Carbon in the Earth's Mantle:

Solubility and speciation in major nominally volatile-free mantle minerals

Dissertation
zur Erlangung des Grades eines Doktors der Naturwissenschaften

der Geowissenschaftlichen Fakultät
der Eberhard-Karls-Universität Tübingen

vorgelegt von

SVYATOSLAV SHCHEKA

aus Wladiwostok (Russland)

2006

Tag der mündlichen Prüfung: 08.02.2006

Dekan: Prof. Klaus G. Nickel, Ph.D.

1. Berichterstatter: Prof. Dr. Hans Keppler

2. Berichterstatter: Prof. Dr. Dr. h.c. Muharrem Satir

Acknowledgements

I want to thank all people who contributed and helped me to make possible this research at Institute for Geosciences, University of Tübingen. I have really enjoyed working here.

First of all, I would like to express my deepest gratitude to Prof. Dr. H. Keppler, for being an outstanding advisor. Thank him for giving me the opportunity to deal with interesting subjects and valuable discussions during this work, for his fruitful assistance and patience, without which composing the current dissertation would not have been possible. His very critical but very true and constructive reviews of earlier versions substantially improved the text of this thesis. Thanks also for allowing me to participate at several conferences and workshops and supporting any kind of travel. His generous support allowed me to concentrate on the research.

I am very grateful to Dr. Michael Wiedenbeck (GFZ Potsdam) for his comprehensive help with SIMS measurements and for his incurable optimism in solving the problems seemed to be unsolvable.

I would like to express my immense gratitude to Dr. Dan Frost (BGI, Bayreuth) and Dr. Paul Balog (Max Planck Institute for Solid State Research, Stuttgart) for introducing me into the multianvil world and for their assistance with preparation and conducting the experiments.

Many thanks are given to my office companion Katrin Mierdel who was helping me every day not only with a routine work, but also with many aspects of my private life, especially during my first months in Germany.

Special appreciation goes to Dr. Cristoph Berthold for hours he spent with me to perform X-ray powder diffraction analyses and to interpret the obtained data. His philosophical and sometimes provoking questions helped me to broaden my general understanding the science.

I am thankful to Dr. Catherine McCammon (BGI, Bayreuth) for critical reading of the manuscript and very productive discussions of its basic points.

I want to thank Bernd Binder and Michael Dorn for their assistance with Raman spectroscopy and Dr. Thomas Wenzel for his thoughtful approach to electron microprobe analyses of my samples.

Acknowledgement

I am grateful to all of my colleagues, who have constructed a very friendly atmosphere for working. This work would not be successful without technical support of our mechanical workshop, particularly, of Norbert Walker and Barbara Maier. Valuable tips of Hubert Schulze (BGI, Bayreuth) on sample preparation saved weeks of my time.

Lastly but not least, I am indebted to my family for their multilateral support, sympathy and prominent encouragement they have always expressed. Above all, I thank my wife, Galina for her love and patience and for taking the burden of the day-to-day activities and responsibilities of our children, when I was occupied with the study. Without her understanding and support it would be impossible to complete this work.

Table of contents

Abstract

(1) Carbon solubility in upper mantle minerals

The solubility of carbon in forsterite, enstatite, diopside, pyrope and $MgAl_2O_4$ spinel has been quantified. Previously reported problems of contamination and slow diffusion of carbon in minerals have been overcome by (1) growing carbon-saturated crystals from carbonatite melts in piston-cylinder (T=900-1100 °C; P=1.5 GPa) and multianvil (T=900-1400 °C; P=6-11 GPa) experiments in the presence of ~1 wt.% water and by (2) using starting materials, isotopically enriched to contain ~99 wt.% of ^{13}C. Secondary ion mass spectrometry (SIMS) was employed to measure the carbon contents of the synthesized minerals.

Carbon solubility in silicates at uppermost mantle conditions is exceedingly low, in the order of a few hundred parts per billion by weight. Solubility increases exponentially as a function of pressure to a maximum of ~12 ppm by weight in forsterite at 11 GPa and 1200 °C. No clear dependence of carbon solubility on temperature, oxygen fugacity and iron content was observed. Carbon solubility in $MgAl_2O_4$ spinel is below the limit of detection of the analytical technique used (i.e., below 30 ppb by weight).

(2) Carbon solubility in minerals of the transition zone and lower mantle

A similar technique was used to obtain the first experimental data on carbon solubility in wadsleyite, ringwoodite, $MgSiO_3$-ilmenite and $MgSiO_3$-perovskite. Experiments were performed in a multianvil press (T=1200-1400 °C; P=16-26 GPa). All high-pressure minerals show no excess of the ^{13}C isotope relatively to the natural ratio of $^{13}C/^{12}C$. The maximum carbon solubility in wadsleyite, ringwoodite, $MgSiO_3$-ilmenite and $MgSiO_3$-perovskite is therefore below the limit of detection of 40-110 ppb by weight.

(3) Carbon speciation in mantle silicates

The observation that carbon solubility in olivine is insensitive to oxygen fugacity implies that the oxidation state of carbon in the carbonatite melt and in olivine is the same, i.e. carbon dissolves as C^{4+} in olivine. The differences in carbon solubilities

between the various minerals studied appear to correlate with the polyhedral volume of the Si^{4+} site, consistent with a direct substitution of C^{4+} for Si^{4+}. The larger size of the Si^{4+} site in minerals of the transition zone and lower mantle and the absence of appropriate polyhedra in $MgAl_2O_4$ spinel prohibit the incorporation of carbon.

(4) Geological implications

The exceedingly low solubility of carbon in major nominally volatile-free mantle minerals implies that the carbon budget of the bulk mantle is dominated by minor carbon-rich phases (e.g. carbonates, diamonds). This is consistent with the possibility of massive carbon enrichment in the shallow mantle. Such carbon-rich reservoirs could be tapped during large volcanic eruptions which may trigger mass extinctions in the biosphere.

Zusammenfassung

1. Kohlenstofflöslichkeit in Mineralen des oberen Erdmantels

Die Löslichkeit von Kohlenstoff in Forsterit, Enstatit, Diopsid und $MgAl_2O_4$-Spinell wurde gemessen. Kohlenstoff-gesättigte Kristalle dieser Minerale wurde aus einer Karbonatitschmelze mit ca. 1 Gew% Wasser auskristallisiert. Für die Experimente wurden eine Piston-Zylinder Apparatur (T =900-1100 °C; P = 1.5 GPa) und eine Multi-Anvil-Presse (T = 900-1400 °C; P = 6-11 GPa) eingesetzt. Der Kohlenstoff im Ausgangsmaterial bestand zu etwa 99 % aus dem Isotop ^{13}C. Durch die Verwendung dieses seltenen Isotops kann der in der Probe gelöste Kohlenstoff eindeutig von Kontaminationen durch isotopisch normalen Kohlenstoff unterschieden werden. Der Kohlenstoffgehalt der synthetisierten Minerale wurde mit Sekundär-Ionen-Massen-Spektrometrie (SIMS) gemessen.

Die Löslichkeit von Kohlenstoff in Silikaten unter den Bedingungen des oberen Erdmantels ist außerordentlich gering. Sie beträgt im Forsterit im obersten Mantel nur einige hundert ppb und steigt als eine Funktion des Druckes bis auf ~12 ppm an (11 GPa und 1200°C). Es wurde keine klare Abhängigkeit der Kohlenstofflöslichkeit von der Temperatur, der Sauerstofffugazität und dem Eisengehalt beobachtet. Im Spinell liegt sich die Löslichkeit von Kohlenstoff unterhalb der Nachweisgrenze von weniger als 30 ppb.

2. Kohlenstofflöslichkeit in Mineralen der Übergangszone und des unteren Erdmantels

Die Experimente zur Kohlenstofflöslichkeit in Wadsleyit, Ringwoodit, $MgSiO_3$-Ilmenit und $MgSiO_3$-Perovskit wurden mit einer Multi-Anvil-Presse (T = 1200-1400 °C; P = 16-26 GPa) durchgeführt. Hierbei wurden ähnliche experimentelle Methoden eingesetzt wie oben beschrieben. Alle synthetisierten Minerale zeigen keinen Überschuß an ^{13}C relativ zum natürlichen $^{13}C/^{12}C$ Verhältnis. Die maximale Kohlenstofflöslichkeit in Wadsleyit, Ringwoodit, $MgSiO_3$-Ilmentit und $MgSiO_3$-Perovskit liegt daher unterhalb der Nachweisgrenze von 40-110 ppb.

3. Kohlenstoff-Speziation in Mantelsilikaten

Da die Kohlenstofflöslichkeit in Olivin unabhängig von der Sauerstoff-Fugazität ist, muß der Oxydationszustand von Kohlenstoff in der Karbonatitschmelze und im Olivin gleich sein, d.h. Kohlenstoff wird im Olivin als C^{4+}gelöst. Die Kohlenstofflöslichkeiten in den verschiedenen Mineralen korrelieren mit dem Volumen des Si^{4+}-Gitterplatzes, wie bei einem direkten Ersatz von C^{4+} für Si^{4+} zu erwarten. Das große Volumen des Si^{4+}-Gitterplatzes in den Mineralen der Übergangszone und des unteren Mantels und die Abwesenheit eines geeigneten Gitterplatzes im $MgAl_2O_4$-Spinell erklären die verschwindend geringe Kohlenstoff-Löslichkeit in diesen Phasen.

4. Geologische Anwendungen

Die außerordentlich niedrige Löslichkeit von Kohlenstoff in den gesteinsbildenden Mineralen des Erdmantels deutet darauf hin, dass das Kohlenstoff-Budget des Mantels durch geringe Mengen an kohlenstoff-reichen Phasen (z.B Karbonate, Diamant) dominiert wird. Damit sind massive Anreicherungen von Kohlenstoff im flachen subkontinentalen Mantel möglich. Kontinentale Flutbasalt-Eruptionen könnten möglicherweise zur schnellen Freisetzung extrem großer Mengen von Kohlendioxid aus diesen Reservoiren führen und damit globale Aussterbeereignisse verursachen.

1. Introduction

1.1 Geochemical significance of carbon

Carbon, although less abundant than hydrogen, may be the most important chemical element in the universe. It is hard to overestimate its significance. Due to its ability to form multiple bonds, stable chains and ring structures, carbon forms more chemical compounds than all the other elements combined. Carbon is the basis of life as we know it.

Carbon and its compounds are a major agent in a large variety of geological processes. Carbon is involved in the regulation of the Earth's surface temperature and ocean chemistry, the formation of gas clathrates and oil deposits as well as in metamorphism and volcanic activity. For example, through the greenhouse effect, the tiny amount of carbon dioxide in the Earth's atmosphere maintains a surface temperature about 35°C above of what it would otherwise be and prevents the freezing of oceans, thereby making life in its modern form possible (Hansen et al., 1984).

Even a rough comparison of terrestrial planets demonstrates that the evolution of the carbon cycle on Earth was fundamentally different from that on Mars and Venus with their CO_2-dominated atmospheres (Rasool and Debergh, 1970). Although carbon compounds surround us everywhere in our routine life, the main carbon reservoir on our planet is located in the interior of the Earth, while most carbon on Venus resides in the atmosphere (Lecuyer et al., 2000).

Understanding the geochemical behavior of carbon in the mantle is of prime importance. For example, when carbonate is present at pressures greater than ~2.7 GPa, the mantle melts initially at temperatures at least 300°C below the carbonate-free solidus (Dalton and Presnall, 1998b; Falloon and Green, 1989). On the contrary, if diamond or graphite is the stable carbon phase under the same conditions, mantle carbon would be much less mobile and its effect on melting relations in the mantle would be minimal (Luth, 1999).

The redox state of regions in the mantle enriched in carbon may be controlled by such equilibria between different carbon-rich phases (Ballhaus, 1993; Blundy et

al., 1991; Canil et al., 1994). Trace amounts of elemental carbon as graphite-like films could influence electrical conductivity and other physical properties (Duba and Shankland, 1982; Karato, 2004; Roberts et al., 1999; Santos et al., 2002) by formation of interconnected phase.

Although carbonates or elemental carbon are stable throughout most of the mantle, there is another possibility – incorporation of carbon in the structure of ordinary mantle minerals which are nominally volatile-free. Water, probably the most important mantle volatile, dissolves in trace amounts in upper mantle silicates (olivine, pyroxenes and garnet), while wadsleyite and ringwoodite, major constituents of transition zone, dissolve water at per cent level, thereby providing an important reservoir of water on Earth (Ingrin and Skogby, 2000; Kohlstedt et al., 1996). If carbon behaved in a similar way, silicate minerals could be the most important host of carbon in our planet.

Although many aspects of the Earth's global carbon cycle are well-constrained, the inaccessibility of the deep interior of the Earth limits our understanding of carbon storage and exchange. This work represents an experimental approach to the problem of carbon solubility in major nominally volatile-free silicates and oxides composing the Earth's mantle. Surprisingly, this issue was firstly brought up more than 25 years ago and, although it was extensively debated and subjected to several reassessments, it still remains ambiguous and unresolved. Nevertheless, if noticeable amounts of carbon can be dissolved by common silicates or oxides, many aspects of mantle geochemistry and petrology, of the global carbon cycle and of the evolution of the carbon distribution in the Earth would need to be re-evaluated.

1.2 Estimates of bulk carbon content of the mantle and carbon global cycle

The Earth's bulk carbon abundance has been deduced from cosmochemical data, based on the observation that despite the relative depletion of meteorites and other planetary objects in volatiles, the ratio of volatiles with similar volatilities is often unaffected by depletion processes. A terrestrial carbon abundance in the order of 0.11 wt.% (6.6×10^{23} g) was derived from the $C/^{36}Ar$ (Otting and Zahringer, 1967) and $C/^{3}He$ (Marty and Jambon, 1987) ratio of chondrites in conjunction with the amount

of rare gases present in the Earth's atmosphere. The resulting total mass of carbon is several orders of magnitude higher than all near-surface carbon reservoirs combined.

Therefore, most of the carbon must reside in the deeper parts of the Earth. Based on geophysical data, it was suggested (Scott et al., 2001; Wood, 1993), that about 10 wt.% of the core is made of light elements and part of it could be carbon. Nevertheless, the mantle is considered to be the largest reservoir of terrestrial carbon (Javoy, 1997).

A number of approaches were used to estimate the bulk carbon abundance in the mantle. They have resulted in a wide range of values (Table 1). Direct measurements in xenoliths and other mantle-derived samples show that 95% of the samples contain less than 500 ppmw (e.g. Figure 3 in Deines, 2002 and references therein), which could be evidence for either a highly heterogeneous distribution of carbon in the source of the measured samples or it could be due to a different degree of carbonate survival during transfer to the surface (Canil, 1990; Wyllie et al., 1983). Values for the oceanic upper mantle (MORB source), derived from studies of MORB glasses, undersaturated melt inclusions in olivine phenocrysts and rare gas systematics as well as data for OIB mantle obtained by mass balance of volcanic gas emissions are all strongly dependent on degree of partial melting and degassing before and during the eruption, which are also somewhat uncertain. In summary, most of the reported estimates of the "average" mantle content are in the range of 50-400 ppmw of carbon (Table 1).

Even if the lowest estimates of carbon concentration were accepted for the mantle, it would still represent the largest reservoir of the Earth's carbon, playing a major role in the carbon global cycle and strongly influencing atmospheric carbon concentration.

Existing models (Berner et al., 1983; Berner, 1994; Lasaga et al., 1985) demonstrate that on a long timescale, the atmospheric CO_2 content is balanced to steady state and controlled by the competing effects of the consumption of atmospheric CO_2 by continental silicate chemical weathering, associated precipitation of marine carbonates and removal of them into the mantle through subduction versus the addition of CO_2 to the atmosphere by mantle degassing (Figure 1.1).

Table 1 Estimates of carbon abundance in various mantle reservoirs and in bulk Earth

Reservoir	Method of estimation	Estimated carbon content, ppmw	Reference
Bulk Earth	$C/^{36}Ar$ systematics of chondrites	1100	Otting and Zahringer, 1967
MORB mantle	Undersaturated melt inclusions	20-73	Saal et al., 2002
	$C/^{3}He$ systematics	40-60	Javoy et al., 1986
	$C/^{3}He$ systematics	74	Zhang and Zindler, 1993
	MORB glasses	185	Blundy et al., 1991; Bottinga and Javoy, 1990
OIB mantle	Mass balance of volcanic gas emissions	40	Greenland et al., 1985
		90	Gerlach and Graeber, 1985; Gerlach et al., 2002
Average cratonic mantle	Ultramafic xenoliths from continental regions	80	McDonough and Rudnick, 1998
Bulk mantle	C content of mantle-derived samples	1-10000	Deines, 2002
	Garnet lherzolites	1-62	Helmstaedt, 1993
	Garnet harzburgites	0.1-130	Helmstaedt, 1993
	Diamondiferous dunites	>1300	Luth, 1999
	Ultramafic xenoliths from hotspots	1-260	Trull et al., 1993; Zheng et al., 2000
	Ultrahigh pressure eclogites	400-4300	Zheng et al., 2000
Bulk upper mantle	C/He systematics of MORB	50-250	Trull et al., 1993
Bulk upper mantle	MORB glasses	400	Javoy, 1997
Primitive mantle	K/C correlation in basalts	80	Canil et al., 1994; O'Nions and Oxburgh, 1988

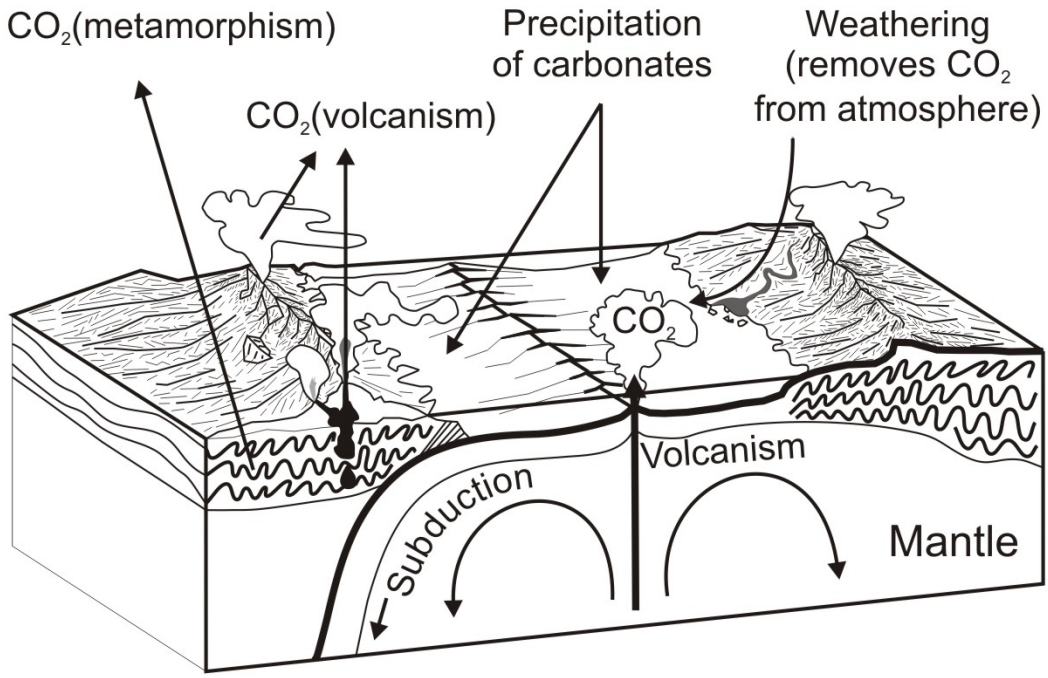

Figure 1.1 Schematic model of carbon global cycle

The rate of carbon degassing was deduced by integration of the CO_2 flux from a variety of sources – volcanic activity in mid-ocean ridges, hotspots and subduction zones (Kerrick, 2001; Marty and Jambon, 1987), metamorphic devolatilization of subducted sediments (Kerrick and Connolly, 2001) and non-volcanic CO_2 degassing. The evaluation of carbon recycling back into the mantle is based on the carbon content of subducted oceanic crust in conjunction with rates of spreading. Although the efficiency of carbon recycling into the mantle via subduction is still debated (Cartigny et al., 1998; Marty and Jambon, 1987), most workers (Javoy et al., 1982; van Achterbergh et al., 2004; Zhu and Ogasawara, 2002) agree, that removal of carbon from the near-surface environment is necessary to maintain the observed balance of carbon. Experimental studies (Dasgupta et al., 2004; Molina and Poli, 2000; Yaxley and Green, 1994) have shown, that subducting carbonate-bearing material (both peridotitic and eclogitic in composition) undergoes only negligible devolatilization, and significant decarbonation is feasible only at lower

pressures (in the forearc region, Figure 3 in Dasgupta et al., 2004) and at relatively high temperatures, when oceanic crust is subducted at slower rates.

1.3 Mantle oxidation state and carbon phases in the mantle

1.3.1 Redox state of the mantle

As observed in mantle-derived samples and supported by experimental studies, carbon can be present in the mantle in various phases. It occurs mostly as CO_2 and CH_4 in fluid inclusions, as carbonate and carbonatite melt, and as graphite and diamond (Luth, 2003). It is generally accepted, that the host for carbon will change systematically with the depth depending on PT-regime, bulk composition and particularly on ambient oxygen fugacity of the mantle which may become more reduced with depth (e.g. McCammon, 2005a,b; Wood et al., 1990).

A strong heterogeneity of the upper mantle by at least four log units in oxidation state derived from studies of natural mantle samples (see Table 2 and reviews of Luth, 1999; Wood, 1991) is considered to result from metasomatism (McCammon, 2001), partial melting events (Ballhaus, 1993) and different tectonic settings (Wood et al., 1990). The highest values of oxygen fugacity (up to 2 log units above fayalite-magnetite-quartz oxygen buffer (FMQ), Table 2) are characteristic for xenoliths from regions influenced by subduction (e.g. island arcs, back-arc basins), while f_{O_2} measured in spinel-bearing suboceanic abyssal samples is in general between FMQ and FMQ-1. Peridotites of garnet facies record a decrease of oxygen fugacity with depth to the values close to WI (wüstite-iron oxygen buffer). Ballhaus (1993) noted, that "isolated samples from cratonic Archean lithosphere may plot as low as FMQ-5". He further assumed the possibility of temporal variations in the redox state of the mantle as a result of different degrees of overprinting metasomatism.

Although the buffering capacity of elements with variable oxidation state in the mantle is largely uncertain (Canil et al., 1994), iron is thought to play a dominant role in controlling the redox conditions in the bulk mantle (McCammon, 2005a). Olivine, the

most abundant mineral of the upper mantle incorporates only negligible Fe^{3+} (Canil et al., 1994; Nakamura and Schmalzried, 1983). Therefore, Fe^{3+} is concentrated in the minor phases spinel and garnet, thereby produces a relatively oxidized environment. Gudmundsson and Wood (1995) have shown that pressure enhances the incorporation of ferric iron in garnet due to the decrease in volume associated with the exchange reaction. Additionally, because of the dissolution of pyroxene in majoritic garnet, the modal fraction of garnet increases with depth, leading to a "dilution of Fe^{3+} in garnet" (Wood et al., 1996) and therefore to a reduction of oxygen fugacity.

O'Neill et al. (1993a,b) found that the major minerals of the transition zone (garnet, wadsleyite and ringwoodite) incorporate significant Fe^{3+} even in equilibrium with metallic Fe. They concluded that f_{O_2} of the transition zone is close to the iron-wüstite buffer, i.e. close to metal saturation.

Based on the high $Fe^{3+}/\Sigma Fe$ (20-75%) of inclusions with pyroxene composition (believed to have originally perovskite structure) in diamonds from Brasil (McCammon, 1997) measured by Mössbauer spectroscopy, it was proposed that a similar situation probably occurs in the lower mantle. This conclusions was supported by the synthesis of aluminous (Mg,Fe)-perovskite with ~50% of its Fe as Fe^{3+} in equilibrium with metallic iron (McCammon, 1997). Recently, Frost et al. (2004) showed that the disproportionation of iron according to the reaction:

$$3FeO \rightarrow Fe + Fe_2O_3$$

is probably the most important mechanism determining the oxidation state of the lower mantle and that the lower mantle contains approximately 1 wt.% of Fe-rich alloy.

In summary, if redox equilibria of iron determine the oxidation state of the mantle, all carbon may be reduced beyond a depth of ~200 km and diamond may be the stable host for carbon at pressures above 7 GPa (Wood et al., 1996). Nevertheless, the high heterogeneity of the carbon distribution in the mantle inferred from geochemical data (see section 1.2) implies that there are regions where the abundance of carbon is sufficient to overwhelm Fe^{2+}/Fe^{3+} equilibria (e.g. subducted marine sediments). In this case, redox reactions involving carbon-bearing phases would govern oxygen fugacity (see section 1.3.3).

Table 2 Oxidation state of mantle-derived samples based on oxygen geobarometry and XANES spectroscopy

Mantle sample	Oxygen fugacity, log units relatively to QFM	Method	Reference
MORB glasses 1200°C, 1 bar	-1.3	Calibration of Fe_2O_3/FeO ratio	Christie et al., 1986
Subcontinental spinel lherzolite 15kb	mean +0.24	$6Fe_2SiO_{4(olivine)}+O_2 = 3Fe_2Si_2O_{6(orthopyroxene)}+2Fe_3O_{4(spinel)}$	Wood and Virgo, 1989
Spinel peridotite from Ronda and Beni Bousera massifs 900-930°C, 9-15kb	-1.1- -1.5	$6\ Fe_2SiO_{4(olivine)}+O_2=3\ Fe_2Si_2O_{6\ (orthopyroxene)}+2\ Fe_3O_{4\ (spinel)}$	Woodland et al., 1992
Abyssal spinel peridotite from Atlantic and Indian ocean 1151°C, 1GPa	mean -0.9	$6\ Fe_2SiO_{4(olivine)}+O_2=3\ Fe_2Si_2O_{6\ (orthopyroxene)}+2\ Fe_3O_{4\ (spinel)}$	Bryndzia and Wood, 1990
Spinel peridotite from San Carlos, Central Asia and Kilbourne Hole 900-1100°C, 15kb	-1.5 - 0	$6\ Fe_2SiO_{4(olivine)}+O_2=3\ Fe_2Si_2O_{6\ (orthopyroxene)}+2\ Fe_3O_{4\ (spinel)}$	Wood et al., 1990
Garnet peridotite from South Africa and Lesotho 900-1100°C, 2.5-6.3GPa	-2.5 - -4.2	$2Fe_3^{2+}Fe_2^{3+}Si_3O_{12\ (garnet)} = 4Fe_2SiO_{4(olivine)}+2FeSiO_{3(orthopyroxene)}+O_2$	Woodland and Koch, 2003
Garnet peridotite from South Africa 1000-1300°C, 2-6.5GPa	-3	$2Ca_3Fe_2Si_3O_{12(garnet)}+2Mg_3Al_2Si_3O_{12(garnet)}+4FeSiO_{3(orthopyroxene)} =2Ca_3Al_2Si_3O_{12(garnet)}+8FeSi_{0.5}O_{2(olivine)}+6MgSiO_{3(orthopyroxene)}+O_2$ $2Fe_3Fe_2Si_3O_{12}= 8FeSi_{0.5}O_{2(olivine)}+2FeSiO_{3(orthopyroxene)}+O_2$	Gudmundsson and Wood, 1995; Luth et al., 1990
Garnet and spinel peridotite from Slave craton	-0.9- -4	$2Fe_3Fe_2Si_3O_{12}= 8FeSi_{0.5}O_{2(olivine)}+2FeSiO_{3(orthopyroxene)}+O_2$ $6Fe_2SiO_{4(olivine)}+O_2 = 3Fe_2Si_2O_{6(orthopyroxene)}+2Fe_3O_{4(spinel)}$	McCammon and Kopylova, 2004
Glass from Kilauea Iki Melt inclusion in olivine from Nikaragua 1200°C	-1.1 +0.2	Vanadium K-edge XANES spectroscopy	Sutton et al., 2005
Spinel peridotite and dunite from Grenada ~850°C, 1.5-3GPa	+1.30 – +1.70	$6\ Fe_2SiO_{4(olivine)}+O_2 =$ $3\ Fe_2Si_2O_{6\ (orthopyroxene)}+2\ Fe_3O_{4\ (spinel)}$	Parkinson and Arculus, 1999; Parkinson et al., 2003

1.3.2 Oxidized carbon

Oxidized forms of carbon (CO_2 and carbonates) are typical for samples from the shallow upper mantle. Mantle-generated silicate melts often contain carbon dissolved as molecular CO_2 or carbonates (Blank and Brooker, 1994). CO_2-rich fluid inclusions are common in minerals from mantle xenoliths (Andersen et al., 1984; Bergman and Dubessy, 1984; Bilal and Touret, 1977; Roedder, 1965). Solid CO_2 inclusions in diamond were described by Schrauder and Navon (1993). Carbonates and carbonatite melts were observed, for instance, as carbonatites (e.g. Ionov and Harmer, 2002; Moine et al., 2004), carbonated mantle xenoliths (e.g. Laurora et al., 2001; Lee et al., 2000) and inclusions in diamonds (Wang et al., 1996).

An overview of experimental studies on carbonate stability in the upper mantle is given in Figure 1.2 and Table 3. In a peridotite upper mantle, CO_2 is stable only at pressures below ~2.7 GPa and readily reacts with silicates to form dolomite and magnesite at higher depth (Wyllie et al., 1983). However, CO_2 persists to higher pressures in eclogitic compositions. Experiments and calculations indicate that magnesite is, among all carbonates, the most stable at high-pressure and high-temperature and it appears to be a very good candidate for hosting oxidized carbon in the mantle (Fiquet et al., 2002; Skorodumova et al., 2005; Zhang et al., 1997). Katsura and Ito (1990) reported that magnesite coexists with enstatite at 8 and 15 GPa and with $MgSiO_3$-perovskite at 26 GPa. Biellmann et al. (1993) found magnesite to coexist with silicate perovskite and ferripericlase at pressures to 50 GPa. Isshiki et al. (2004) demonstrated that magnesite and its high pressure modification (probably with pyroxene- or $CaTiO_3$-like structure (Skorodumova et al., 2005) is stable to the pressure corresponding to the base of the lower mantle.

Dalton and Presnall (1998a,b) and Gudfinnsson and Presnall (2005) showed that in carbonate-bearing mantle low-degree near-solidus melts are carbonatitic with ~45 wt% of CO_2 and the presence of carbonate dramatically decreases the solidus temperature of peridotite. The segregation and migration of low-viscosity carbonatitic liquids (Dobson et al., 1996) formed at low temperature could result in a highly heterogeneous carbon distribution in the mantle. The local enrichment in carbon may be sufficient to overcome the reducing capability of iron equilibria and to stabilize oxidized forms of carbon in the deeper mantle.

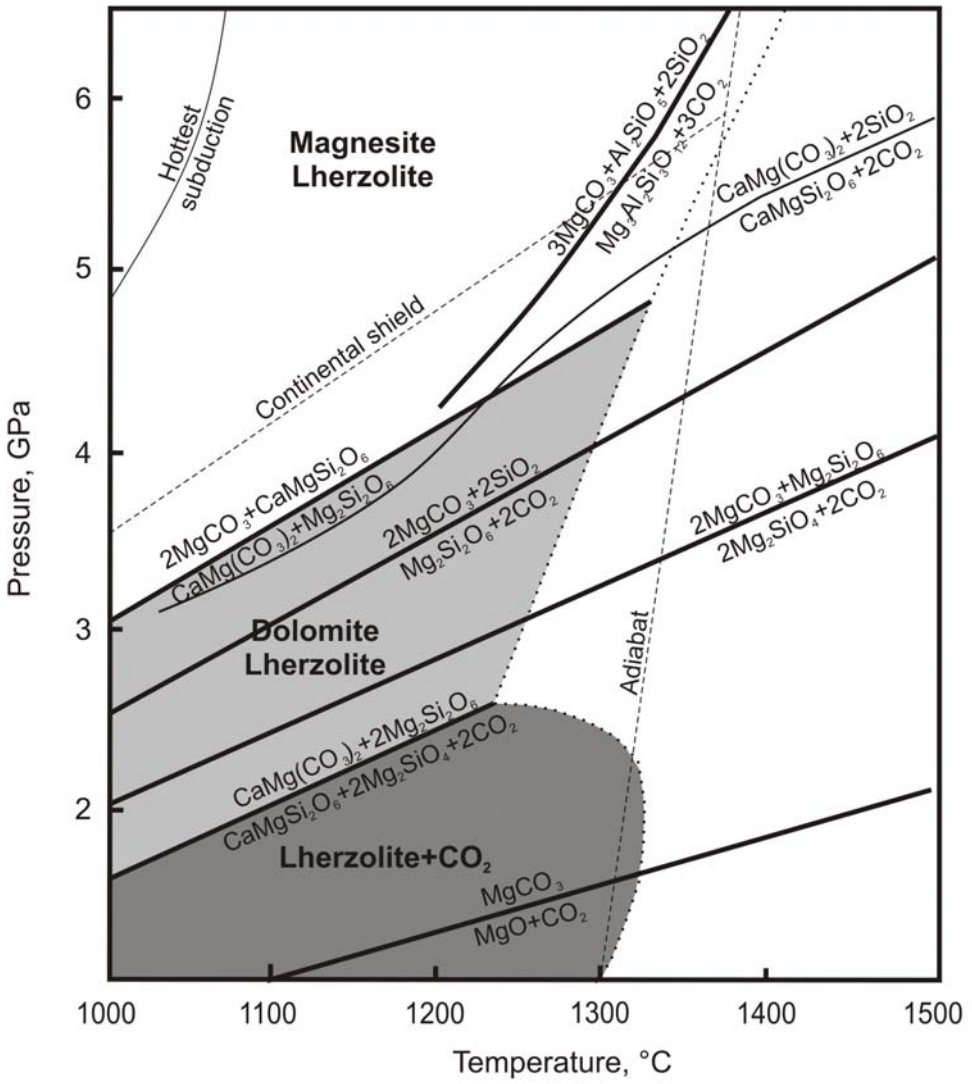

Figure 1.2 Summary of experimental studies of carbonation reactions relevant to peridotites and eclogites of the upper mantle (see Table 2 for references). Solidus curve for model carbonated lherzolite (CMAS.CO_2 system) is from Dalton and Presnall (1998b). Also shown are an average mantle adiabat (McKenzie and Bickle, 1988), a continental shield geotherm (Chapman, 1986) and the maximum estimate of temperatures in subduction zones ("Hottest subduction", van Keken et al., 2002).

Although stability of oxidized forms of carbon is suggested by several authors to be limited to the uppermost ~200km of the mantle (e.g. Luth, 1999; Wood et al., 1996), the redox equilibria involving carbon and iron are poorly understood at the conditions of the lower mantle and there is no reliable experimental evidence for the large-scale reduction of carbon at a greater depth.

Table 3 Selected experimental studies of carbonation reactions for model peridotitic and eclogitic compositions

Phase equilibrium studied	Reference
$MgCO_3=MgO+CO_2$	Ellis and Wyllie, 1980
$CaMgSi_2O_6+Mg_2SiO_4=CaMg(CO_3)_2+Mg_2Si_2O_6+CO_2$	Canil, 1990; Dalton and Presnall, 1998b; Haselton et al., 1978; Wyllie et al., 1983
$2MgCO_3+Mg_2Si_2O_6=2Mg_2SiO_4+2CO_2$	Newton and Sharp, 1975
$2MgCO_3+2SiO_2=Mg_2Si_2O_6+2CO_2$	Wyllie and Huang, 1976
$CaMg(CO_3)_2+Mg_2Si_2O_6=2MgCO_3+CaMgSi_2O_6$	Brey et al., 1983; Dalton and Presnall, 1998b
$CaMgSi_2O_6+2CO_2=CaMg(CO_3)_2+2SiO_2$	Luth, 1995
$Mg_3Al_2Si_3O_{12}+3CO_2=3MgCO_3+Al_2SiO_5+2SiO_2$	Knoche et al., 1999

1.3.3 Neutral carbon

Elemental carbon is potentially stable in the mantle as graphite at low pressure and as diamond at higher pressure. This is supported by observations of both polymorphs in mantle-derived xenoliths (Viljoen, 1995) and graphite pseudomorphs after diamonds in some peridotite massifs (Davies et al., 1993). According to mineral composition of inclusions in some ultradeep diamonds, the latter have formed in the transition zone and lower mantle (Stachel et al., 2005). The origin of poor-crystallized carbonaceous films on grain boundaries and cracks in mantle minerals (Mathez et al., 1984; Mathez, 1987; Pasteris, 1988; Pineau and Mathez, 1990) is poorly understood and was interpreted as decomposition product of C-O-H fluid adsorbed on the mineral surface during cooling of host magma. However, Pineau and Mathez (1990) described

cracks with carbonaceous material in minerals in websterites, which were partially annealed before the incorporation of the xenoliths in the transporting magma.

The potential stability of elemental carbon is constrained by the reaction:

$$C+O_2=CO_2$$

(Frost and Wood, 1997; Frost and Wood, 1998; Pineau and Mathez, 1990). In natural systems, however, carbon-bearing phases coexist with silicates, and the redox equilibria of type:

$$MgSiO_3+MgCO_3=Mg_2SiO_4+C+O_2 \text{ (EMOG/D, Eggler and Baker, 1982)}$$

and

$$2SiO_2+CaMg(CO_3)_2=CaMgSi_2O_6+2C+2O_2 \text{ (DCDG/G, Luth, 1993)}$$

are suggested to determine maximum oxygen fugacity at which elemental carbon is stable in peridotite and eclogite assemblages, respectively (Figure 1.3).

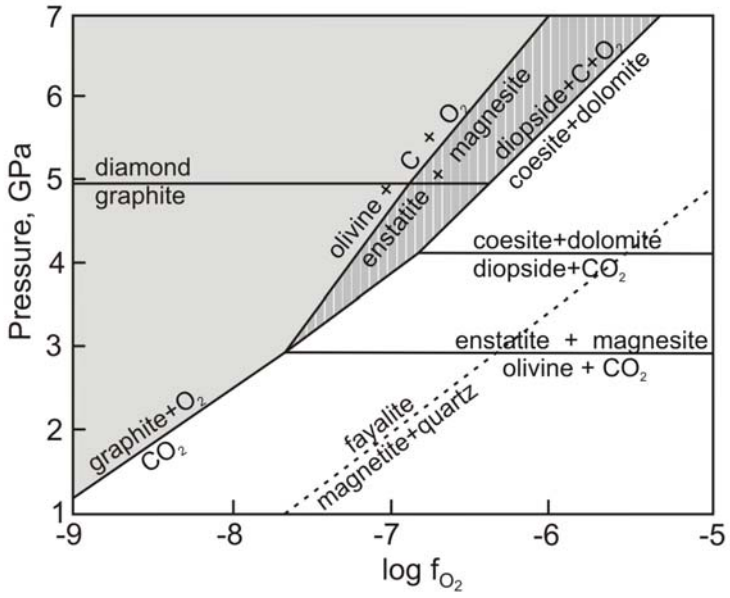

Figure 1.3 Position of basic equilibria determining the stability of C-bearing phases in the mantle on a pressure-log f_{O_2} projection at T=1200°C (after Luth, 1999). Shaded region represents P- f_{O_2} space where graphite or diamond is stable. Vertically-ruled area corresponds to the conditions where diamond is stable in eclogitic mantle but carbonate - in peridotitic assemblage. Non-redox reactions (parallel to log f_{O_2} -axis) and the FMQ oxygen buffer (dotted line) are shown for reference.

Generally, graphite or diamond is stable to higher f_{O_2} in eclogites, implying the possibility of coexistence of carbonated peridotite with diamond-bearing eclogites.

Blundy et al. (1991) suggested that carbon redox equilibria similar to those shown on Figure 1.3 buffer oxygen fugacity in the mantle so that both oxidized and reduced forms of carbon coexist. However, estimates of bulk mantle carbon limit this possibility to carbon-rich parts of the mantle.

1.3.4 Reduced carbon

Reduced carbon occurs in the mantle as CH_4 in fluid (Melton et al., 1972) and moissanite (Mathez et al., 1995). Some models (Scott et al., 2004; Taylor and Green, 1988) suggest that CH_4-dominated fluids are common in the deeper mantle, but they react with the more oxidized upper mantle during ascending. Formation of moissanite probably requires a very reduced environment (Kadik et al., 2004) which probably occurs only in limited regions of the mantle.

1.4 Carbon in nominally volatile-free mantle minerals

In pyrolite mantle model (Ringwood, 1962), which is based on the complementary melt-residuum relationship between basalts and peridotite, the upper mantle is composed of olivine, two pyroxenes and an Al-bearing phase (depending on depth, plagioclase, spinel or garnet). With increasing pressure, olivine transforms to wadsleyite at ~410 km and ringwoodite at ~520 km. Pyroxenes convert to $MgSiO_3$-ilmenite and dissolve in garnet to form majorite. At the top of the lower mantle minerals of the transition zone transform to assemblage of $MgSiO_3$-perovskite and ferropericlase with a minor amount of $CaSiO_3$-perovskite (Figure 1.4).

Although carbon may exist in the mantle in separate C-rich phases, ordinary mantle silicates and oxides could be a potential host of mantle carbon as well. Moreover, it is conceivable that these minerals may incorporate carbon in any oxidation state, involving the substitution of either cations or anions in the crystal lattice or involving neutral carbon in defects in the structure. In this case, the stability of other C-rich phases (see section 1.2) should depend on the modal mineralogy of the

mantle and should be controlled by the solubility of carbon in the constituent minerals.

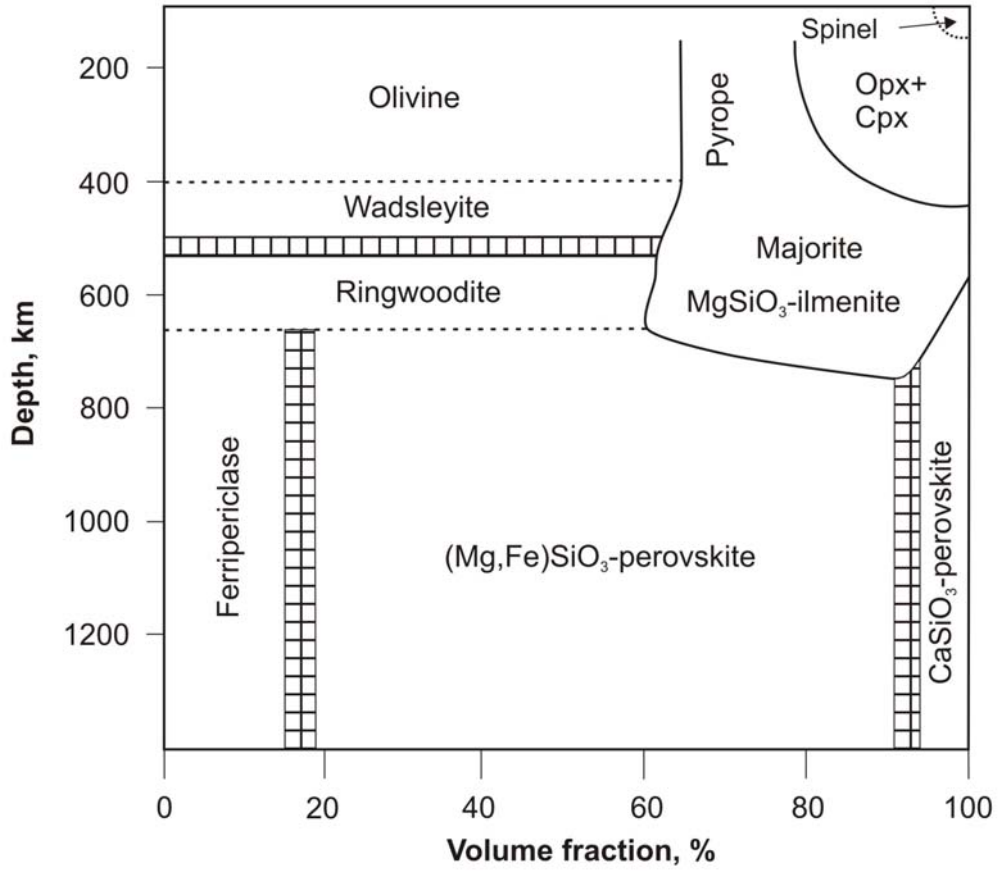

Figure 1.4 Major phase proportions in a pyrolite mantle. Compilation of data of Bina (1998), Ita and Stixrude (1992) and Ringwood (1989). Modified after Bina, 2003.

Some evidence for significant carbon solubility in upper mantle minerals came from studies of fluid inclusions. The ubiquitous presence of tiny (<1 μm) bubbles, filled with "a mysterious fluid with remarkable physical properties" (Brewster, 1823), identified later as nearly pure liquid carbon dioxide (Vogelsang, 1869; Vogelsang and Geissler, 1869) in minerals from peridotite xenoliths in alkalic basalts, could imply that these inclusions have formed by exsolution of carbon dioxide (Green and Radcliffe, 1975; Green, 1972; Green and Gueguen, 1974), originally dissolved in host minerals at higher pressure. However, alternatively, the fluid may be trapped during

crystal growth from a melt or during subsequent healing of fractures in crystals (Roedder, 1965; Roedder, 1984). The following observations support the former interpretation: (1) the extremely small size of the bubbles, (2) the location on dislocations in the crystal structure, (3) the concentration on the boundaries of inclusion-free recrystallyzed grains and (4) the dissolution of CO_2 bubbles in the host olivine at pressures up to 110 kbar in experiments of Ernst et al. (1982).

Green and Gueguen (1974) have estimated that the volume fraction of carbon dioxide inclusions in olivine from peridotite xenolith in kimberlite corresponds to a carbon solubility of 160 ppmw, assuming a positive pressure dependence of solubility. Comparing of this number with estimates of bulk carbon abundance of upper mantle (see Section 1.1) would suggest, that there might be regions in the upper mantle, where a significant fraction of carbon (if not all) could be locked in normally volatile-free silicates.

Previously, numerous attempts to measure carbon solubility in major mantle mineral have been undertaken. Major problems in these studies were often due to contamination.

Most attention previously has focused on carbon solubility in olivine, the main constituent of the upper mantle down to the top of the transition zone, where it converts to wadsleyite. In the early 1980s Freund and co-workers reported a significant solubility of carbon in natural olivine (Freund et al., 1980; Freund, 1981; Kathrein et al., 1983; Oberheuser et al., 1983) measured by X-ray-photoelectron spectroscopy and by the $^{12}C_{(d,p)}{}^{13}C$ nuclear reaction. They suggested that carbon is truly dissolved in olivine forming CO_2^{2-}-complexes, with high mobility in the crystal lattice and a tendency to segregate from the bulk toward crystal surfaces. Mathez et al. (1984), Tsong et al. (1985) and Tsong and Knipping (1986) could not reproduce the earlier results using the same methods and secondary ion mass spectrometry. They pointed out the poor vacuum conditions of the previous studies and demonstrated that at 10^{-8} torr (analytical conditions in the studies of Freund and coworkers) a monolayer of contamination on the sample surface forms in only ~100s. The reported solubility was below the limits of detection of the techniques used (in the order of several 10's ppmw). 425 ppmw of carbon in one olivine crystal reported in Mathez et al. (1984) were attributed to discrete C-rich phase(s) in submicroscopic inclusions or microcracks.

Another approach was used by Tingle et al. (1988). Single crystals of natural olivine from San Carlos were annealed in ^{14}C-labeled CO_2, CO_2-H_2O, and graphite at upper mantle conditions. Samples were studied by beta-track mapping. No evidence for carbon solubility above the limit of detection of 30 ppmw was found. However, these experiments do not rule out a significant carbon solubility, if the diffusion of carbon in olivine at 1400°C is lower than 10^{-14} cm^2/s.

Data on other upper mantle minerals are scarce and based exclusively on the $^{12}C_{(d,p)}{}^{13}C$ nuclear reaction technique. Mathez et al. (1984) and Wilmart et al. (1993) tried to measure carbon in pleonaste megacrysts from spinel lherzolite and spinel grains from hyperstene granite, respectively and found no evidence for dissolved carbon. Kadik et al. (1996) reported the carbon content of orthopyroxene and garnet in garnet lherzolite nodule in an alkaline basalt from Mongolia to be in the order of 75-168 ppmw, but they did not provide technical details and these data are questionable because of possible contamination or the presence separate C phases.

Recently, Keppler et al. (2003) demonstrated that usual upper mantle silicates incorporate only traces of carbon (1-5 ppm by weight). However, their C-saturated crystals were synthesized at conditions of the uppermost mantle, and it is not clear if these results could be applied to the whole pressure-temperature range of the upper mantle. Moreover, ion probe data on carbon solubility in enstatite, diopside, pyrope and spinel were calibrated against a glass standard, which does not match measured samples compositionally and structurally. Taking into account the matrix dependence of ion yields during ion probe analysis significant systematic errors are possible.

Little is known about the behavior of carbon in the transition zone and lower mantle. It was experimentally shown that while the main host for oxidized carbon is probably magnesite and its high-pressure polymorphs (Biellmann et al., 1993; Isshiki et al., 2004; Wang et al., 1996), diamond is the stable carbon phase in more reduced regions (McCammon, 2001; Stachel et al., 2005). No data on carbon solubility in the common silicates of the transition zone - wadsleyite, ringwoodite and $MgSiO_3$-ilmenite and in the major phase of the lower mantle – $MgSiO_3$-perovskite exists up to now. However, because $MgSiO_3$-perovskite is thought to be the most abundant mineral in the Earth, even a moderate solubility of carbon in it would make $MgSiO_3$-perovskite the Earth's major reservoir of carbon.

2. Experimental procedure

2.1 Sample synthesis

2.1.1 Starting materials

The main criteria to choose starting materials in this study were (1) the necessity to produce relatively large crystals of silicates and spinel (>50μm in diameter), (2) saturated with carbon, staying in a (3) compositional range as close as possible to real natural systems. For these reasons bulk compositions corresponding to carbonatite were used. Carbonates are stable at mantle conditions (Biellmann et al., 1993, Isshiki et al., 2004; Santillan et al., 2003). Moreover, various amounts of carbonates are often observed in mantle samples, as inclusions in minerals in mantle xenoliths (Ionov et al., 1993; Pineau and Javoy, 1975) or as kimberlite and carbonatite melts (e.g. Kamenetsky et al., 2004), although it was shown (Canil, 1990; Wyllie et al., 1983) that the carbonates in most cases do not survive the entrainment and ascend to the surface. Sodium carbonate was used as a source of carbon because of its fluxing properties and because only traces of sodium dissolve in the structures of the investigated mantle minerals (Table 7).

Stoichiometric mixtures corresponding to each mineral of interest were prepared from high purity oxides and hydroxides (Table 1). Before weighing, chemicals were dried at ~150°C for several hours to remove adsorbed water, afterwards, they were stored in desiccator. Mixtures were ground in ethanol together with 20% of Na_2CO_3 certified to contain 99% of the ^{13}C isotope, for 30 minutes using a planetary mill. For piston cylinder experiments approximately 120 mg of these mixtures together with about 1 wt. % of water were loaded in 10mm long capsules with an outer diameter of 5mm and a wall thickness 0.3 mm, made of platinum-rhodium (95 wt.% Pt, 5 wt.% Rh), iron, cobalt or nickel. Platinum-rhodium capsules were sealed by arc welding. During this procedure the capsule was submerged into an ice-water mixture to avoid evaporation of water during sealing. Iron, cobalt and nickel capsules were closed by hammering the upper lid into the capsule. The lid had a ledge with 0.1mm larger diameter than inner diameter of the capsule. Final sealing was

reached by fast assembling and compressing the capsule to the target pressure. In multianvil runs platinum capsules (1-3.5 mm long, 1-2 mm in diameter) made from 0.1 mm thick foil and closed by compression were used.

Table 4 List of chemicals used for preparation of starting mixtures

Chemical	Chemical purity	Producer
MgO	97%+	Merck
SiO_2	99.99%	ChemPur
Al_2O_3	99%+	Merck
$Ca(OH)_2$	96%+	Merck
FeO	99.5%	ChemPur
LiOH	98%+	Merck
MoO_3	99.5%+	Merck
V_2O_5	98%+	ChemPur
Na_2CO_3 (99% ^{13}C)	98%+	Cambridge isotope laboratories

The size of crystals, grown from such a homogeneous starting material was satisfactory only for enstatite in all runs and for minerals synthesized in the multianvil press at temperatures of 1200°C and higher. All attempts to grow large enough grains of olivine, diopside and spinel in piston cylinder experiments in the temperature range of 900-1100°C failed because of the very fast nucleation rate resulting in production of many small crystals with a diameter of <15-20μm. Therefore, a slightly modified setup described in Mierdel and Keppler (2004) was used (Figure 2.1). Instead of using homogeneous, stoichiometric mixtures of chemicals, the capsules were filled with alternating layers of two types: (1) SiO_2 + 20 wt.% of Na_2CO_3 and (2) MgO or $Mg(OH)_2$ ± $Ca(OH)_2$ ± γ-Al_2O_3 + 20 wt.% of Na_2CO_3 with bulk stoichiometry corresponding to olivine, diopside or spinel mixed with 20 wt.% of Na_2CO_3. Such a layering of material in the capsule leads to nucleation of crystals only along the boundaries between layers while Na_2CO_3 is present in excess within the whole capsule. The reduced number of nucleation centers results in a larger size of individual crystals.

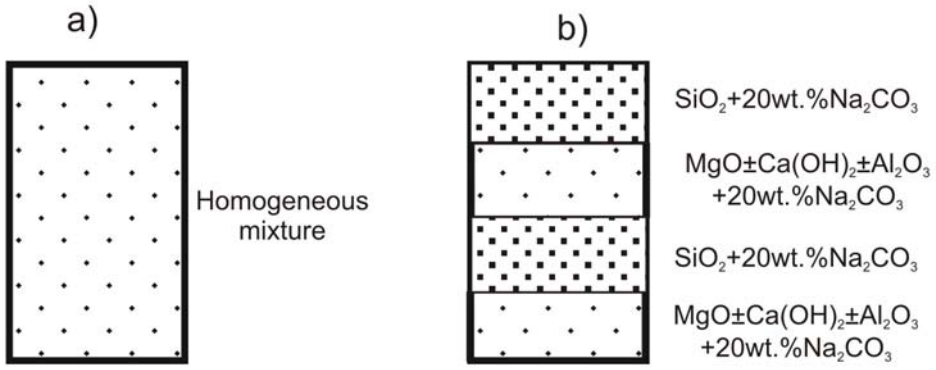

Figure 2.1 Configuration of sample capsule for high-pressure high temperature synthesis of minerals: a) type used in all multianvil runs and for enstatite in piston-cylinder runs; b) type used for forsterite, diopside, spinel in piston-cylinder runs.

2.1.2 High-pressure experiments

An overview of the experimental approach is shown on Figure 2.2. This procedure was found to be most effective in growing and separating carbon-saturated minerals. The use of starting materials enriched in the isotope ^{13}C (with natural abundance of ~1.1%) was essential to distinguish structurally bound carbon and external contamination.

2.1.2.1 Piston-cylinder apparatus

In a piston-cylinder apparatus, a small piston is forced into a cylindrical cavity that contains a sample. A large hydraulic ram is used to transmit force to the smaller piston. Since pressure equals force/area, going from a relatively large area (ram) to a small area (piston) results in high pressures on a small sample.

Experiments at the uppermost mantle conditions (P=1.5 GPa, T=900-1100 °C) were carried out in a non-endloaded Johannes-type (Johannes, 1973) piston cylinder (PC) apparatus (Figure 2.3).

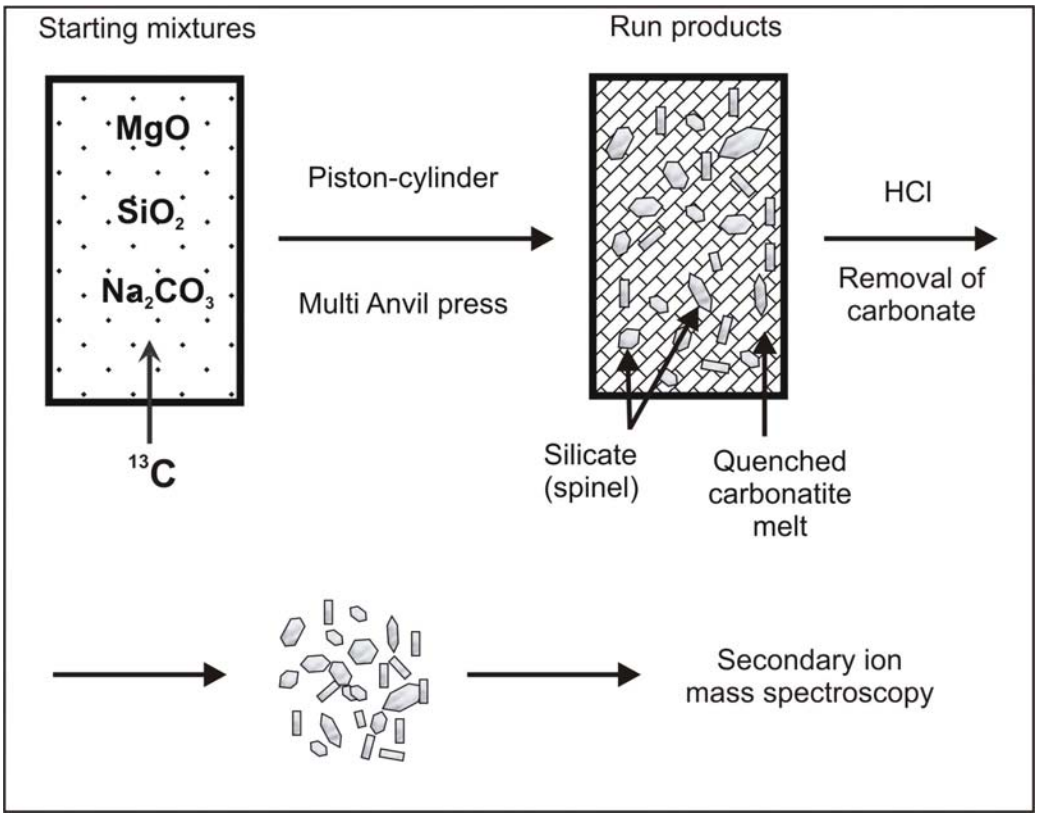

Figure 2.2 Experimental procedure used in this study

This press was used to synthesize forsterite, enstatite and diopside at 900, 1000 and 1100°C, $MgAl_2O_4$ spinel at 1100°C as well as olivine with various Fe content at 1100°C. Additionally, experiments with olivine composition at different redox conditions were performed using piston cylinder press. Assemblies (22 mm diameter, 45 mm long) used consisted of NaCl pressure medium, pyrex glass, crushable alumina, pyrophyllite and graphite (Figure 2.4). A tapered graphite heater was used to minimize thermal gradient (Schilling and Wunder, 2004). Before loading the assembly, the inner walls of the bomb were coated with a suspension of molybdenum sulfide powder in mineral oil to facilitate extraction of sample after the experiment.

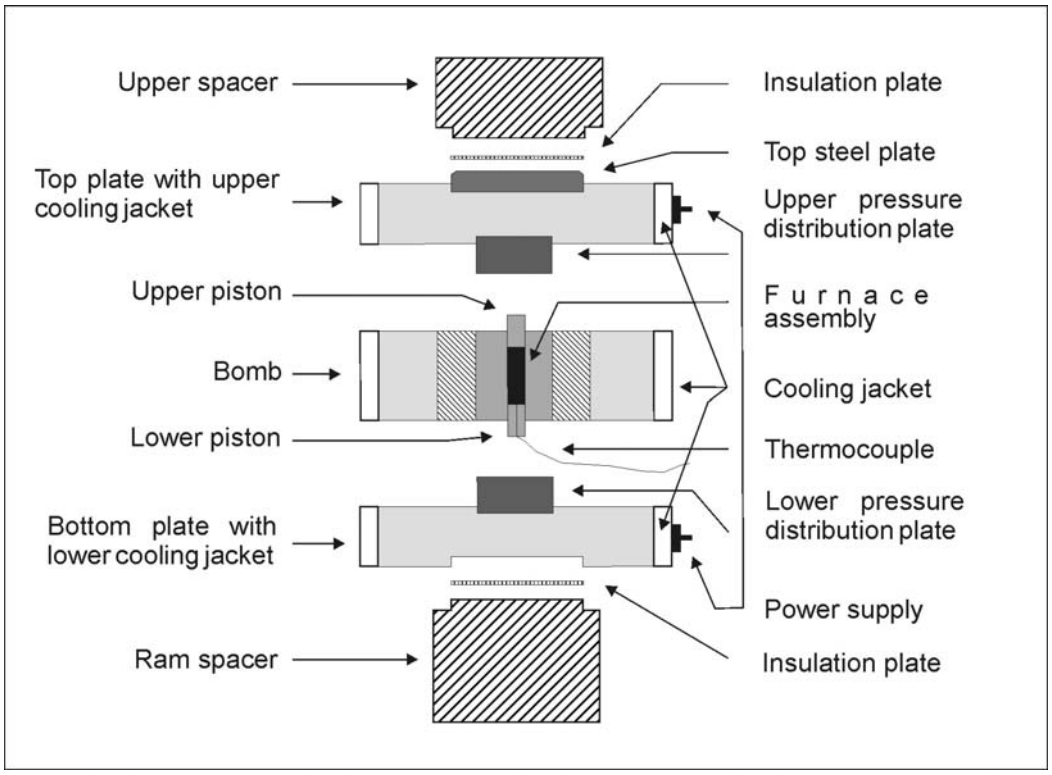

Figure 2.3 Details of non-endloaded piston-cylinder apparatus

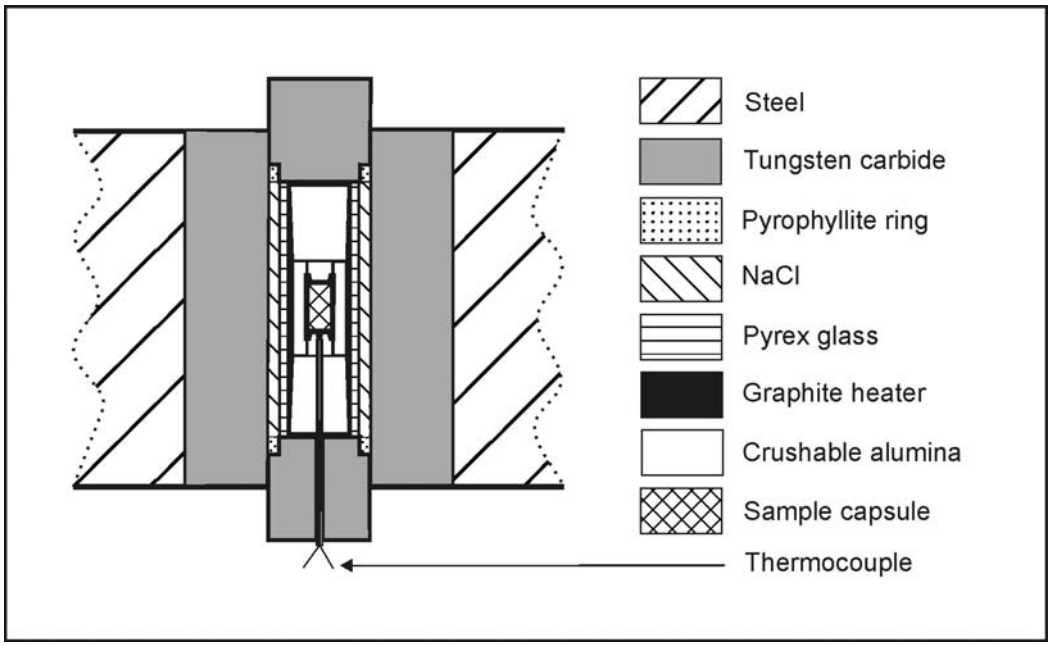

Figure 2.4 Details of assembly for piston cylinder experiments

Temperature was measured by a NiCr-Ni (type K) thermocouple touching the sample capsule and controlled by a Euroterm 2416 temperature controller. Pressures reported include a 10% friction correction. Pressures and temperatures are estimated to be accurate to ± 1 kbar and ±25°C, respectively. Oxygen fugacity was not strictly controlled in runs with PtRh capsules, but the reaction of traces of water with the graphite heater probably results in an oxygen fugacity close to Ni-NiO buffer. Oxidation of Fe, Co and Ni capsules in experiments Ol11F1, Ol11C and Ol11N produced an oxygen fugacity corresponded to IW (Fe-FeO), Co-CoO and Ni-NiO buffer reactions respectively.

2.1.2.2 Multianvil press

Multianvil experiments were carried out at Bayerisches Geoinstitut, Bayreuth. The pressure in this type of press is generated in two steps (Figure 2.5). In the first compression stage (Figure 2.5A) six steel anvils embedded in hemispheres of guide blocks transform the uniaxial force of the hydraulic press to a concentric force on the inner anvils. The inner anvils are placed in the cubic cavity formed by steel anvils and consist of eight corner-truncated tungsten cubes (Figure 2.5.). The truncation (second compression stage) creates an octahedral cavity where the sample assembly is placed (for details see Rubie, 1999; Walker et al., 1990). Varying of the truncation edge length allows experiments in the pressure range of 5-26 GPa. Experiments in the pressure range of 6-26 GPa and 900-1400°C were performed in a 500- and 1000-tonne multianvil presses using 32 mm Toshiba tungsten carbide cubes, pyrophyllite gaskets and 18/11 (octahedral edge length/truncation edge length), 14/8, 10/5, 10/4 and 8/3 octahedral sample assemblies (Figure 2.6.) made of partially sintered MgO doped with 5% Cr_2O_3 to reduce heat loss by radiation. The $LaCrO_3$ heater (with stepped design in the 18/11 and 14/8 assemblies to reduce temperature gradients (Rubie et al., 1993) was separated from the octahedron by a ZrO_2 sleeve and from the capsule by an MgO sleeve. The capsule was positioned near the middle of the assembly using crushable alumina or MgO spacers. A W3Re97-W25Re75 thermocouple was inserted axially in a four-bore Al_2O_3 ceramic rod with the hot junction next to Re-foil disc, placed between thermocouple and capsule to prevent puncturing of the capsule. No correction for pressure effect on the emf of the

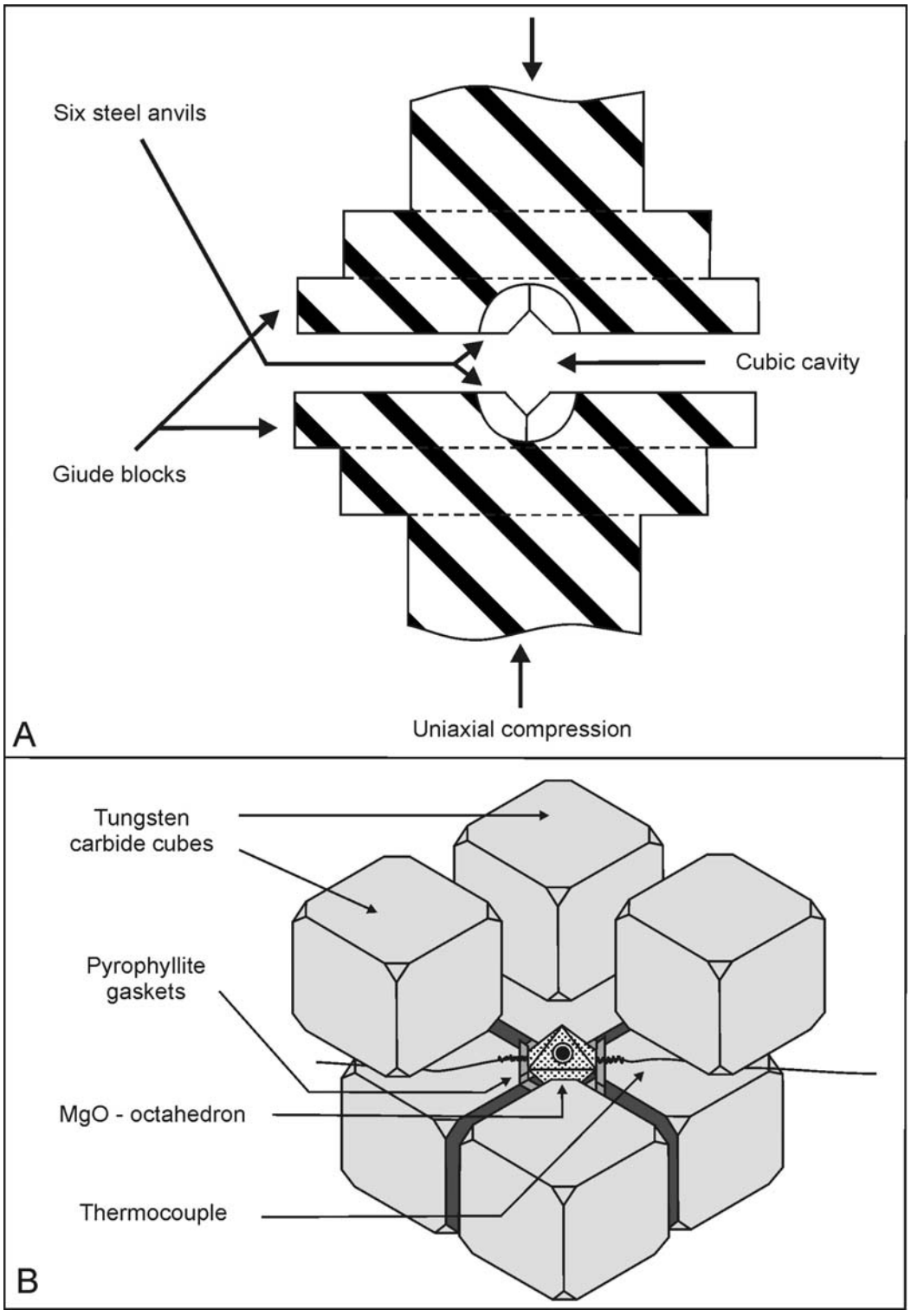

Figure 2.5 Details of multianvil press: A - 6 outer steel anvils embedded in guide blocks form a cubic cavity; B - eight inner cubes with triangular truncation form an octahedron for the sample assembly.

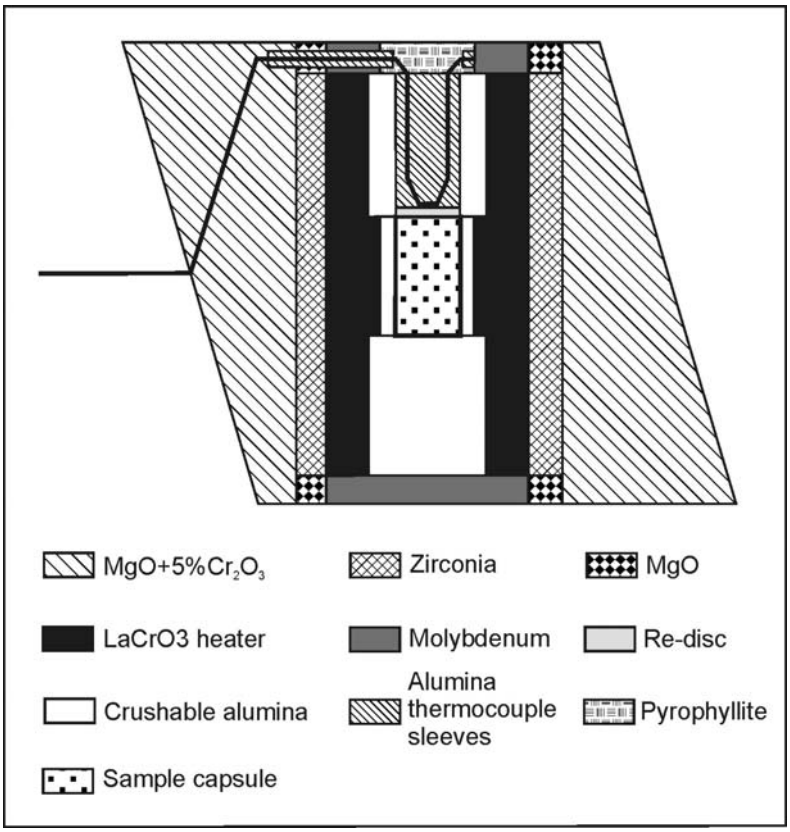

Figure 2.6 Details of 18/11 assembly

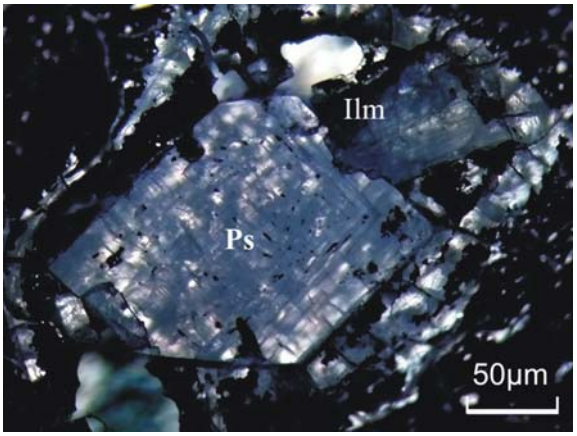

Figure 2.7 Coexisting $MgSiO_3$-perovskite and $MgSiO_3$-ilmenite from multi anvil run MA-Ps-25. Black areas represent remains of gold coating. The coexistence of the two phases implies that at a run temperature of 1400±25 °C, the pressure was ~25±1.25 GPa (Fei and Saxena, 1990).

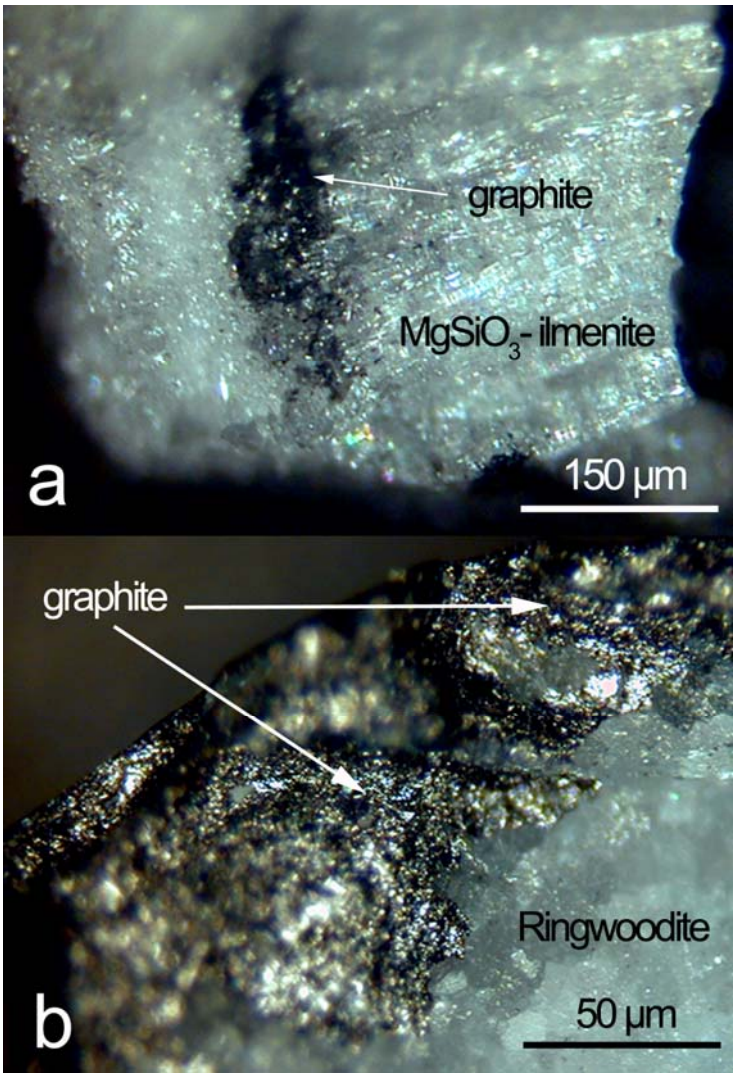

Figure 2.8 Optical photomicrograph of run products in multianvil press after removal of carbonates. A – run MA-R-21; b – run MA-I-25.

thermocouple was applied. Pressure calibrations for various assemblies were carried out using phase transitions in the Mg_2SiO_4, $MgSiO_3$ and SiO_2 systems and were published elsewhere (Bolfan-Casanova, 2000; Canil, 1994; Fei and Saxena, 1990; Frost et al., 2001 and references therein). The accuracy of these calibrations is estimated to be of the order of ±5%. In some cases, the actual pressure was documented by the coexistence of minerals in run products (Figure 2.7). As in most of piston-cylinder experiments, the redox state was not controlled, but the presence of poorly crystallized graphite-like carbonaceous material (Figure 2.8) coexisting with

carbonates in several runs shows that equilibria similar to $MgSiO_3+MgCO_3 = MgSiO_4+C+O_2$ (Eggler and Baker, 1982; Luth, 1999) probably yield an oxygen fugacity between EMOG(D) (enstatite-magnesite-olivine-graphite/diamond) and GCO (graphite/diamond-carbon dioxide) buffer (Frost and Wood, 1997; Frost and Wood, 1998; Luth, 1999).

2.2 Synthesis of reference materials

For secondary ion mass spectrometry (see Section 3), it was necessary to have homogeneous carbon- and inclusion-free crystals of each mineral of interest as reference materials. For this purpose, carbon-free diopside, enstatite, and pyrope were synthesized. Crucial in the selection of the growth technique was the required size of crystals larger than 300-500 μm in diameter.

Large (up to 2 mm length) euhedral crystals of orthoenstatite were synthesized using a method, similar to that developed by Grandin de L'Eprevier (1972) for forsterite and applied to orthoenstatite by Ito (1975). A difficulty in growing orthoenstatite is that at around 1000°C it converts to protoenstatite before melting incongruently at 1557°C (Boyd and England, 1965). By adding a large amount of solvent to an incongruently melting phase it is possible to reduce the melting point and to saturate the phase congruently in the solvent. This is the physical basis of the method used.

Lithiumvanadomolybdate (51.2 mol % Li_2O, 42.8 mol % MoO_3, 6.0 mol % V_2O_5) was used as a flux in this study. About 20g of the homogeneous mixture (see Table 2 for the composition) was loaded in a platinum crucible and heated to 930°C in a muffle furnace. The temperature was kept constant for 10 days in order to completely dissolve solids and then it was decreased at 1.5°C per hour to 650°C. After subsequent rapid cooling to room temperature, the solvent was washed out with warm distilled water. Crystals grown were either euhedral or terminated at one end, and elongated in ***c*** direction, with a length up to 2 mm. Cleavage cracks characteristic for natural enstatite are not present and inclusions of flux are rare (Figure 2.9). The only two differences from the technique of Ito were: (1) using of lithium hydroxide instead of carbonate for growth of carbon-free enstatite; and (2) lower (by factor 3) ratio enstatite/solvent in starting mixture, resulting in the synthesis of of larger crystals.

Table 5 Composition of starting mixture for synthesis of C-free enstatite by the flux growth method

Chemical	Charge composition, wt.%
LiOH	24.56
MoO_3	61.68
V_2O_5	10.97
SiO_2	1.67
MgO	1.12
Enstatite	3.074
Flux	96.926
Mg/Si atomic ratio	1

Attempt to apply this method to diopside failed due to formation of tetragonal-dipyramidal powellite $CaMoO_4$ crystals. Therefore, diopside was grown directly from the melt using a stoichiometric mixture of SiO_2, MgO and $Ca(OH)_2$. A platinum crucible with starting material was heated to a temperature 1500°C which is above melting point of diopside (1392°C), kept at 1500°C for several hours and then slowly cooled at 20°C per hour to 1250°C. This rate of temperature decrease was low enough to grow polycrystalline aggregates with the size of individual grains up to several millimeters, however, cleavage cracks were common and transparent clear fragments acceptable for SIMS did not exceed 1 mm in diameter.

500μm-sized pyrope crystals were synthesized from a stoichiometric mixture of oxides in an end-loaded piston cylinder apparatus (Boyd and England, 1960) at 3.5 GPa and 1100 °C and 1 week run duration.

A single crystal of $MgAl_2O_4$ spinel purchased from "Gram Faceting"(USA) (Figure 2.10) was synthesized by a flame fusion technique (Verneuil process), which involves melting of powdered starting material of spinel composition in the flame. Drops of melt fall onto a growing seed crystal that is lowered as it grows (Figure 2.11). Although this spinel is non-stoichiometric ($Mg_{0.309}Al_2O_{3.309}$), X-ray powder diffraction data (Figure 2.12) show that the non-stoichiometry results in decrease of

the unit-cell parameter ***a*** from 8.080 Å to 7.976 Å only, without change of symmetry or structure.

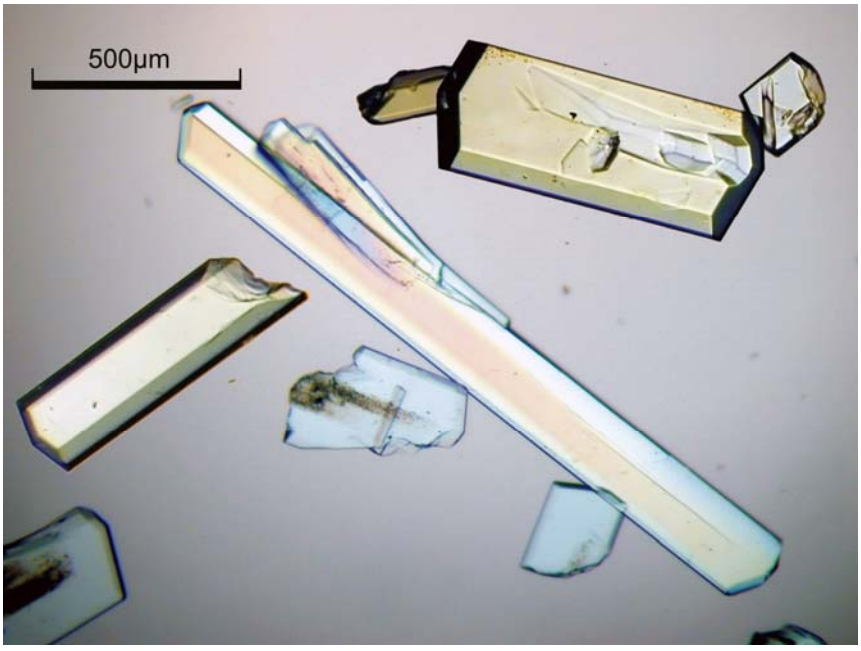

Figure 2.9 Optical micrograph of orthoenstatite crystals, grown using a lithiumvanadomolybdate solvent

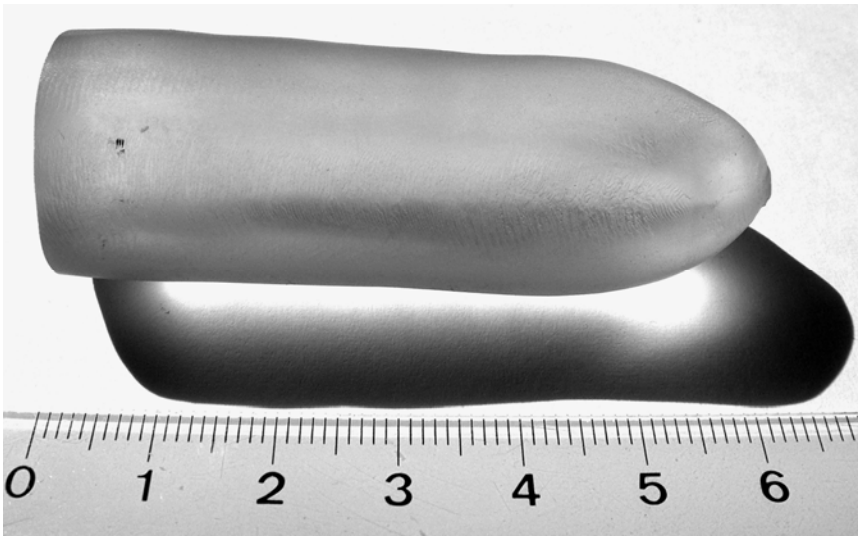

Figure 2.10 Synthetic spinel single crystal grown by Verneuil method

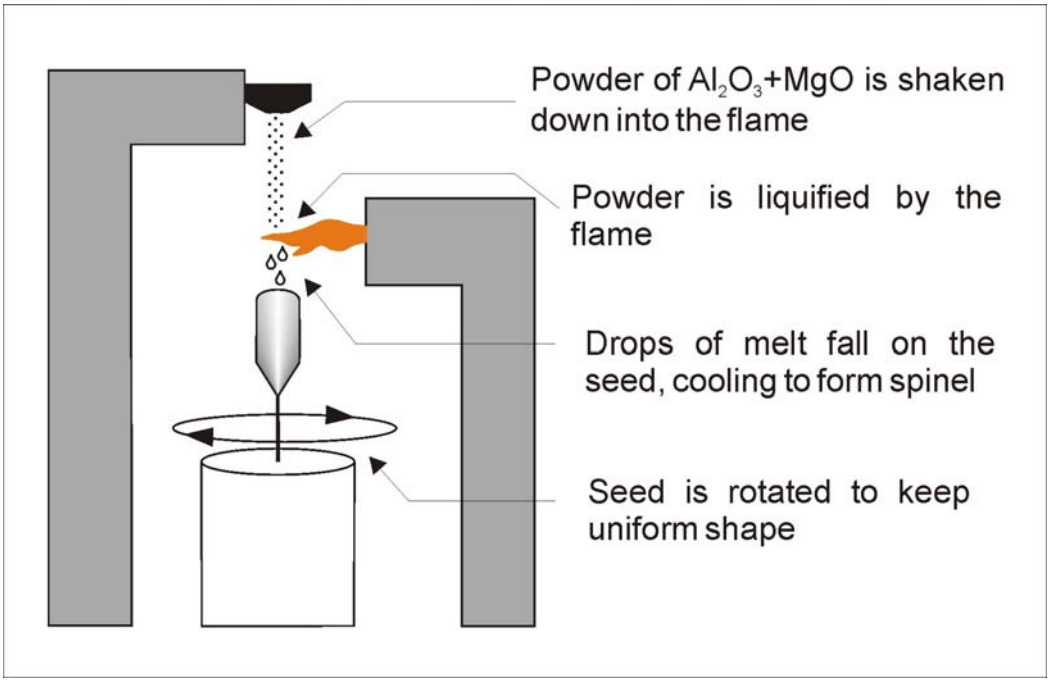

Figure 2.11 Principles of flame-fusion synthesis of spinel (Ueltzen, 1993, Verneuil, 1902)

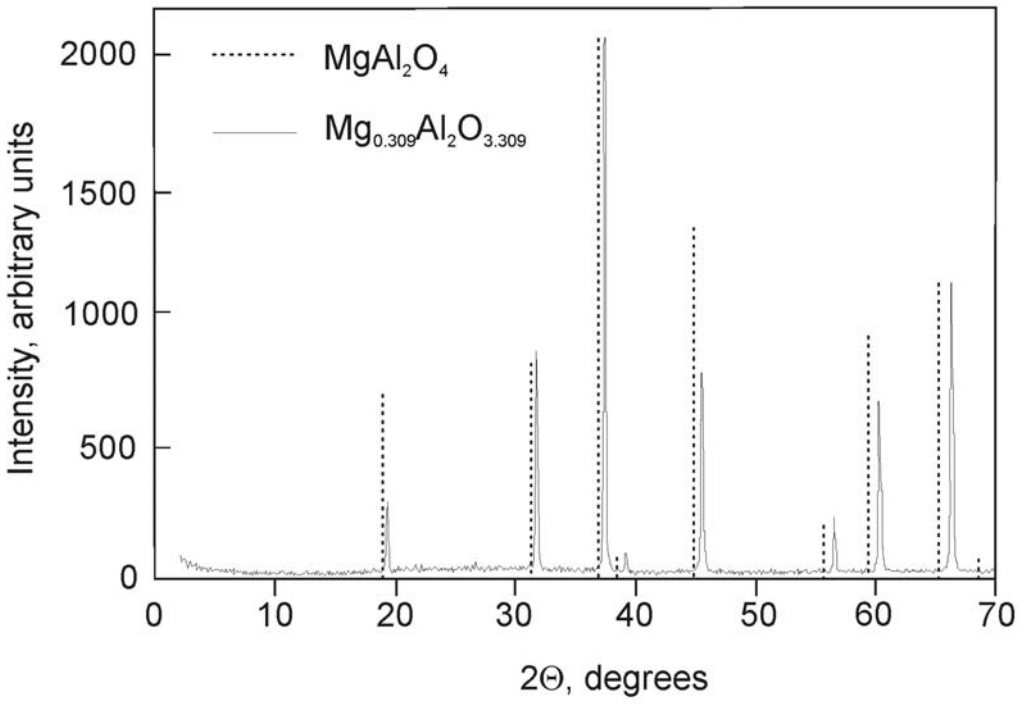

Figure 2.12 X-ray diffraction pattern (Cu Kα-radiation) of synthetic spinel used in this study compared to that of stoichiometric spinel (Tsirelson et al., 1986).

Additionally, three tholeiite glasses (see Table 3 in section 3.5 for the composition) doped with 793, 1484, and 3130 ppm of ^{13}C were produced in piston cylinder experiments at 1.5GPa, 1450°C and 3 hours run duration.

2.3 Sample characterization

Recovered capsules were punctured, dried at 150°C for 1 hour and weighed before and after drying. A loss of weight indicated that the capsule had been closed during the experiment. Another sign of the impermeability of the capsule was the emission of carbon dioxide when nitric acid was added to the run products. Those experiments, which did not show both features, were discarded.

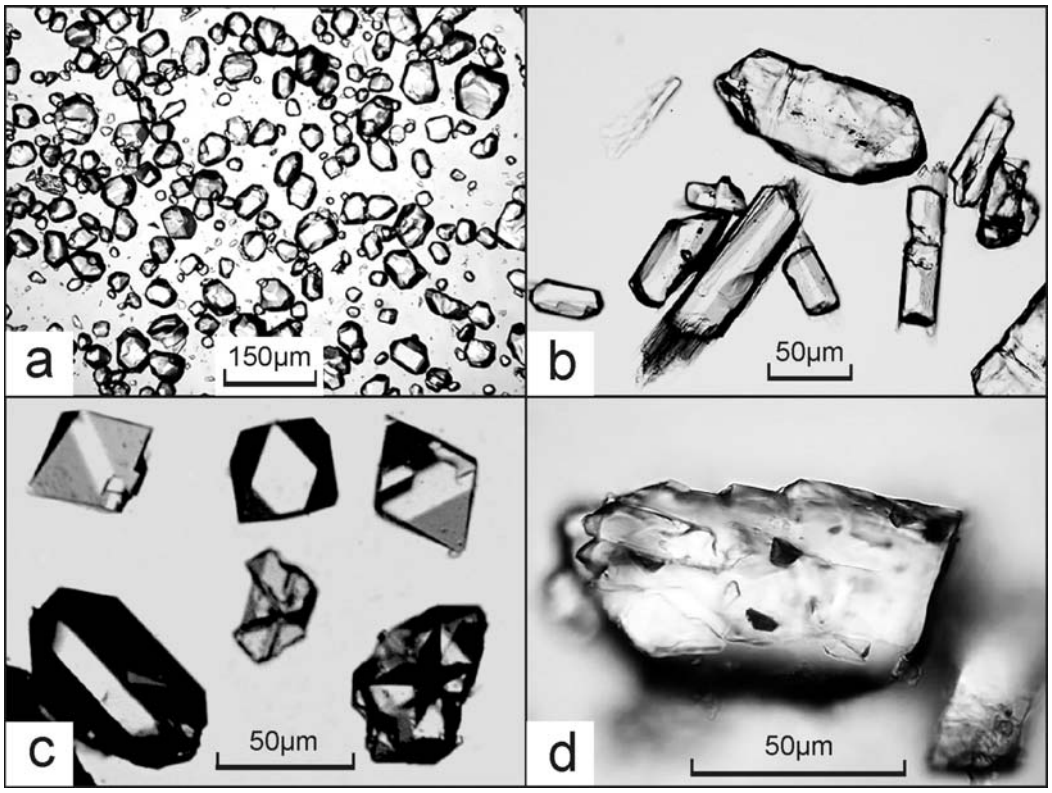

Figure 2.13 Optical micrograph of run products after removal of carbonates; **a**-olivine, **b**- enstatite, **c**- $MgAl_2O_4$-spinel, **d**-$MgSiO_3$-ilmenite.

Run products in most experiments were euhedral or subhedral crystals of silicates (or spinel) free of inclusions (Figure 2.13), embedded in a fine-grained matrix of carbonates, representing quenched carbonatite melt. Grain size varied from 30-40 micrometers to a few hundred micrometers. The growth of large crystal was probably enhanced by the carbonate flux.

Because the aim of the experiments was to produce crystals saturated with the ^{13}C isotope, and because diffusion of carbon from the graphite heater into the Pt capsule in piston cylinder runs might be significant (see Brooker et al., 1998 for review), infrared spectra of carbonates recovered after runs were compared to that of $Na_2{}^{13}CO_3$ used in starting mixtures and to Na_2CO_3 with natural isotopic composition. Figure 2.14 demonstrates that only traces of ^{12}C are present in the capsule, and they can be at least partly attributed to carbon contamination during preparation of the sample for infrared analysis.

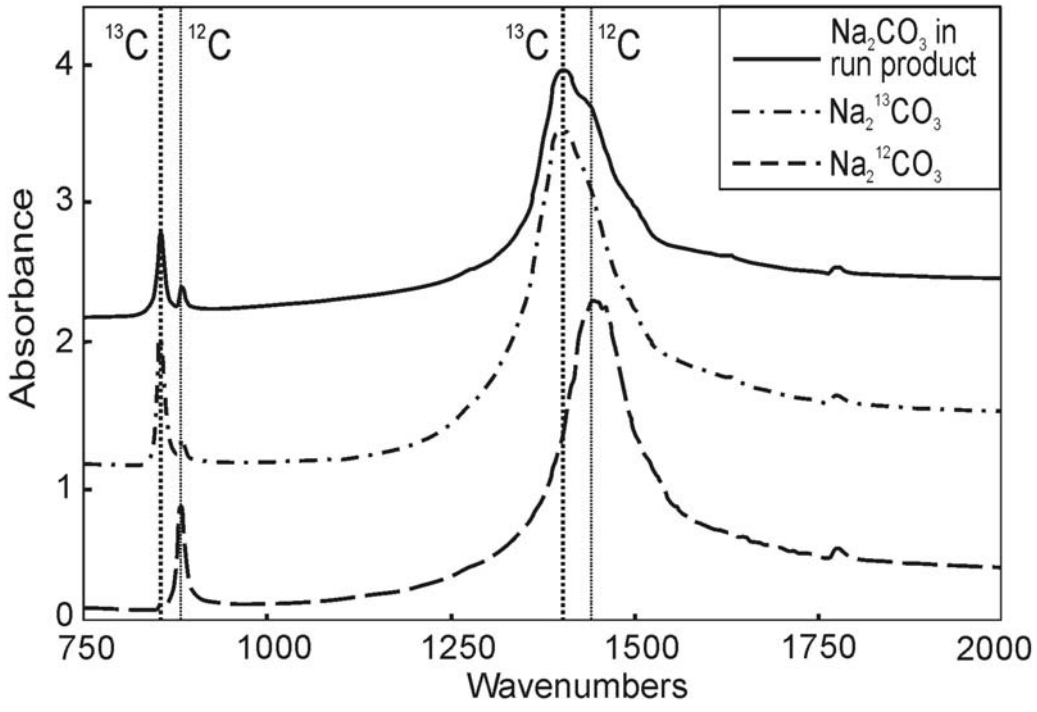

Figure 2.14 Infrared spectra (KBr-pellets) of isotopically "normal" Na_2CO_3 ($^{12}C/^{13}C$ ~ 89.91), of Na_2CO_3 certified to contain 99 % of the isotope ^{13}C and of the carbonate recovered from a piston cylinder experiment. The samples rich in ^{13}C probably exchanged some carbon dioxide with the air during preparation of the KBr-pellet.

Carbonates were removed by etching with nitric or hydrochloric acid. Mineral phases synthesized with piston-cylinder apparatus were identified using X-ray powder diffraction (Bragg Brentano setup, Philips PW 1060, computer controlled, Cu-Kα, secondary graphite monochromator, 40kV/20mA, 2θ-step 0.05°, integration time 5 seconds, (001)-oriented silicon wafer with forbidden reflection at 2θ≈33°). Due to the limited amount of material produced in multi-anvil experiments, higher-pressure silicates were identified with Raman spectroscopy. Raman spectra were recorded using a LabRam II (Dilor, France) Raman microspectrometer equipped with a microscope for focusing the incident laser beam to a 1-μm spot. The 488nm (Ar^+ ion laser) excitation line was used. The acquisition time varied from 10 to 30 s depending on the sample and the intensity of the laser beam. The beam intensity was kept low while measuring $MgSiO_3$-perovskite, because it easily decomposes to amorphous phase at a laser intensity higher than 3 mW .

Carbon contents of synthesized minerals were measured with secondary ion mass spectrometry.

3. Secondary ion mass spectrometry (SIMS)

3.1 Principles of SIMS

The Cameca ims 6f ion microprobe at GeoForschungsZentrum Potsdam was used to measure the carbon content of synthesized minerals. An ion probe employs a focused primary ion beam which bombards the sample surface and sputters material of the domain to be analyzed. Principles of SIMS are schematically shown in Figure 3.1 and Figure 3.2. While many of the matrix atoms are sputtered away as neutral particles, some are released as ions and ionized molecules (Figure 3.1). The secondary ion beam

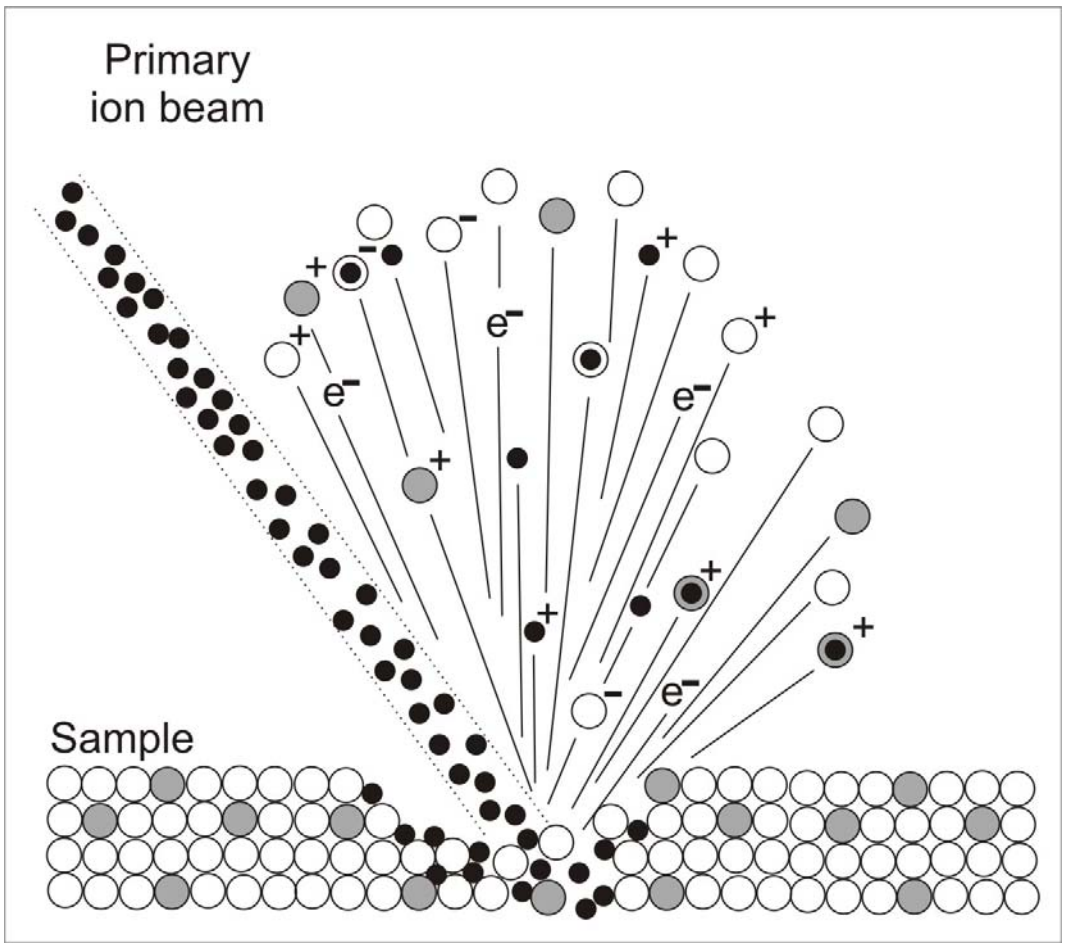

Figure 3.1 "In-situ" ionization of the sample material by primary ions

is extracted by using an accelerating voltage and an ion optical system followed by energy filtering which leads to a mass spectrometer for nominal mass (mass-to-charge ratio) separation and finally to an ion counting unit (Figure 3.2). Unlike conventional mass spectrometry, the SIMS primary beam produces ions from solid samples without prior vaporization. In light of the high sensitivity of carbon analyse to external contamination (see section 1.3) numerous precautions (see sections 3.2; 3.4) and specific analytical procedures were necessary to resolve most of problems of previous studies.

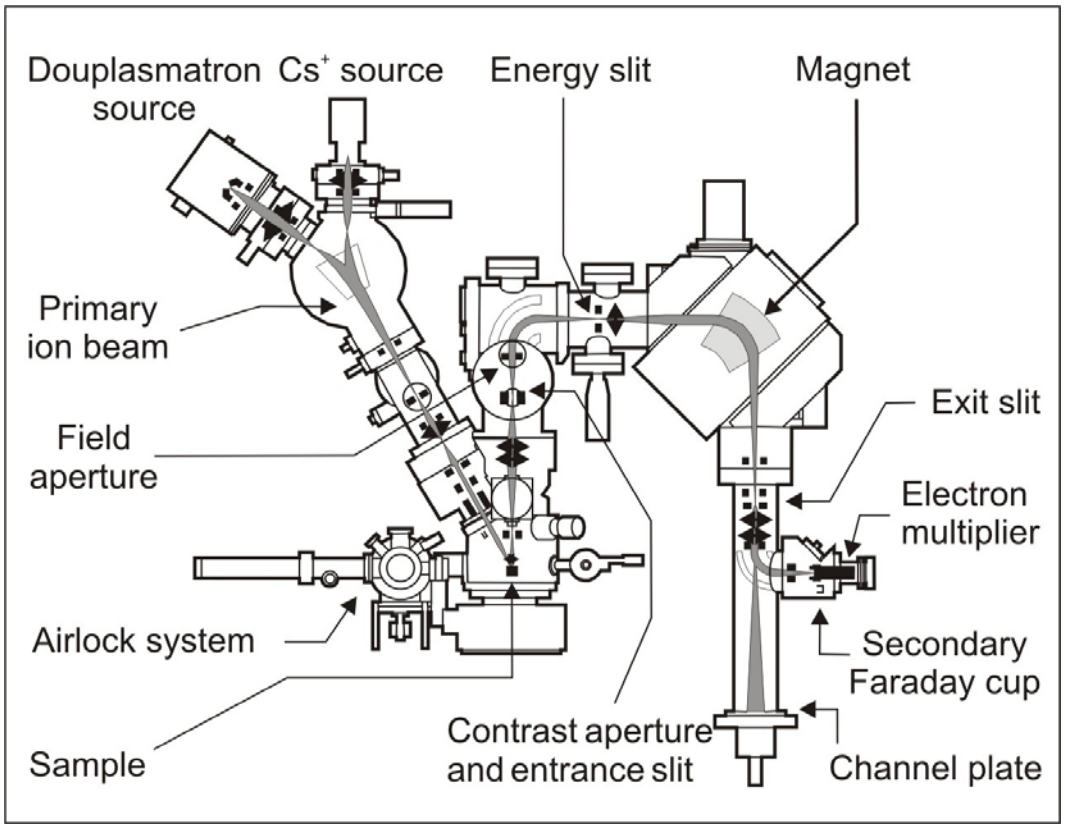

Figure 3.2 Main elements of Cameca ims 6f magnetic sector SIMS microprobe (modified from a Cameca document, courtesy of GFZ Potsdam - Dr. M. Wiedenbeck).

3.2 Sample preparation

The synthesized ^{13}C-saturated individual crystals were mounted on 2.5 cm-diameter round glass slides using a small amount of carbon-free ceramic glue (aqueous solution of Na_2SiO_3). The samples were subsequently dried one day in air at 70°C to remove absorbed water. Independently on drying rate and mode, the glue was subjected to intense cracking due to water evaporation, which caused conductivity problems during SIMS. To overcome this effect, a small amount (5-10% by weight) of powdered silicate glass was added to the glue as a binder. Crystals were polished with 0.25μm polycrystalline diamond powder to produce a flat surface, at most a few tens of microns above the surface of the glass slide. Glass slides were cleaned in an ultrasonic bath with high-purity ethanol which evaporated completely during drying in air. Care was taken to make sure that good contact was established between the crystal edges and the glue, to assure electrical conduction during SIMS analysis. Moreover, the flat polished area of crystals surrounded by glue was at least 200μm in diameter in order to have a uniformly distributed charge compensating electron cloud during ion sputtering. This method of preparing the samples was found to give the best results, however it also had the drawback that the glue disintegrated on some samples after they had been exposed to air for several weeks.

3.3 Calibration

SIMS is a comparative technique, and for a quantification standards are necessary. The main limitation of SIMS is that secondary ion yields are extremely matrix-dependent. In order to have matrix-matched reference materials, synthetic nominally carbon-free crystals of each of the upper mantle minerals olivine, enstatite, diopside, and pyrope were prepared on mounts as described above. The commercially purchased large spinel single crystal was cut into three 7.5 x 7.5 mm plates. All of these crystals were polished to a sample surface roughness of <10nm using 0.25μm polycrystalline diamond powder and 30nm neutral alumina suspension on aluminum foil. These samples were cleaned in high-purity ethanol, were dried in air at ~70˚C and were then sent for commercial ion implantation (Panalytic GmbH, Dresden). A schematic diagram of an ion implanter is shown on Figure 3.3. Thermally

decomposed $Na_2{}^{13}CO_3$ was used as a source material for the 60 kV implantation of a known dose ($3x10^{14}$ ± 3% At/cm^2) of ^{13}C. The extraction and suppression electrodes were used for extracting ions from the source to form an ion beam. A mass analyzing magnet positioned along the beam path between the source and the acceleration tube filtered ions from the beam by mass to charge ratio while allowing ^{13}C ions to enter the acceleration tube. The acceleration system was used for post filtering acceleration of the ion beam to a selected final energy. The ion optical system generated a focused beam with a uniform intensity over the target area. The dose control system is based on measuring and integrating the current passing through a Faraday cup, placed on the sample wafer.

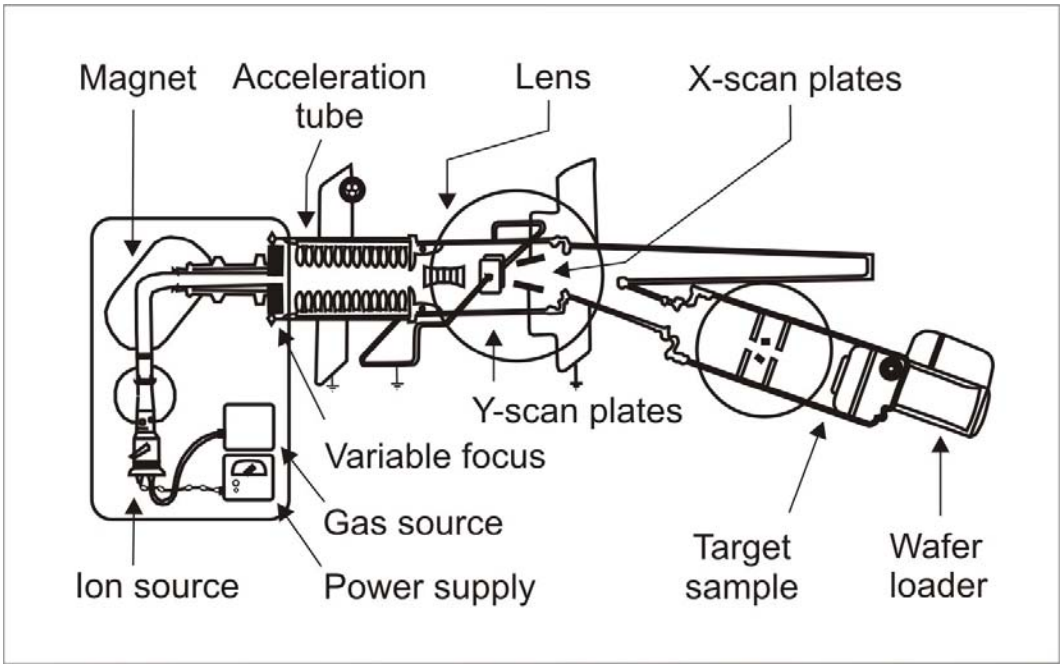

Figure 3.3 Schematic diagram of the ion accelerator used for implanting of ^{13}C-ions in reference carbon-free samples (Rimini, 1995).

The ion implanting procedure could not be used for minerals of the transition zone and lower mantle, because it would most probably convert these metastable phases to amorphous aggregates. Synthetic tholeiite glasses doped with a known amount of ^{13}C were employed instead. The concentration of carbon in these samples has been determined gravimetrically based on the material used to synthesize the glasses.

The natural ratio of carbon isotopes used to estimate isotope fractionation during analysis was calibrated against two natural spurrite ($Ca_5CO_3(SiO_4)_2$) specimens from Durango, Mexico, and New Mexico, USA.

3.4 Analytical conditions

SIMS analyses were conducted on the Cameca ims 6f at the GeoForschungsZentrum Potsdam. This instrument had been modified from its original design by replacing all pumps by oil-free pumps, including a scroll pump for achieving roughing pressures. In order to suppress outgassing of the samples, the mounts were stored for at least 24 hours in an in-house designed UHV sample storage chamber (Wiedenbeck et al., 2004). Further vacuum improvements (by a factor of about 3) were achieved by using a liquid nitrogen cold trap, such that the source operating pressure of the instrument was on the order of $1x10^{-9}$ Torr when samples were present. Prior a measurement session the multiple immersion lens of the SIMS was shifted to a new position.

Each of the ^{13}C-saturated samples was cleaned in an ultrasonic bath in high-purity ethanol, dried and coated with between 50 and 80 nm of high-purity gold. The actual SIMS analyses employed a nominally 12.5kV, 1 to 2 nA $^{133}Cs^+$ beam, which was focused to a ~5x8 μm spot on the sample surface. In order to reduce the impact of surface carbon contamination, each domain which was to be analyzed was pre-sputtered with a 25x25 μm rastered beam for 3 minutes before the actual analysis. Furthermore, as a part of the analysis a 3-minute spot preburn was conducted in order to establish equilibrium sputtering conditions. Charge compensation used a normal incidence electron flood gun operated at the same voltage as the sample stage.

The secondary side of the SIMS was operated at high mass resolving power of $M/\Delta M \approx 4300$ which over-resolved the $^{12}CH^-$ interference from the lighter $^{13}C^-$ mass position (Figure 3.4). Mass resolving power was measured at the beginning of every analytical session by scanning the magnet over a selected mass. The carbon signal derived from any surface contamination sputtered by stray neutral primary atoms was suppressed from the mass spectrum by employing a 400 μm field aperture which was equivalent to a 30 μm field-of-view at the sample surface. The energy window of the instrument was centered using the $^{28}Si^-$ signal obtained from a piece of Si metal.

Subsequent to centering, the window was opened to a width of 25V; no energy offset was applied. The actual analyses employed the peak stepping sequence 11.5 background (0.1 seconds per cycle), ^{12}C (4 s), ^{13}C (15 s) and ^{28}Si (4 s) (or alternatively ^{27}Al in the case of spinel). Twenty cycles of this peak stepping sequence, in conjunction with the 3 minute spot preburn, gave a total analysis time of 11.7 minutes. Count rates on the reference isotopes (i.e., $^{28}Si^-$ or $^{27}Al^-$) were typically 500 to 900 kHz and were limited by counting capability of the electron multiplier ion detector.

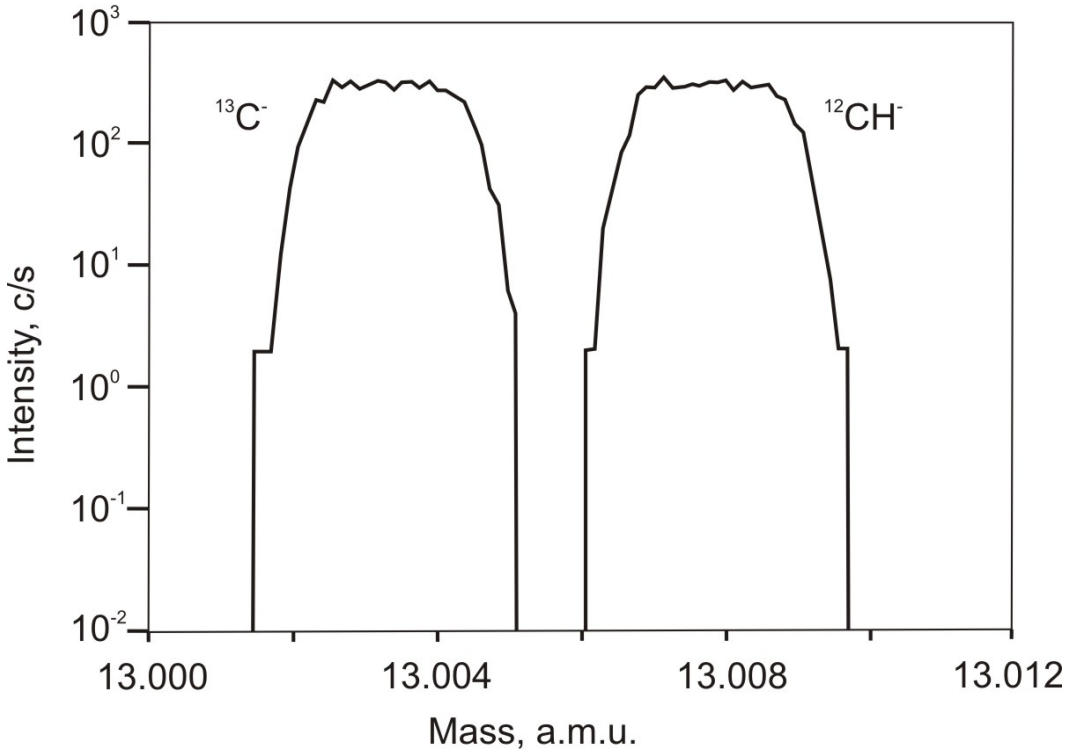

Figure 3.4 Filtering of $^{12}CH^-$ from the lighter $^{13}C^-$ using high mass resolution capability of Cameca ims 6f

3.5 Calculations

Despite all the efforts described above, laboratory contamination was a major contributor of carbon to our analyses. It was therefore essential to employ the rare isotope ^{13}C (with natural abundance 1.1%) for all the work reported. Unlike samples with natural isotopic composition (spurrite; $^{13}C^-/^{12}C^-=0.011\pm1.38\%$, n=25) synthesized crystals demonstrated elevated $^{13}C^-/^{12}C^-$ ratios up to 0.3. Saturating of crystals with the rare isotope ^{13}C allowed us to subtract contribution of contaminated carbon, which were assumed to have natural $^{13}C/^{12}C$ ratio. Therefore, the "true" absolute concentration of the ^{13}C dissolved in carbon-saturated silicates could be determined by measuring $^{13}C^-/^{28}Si^-$ and $^{12}C^-/^{13}C^-$ratios in conjunction with the known isotopic composition of the extraneous carbon, and by knowing the relative sensitivity factor (RSF) for C/Si, using the "fundamental SIMS equation":

$$RSF=\left[\frac{\left(^{13}C^-/^{28}Si^-\right)_{measured}}{\left(^{13}C_{ppm}/^{28}Si_{wt.\%}\right)}\right]_{standard} = \left[\frac{\left(^{13}C^-/^{28}Si^-\right)_{measured}}{\left(^{13}C_{ppm}/^{28}Si_{wt.\%}\right)}\right]_{unknown}$$

An identical approach, based on ^{27}Al, was used for calculating the carbon content in spinel.

To determine RSF for each upper mantle mineral we conducted multiple depth profiles on the implanted reference samples. SIMS depth profiles used parameters similar to those employed during the analysis of the samples, the main difference being that data were collected with an 80x80 μm raster. In order to eliminate contamination from the crater walls, the beam was centered under the field aperture using the scanning ion image capability of the Cameca ims 6f. After an initial pulse of carbon derived from surface contamination, an excess in ^{13}C well above the natural isotopic composition was clearly detected (Figure 3.5). To eliminate the impact of the extraneous surface carbon, we only used those data collected after two cycles subsequent to the penetration of the gold coat, when a precipitous drop in the reference isotope (^{28}Si or ^{27}Al) was observed. The data from the depth profile,

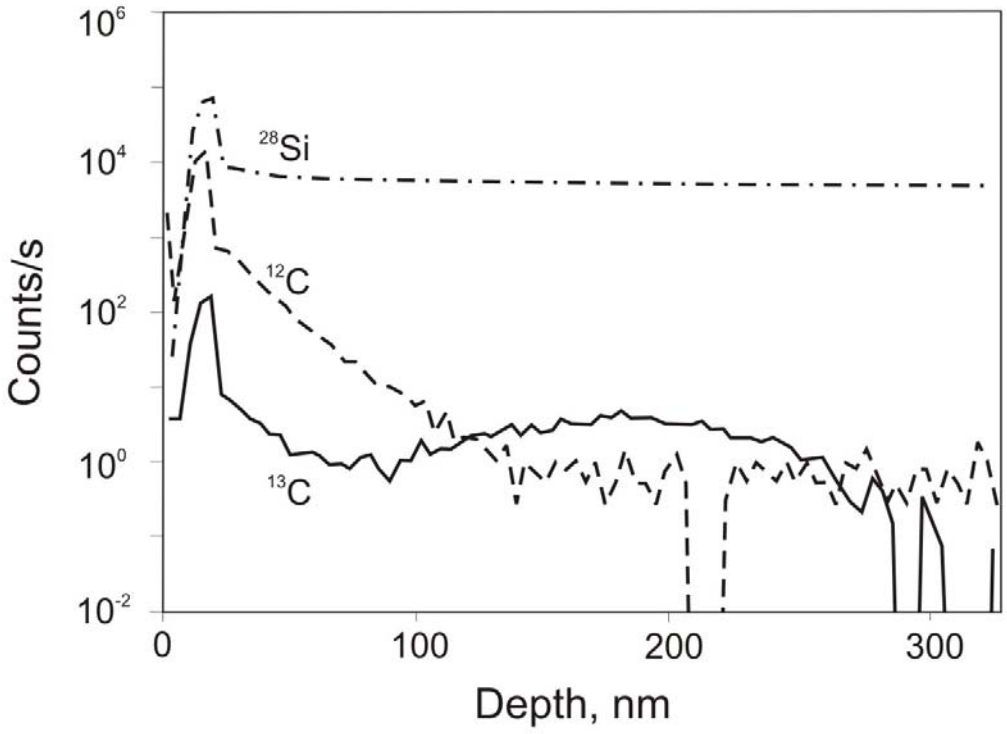

Figure 3.5 Depth profile of synthetic enstatite, imlanted with known dose of the ^{13}C isotope. Note a "spike" of carbon with natural isotopic composition due to contamination of the surface of crystal before gold coating.

including a correction for the extraneous ^{12}C-rich carbon, were converted into the required RSF (Table 3) using the formula:

$$RSF = \frac{\left(mean^{13}C^{-}_{cps} \Big/ mean^{28}Si^{-}_{cps} \right)_{measured}}{\left(flux^{13}C \Big/ (depth \cdot \rho \cdot Si_{wt\%} \cdot (N_A / At_{wt}Si) \cdot (at^{28}Si / Si_{total})) \right)},$$

where $flux^{13}C$ is implanted dose of ^{13}C, *depth* – crater depth, ρ and $Si_{wt\%}$– density and weight per cent of Si (Al for spinel) of analyzed mineral respectively, N_A – Avogadro's number, $At_{wt}Si$ – atomic weight of silicon; $at^{28}Si/Si_{total}$ – mole fraction of ^{28}Si. Crater depths, typically on the order of 300 nm deep, were determined with a

Dektak3 stylus profilometer which has an accuracy of better than ±2 %. The external reproducibility of this method was estimated to be of the order of 2.4-4.8%.

For the wadsleyite, ringwoodite, $MgSiO_3$-ilmenite and $MgSiO_3$-perovskite we were compelled to use a different approach for defining the RSF. Three synthesized tholeitic glasses were used to determine a calibration curve (Figure 3.6.) for which the best-fit line of the 18 analyses was forced through the origin and the slope of this line was used to determine the RSF for these minerals. The external precision of this method was ±13.9% (1σ). In view of the potential impact of using non-matrix matched reference samples and the uncertain compositions of the concentration values for the reference basaltic glasses, the accuracy of the quantitative results for the minerals of transition zone and lower mantle is likely to be not as good as those obtained for the upper mantle mineral phases.

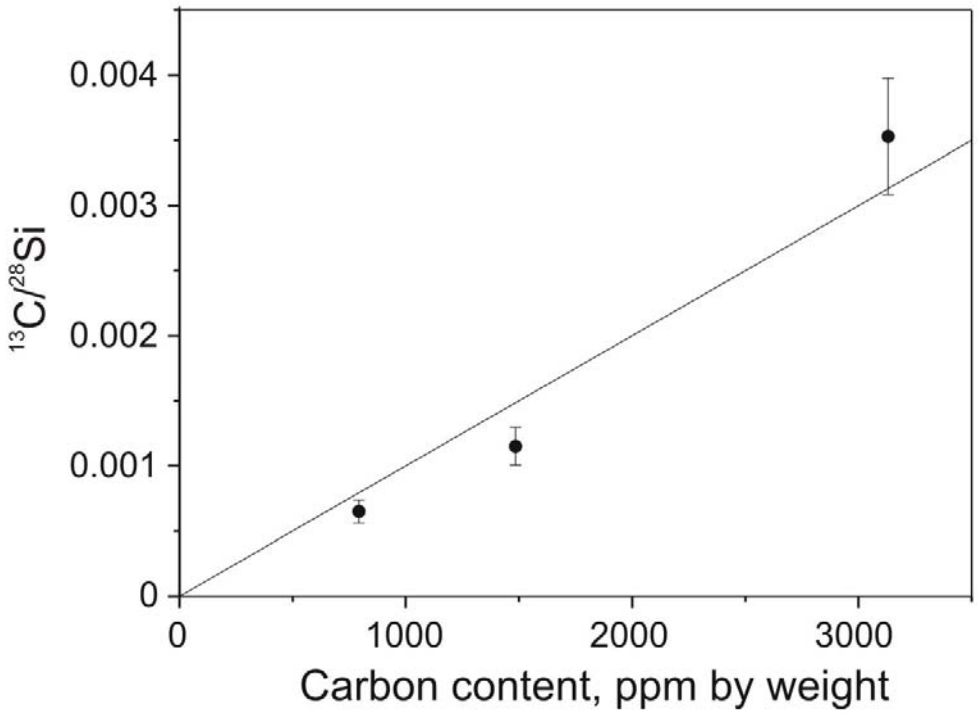

Figure 3.6 Calibration curve to calculate the relative sensitivity factor of C and Si for wadsleyite, ringwoodite, $MgSiO_3$-ilmenite and $MgSiO_3$-perovskite, based on three ^{13}C-doped tholeiite glass standards.

Relative sensitivity factors derived from the C-implanted crystals, tholeiite glasses and natural spurrite are compared in Table 6. The cause for variability of RSF for Si and C among silicates could not be established unambiguously.

Table 6 Relative sensitivity factors (RSF) of various reference materials

Mineral	Measured ratio	RSF	Number of measurements
Tholeiite glasses[a] (^{13}C-doped, synthetic)	$^{13}C/^{28}Si$	0.297±0.055	6
Spurrite[b] (natural)	$^{13}C/^{28}Si$	0.421±0.062	25
Forsterite (^{13}C-implanted, synthetic)	$^{13}C/^{28}Si$	0.411±0.025	6
Enstatite (^{13}C-implanted, synthetic)	$^{13}C/^{28}Si$	0.753±0.031	3
Diopside (^{13}C-implanted, synthetic)	$^{13}C/^{28}Si$	0.707±0.023	3
Pyrope (^{13}C-implanted, synthetic)	$^{13}C/^{28}Si$	0.810±0.039	3
Spinel (^{13}C-implanted, synthetic)	$^{13}C/^{27}Al$	3.498±0.161	3

[a] Composition: 60.5 wt.% SiO_2, 2 wt.%TiO_2, 14.5 wt.% Al_2O_3, 9.9 wt.% MgO, 8.8 wt.% CaO, 3.3 wt.% Na_2O, 1.6 wt.% K_2O, doped with 793, 1484, and 3130 ppm of ^{13}C

[b] Natural samples from New Mexico (USA) and Durango (Mexico)

For many of our analyses the observed excess ^{13}C was too low to detect, implying extremely low carbon solubility. The limit of detection for carbon for individual analysis was calculated from the 3σ uncertainty in the measured isotopic ratios:

$$LOD = 3 \cdot \sqrt{\left(\left(\sigma_{\left(\frac{^{12}C^-}{^{28}Si^-}\right)_{unknown}} \right)^2 + \left(\sigma_{\left(\frac{^{12}C^-}{^{13}C^-}\right)_{spurrite}} \right)^2 \right)} \cdot \frac{\left(\frac{^{12}C^-}{^{28}Si^-}\right)_{unknown}}{\left(\frac{^{12}C^-}{^{13}C^-}\right)_{spurrite}} \cdot \frac{Si_{wt.\%}}{RSF} \cdot 10^6$$

Obviously the limit of detection depends essentially on the carbon background due to contamination. Usually it is in the rang of 30-200 ppbw.

4. Results

4.1 Run products

All major mantle minerals were synthesized in the iron-free system MgO-SiO_2 or MgO-Al_2O_3. This includes forsterite, enstatite and their high-pressure equivalents (Figure 4.1), as well as diopside, pyrope and $MgAl_2O_4$-spinel. A few experiments (open circles on Figure 4.1) produced not only the mineral of interest in carbonate matrix, but also coexisting phases from adjacent P-T regions (Figure 4.2). The observed differences between expected and obtained run products are probably due to temperature gradients in the capsule or errors in pressure calibration.

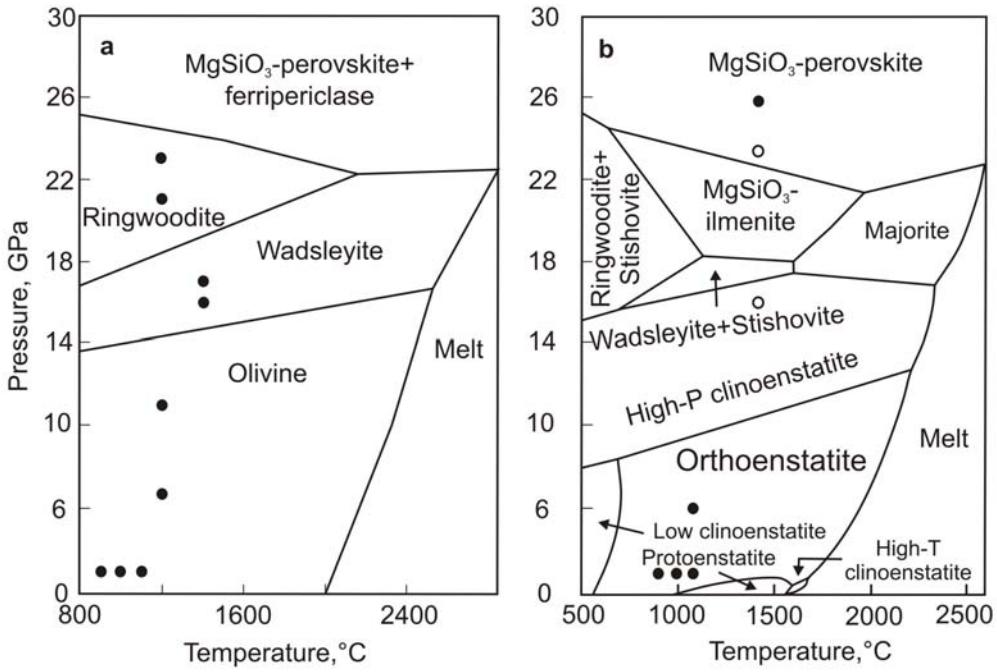

Figure 4.1 Phase diagrams of Mg_2SiO_4 (a) and $MgSiO_3$ (b) systems (simplified after Fei and Saxena, 1990 and Gasparik, 2003). Circles represent experimental points in this study. Runs shown as open circles contain more than one silicate mineral.

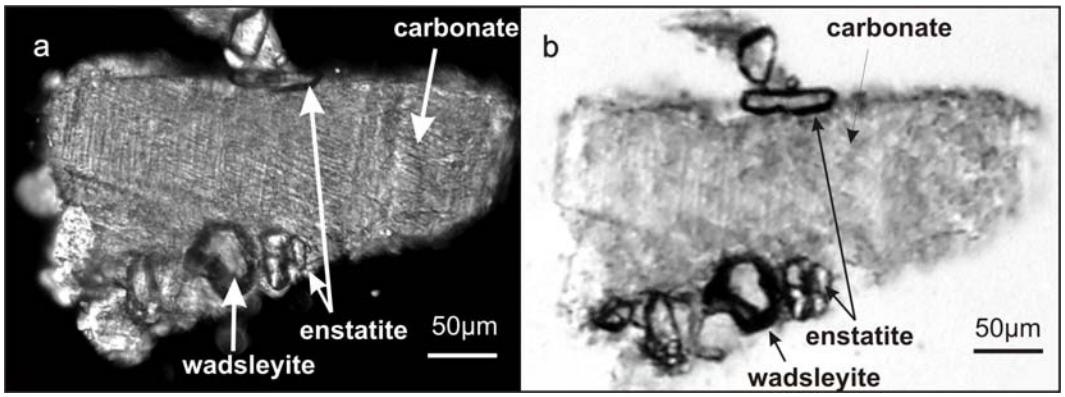

Figure 4.2 Optical photomicrograph of coexisting wadsleyite and enstatite (former high-clinoenstatite, see section 4.2.2) embedded in carbonate recovered from run MA-W-6. A - crossed nicols; b - parallel nicols.

Electron microprobe analyses of synthetic crystals show that they have nearly ideal stoichiometry. For instance, the concentration of Na_2O, the major impurity in the upper mantle minerals grown, does not exceed 0.03 wt.% in forsterite, 0.12 wt.% in diopside and 0.09 wt.% in enstatite (Table 7).

Table 7 Electron microprobe analyses of selected run products

Wt.% oxide	**Forsterite Ol11 (n=14)**	**Enstatite E9 (n=9)**	**Enstatite E11 (n=4)**	**Diopside D9 (n=18)**
SiO_2	42.12 (0.276)	60.35 (0.340)	58.99 (0.548)	55.18 (0.248)
Al_2O_3	0.01 (0.008)	0.04 (0.032)	0.09 (0.068)	0.03 (0.014)
MgO	57.82 (0.256)	40.16 (0.246)	40.22 (0.616)	18.56 (0.165)
CaO	0.003 (0.004)	0.00 (0.01)	0.02 (0.033)	25.43 (0.081)
Na_2O	0.01 (0.01)	0.10 (0.044)	0.09 (0.021)	0.06 (0.037)
Total	99.97 (0.235)	100.65 (0.417)	99.40 (0.107)	99.26 (0.309)

Numbers in brackets are one standard deviation of n analyses

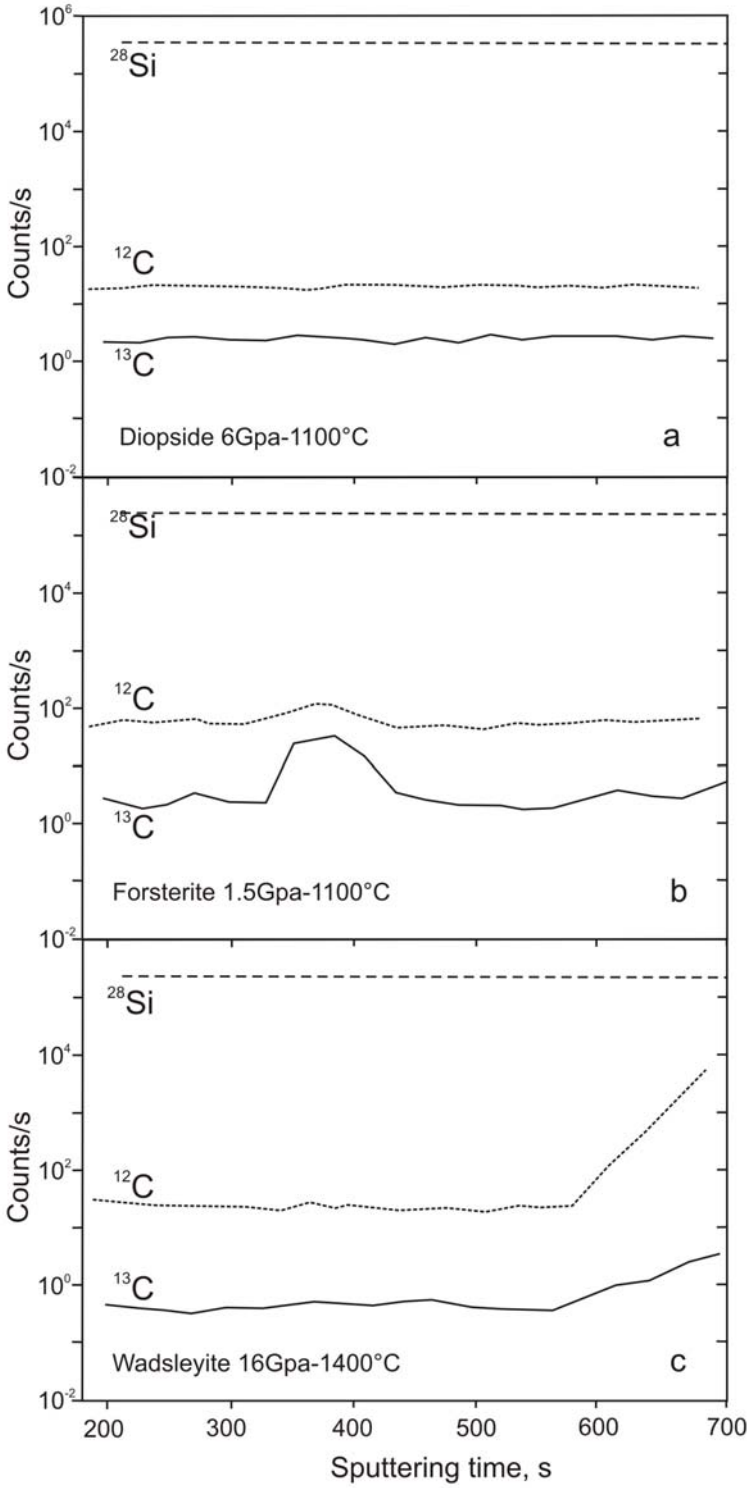

Figure 4.3 Data accumulation during an individual measurement. **A** - usable analysis; **b** - sputtering of ^{13}C-rich inclusion; **c** - measurement affected by external contamination

Only the measurements with steady count rates of sputtered carbon ions within the whole accumulation time were taken into account (Figure 4.3a). Although crystals were inspected with an optical microscope to assure the absence of inclusions prior to SIMS, several analyses yielded local carbon contents in the order of tens or hundreds ppm of ^{13}C by weight (ppmw). These high concentrations, which were observed only on certain spots of the respective sample, are attributed to the sputtering of carbon-rich inclusions or fractures in a host grain. Generally, a single carbonaceous impurity smaller than 1 micrometer increases the count rate of ^{13}C at least by a factor of 8-10 while the influence on the ^{12}C intensity is only small (Figure 4.3b). Larger cracks in measured areas were observed by optical microscopy after SIMS analysis (Figure 4.4). On the contrary, sputtering of carbon with natural isotopic composition due to contamination resulted in a more intense increase of the ^{12}C count rate relatively to ^{13}C (Figure 4.3c). Thus, any extraneous carbon species were confidently distinguished from structurally dissolved carbon intrinsic to the host.

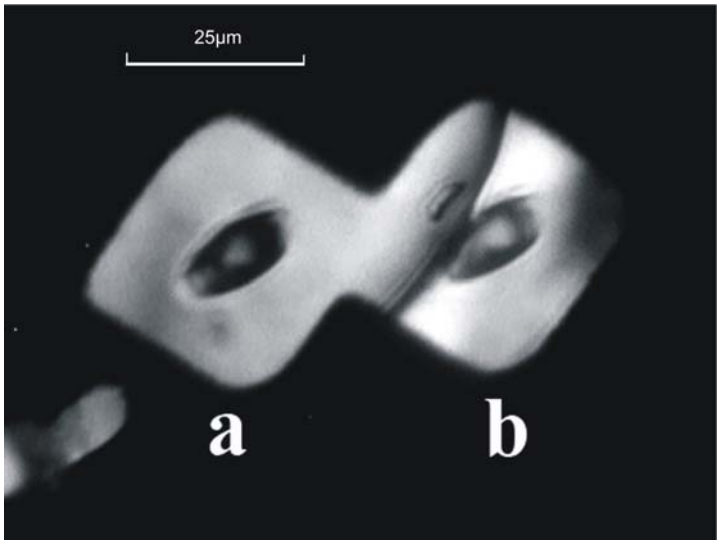

Figure 4.4 Optical photomicrograph of analyzed points in transmitted light. The black area is a polished crystal surface coated with gold. Rectangular regions are pre-burned with a rastered ion beam. Only ions, sputtered from the centers, were used for data accumulation. A - usable analysis, b – discarded analysis (fracture close to measured spot).

4.2 Carbon solubility in minerals of the upper mantle

4.2.1. Olivine

In a pyrolite model, olivine is estimated to constitute ~60% by volume of the upper mantle by volume and potentially, it could be as a major carbon reservoir. Although an exceedingly low carbon solubility in olivine was recently reported (Keppler et al., 2003), it is not clear whether these results are applicable to the entire pressure range of the upper mantle.

Four series of experiments were conducted to determine the influence of pressure, temperature, redox conditions and composition on carbon solubility in olivine. A summary of the experimental results is shown in Table 8.

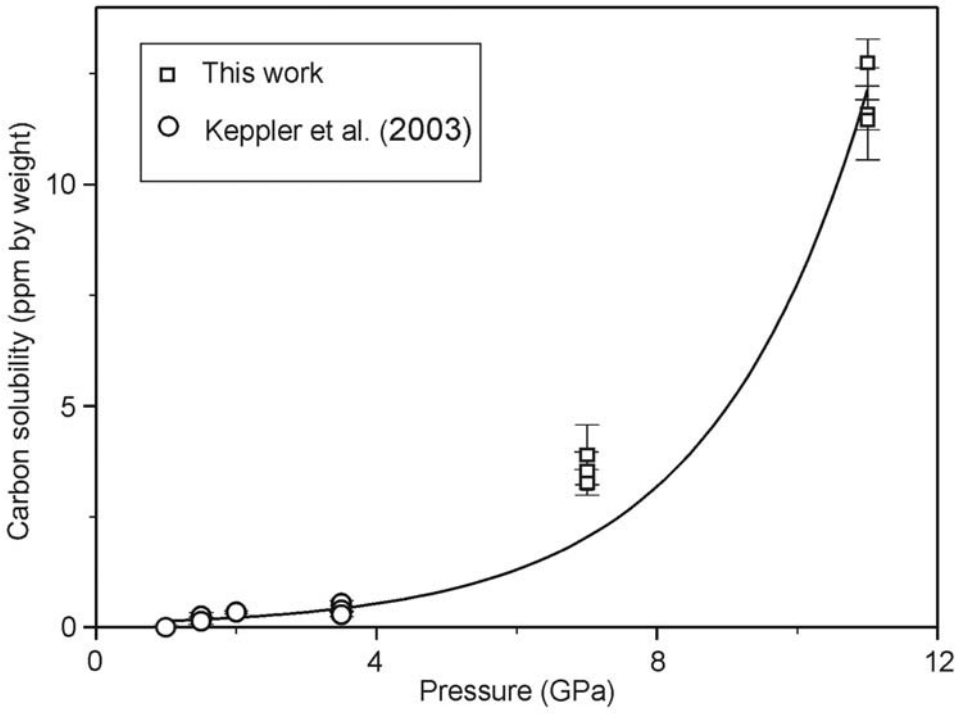

Figure 4.5 Carbon solubility in forsterite as a function of pressure for T=1200 °C. Error bars are one standard deviation. The curve shown is a best fit of the experimental data to an equation $C=A \exp(-P\Delta V/RT)$ with A = 0.089 ppmw and ΔV = -5.47 cm^3/mol.

Table 8 Experimental data on carbon solubility in olivine

Run	Mineral	*T* (°C)	*P* (GPa)	$log(f_{O_2})$	*t* (h)	C content[a] (wt. p.p.m.)
Ol9	Forsterite	900	1.5	not buffered	144	0.38±0.09
						0.29±0.07
Ol10	Forsterite	1000	1.5	not buffered	168	0.12±0.03
						0.10±0.03
Ol11	Forsterite	1100	1.5	not buffered	144	<0.09[b]
						0.10±0.03
Ol11F2	Olivine[c]	1100	1.5	not buffered	144	0.21±0.06
						0.20±0.03
Ol11F3	Olivine[c]	1100	1.5	not buffered	144	0.34±0.02
						0.30±0.03
MA-Ol-7	Forsterite	1200	7	not buffered	10	3.90±0.68
						3.27±0.29
						3.53±0.43
MA-Ol-11	Forsterite	1200	11	not buffered	10	12.75±0.53
						11.57±0.34
						11.59±1.04
Ol11F1	Olivine[c]	1100	1.5	-12.7	96	0.52±0.06
						<0.04 [b]
						<0.07 [b]
Ol11C	Olivine[c]	1100	1.5	-10	96	0.29±0.08
						0.22±0.06
Ol11N	Olivine[c]	1100	1.5	-8.2	96	0.34±0.12

Runs with prefix "MA" were carried out in the multi-anvil press, all other experiments were performed in a piston cylinder apparatus. Errors are one standard deviation.

[a] If several numbers are given , they represent analyses of different crystals in the charge.

[b] Values are below detection limit.

[c] For composition see Table 9 .

While in the all lower pressure experiments, olivine dissolved below 1 ppmw of carbon, the solubility in pure forsterite increases exponentially by two orders of magnitude when pressure rises from 1 to 11 GPa at constant temperature (Figure 4.5).

Because at constant temperature

$$\frac{d\Delta G}{dP} = \Delta V \text{ and } \Delta G = -RT \ln K ,$$

the pressure dependence of the equilibrium constant is given by

$$\frac{d \ln K}{dP} = -\frac{\Delta V}{RT},$$

where ΔG is free Gibbs energy, R = gas constant, K = equilibrium constant of reaction of carbon incorporation in forsterite, P = pressure and T = temperature. Since the carbon concentration in forsterite is proportional to the equilibrium constant, the volume change during the carbon dissolution was calculated to be $\Delta V = -5.47 cm^3/mol$ by fitting the data plotted on Figure 4.5 to the equation:

$$C_{C(ppmw)} = A \exp\left(\frac{-P\Delta V}{RT}\right), \quad (4.1)$$

where A = 0.089 ppmw and gives the carbon solubility at zero pressure.

Experiments performed at constant pressure and different temperatures (900-1100 °C) showed no systematic effect. Although a decrease in carbon solubility could be inferred from the data in Table 4 (runs OL9-OL11), the results from Keppler et al. (2003) together with the size of the error bars make this trend uncertain (Figure 4.6).

Experiments Ol11F1, Ol11C and Ol11N were carried out using Fe, Co and Ni as a capsule material, respectively, to produce various oxygen fugacities corresponding to the Fe-FeO, Co-CoO, and Ni-NiO buffers. These data show that a 4.5 log unit difference in oxidation state resulted in no noticeable changes in carbon solubility. However, it should be noted, that using Fe, Co and Ni as capsule material resulted in the incorporation of these elements in olivine (Table 9). While the effect of Co and Ni on ion yields was negligible, the observed count rate of Si slightly increased in olivine with the highest Fe-content (run Ol11F1 in Table 8 and 9). Similar matrix effects, associated with Fe-bearing minerals were documented in

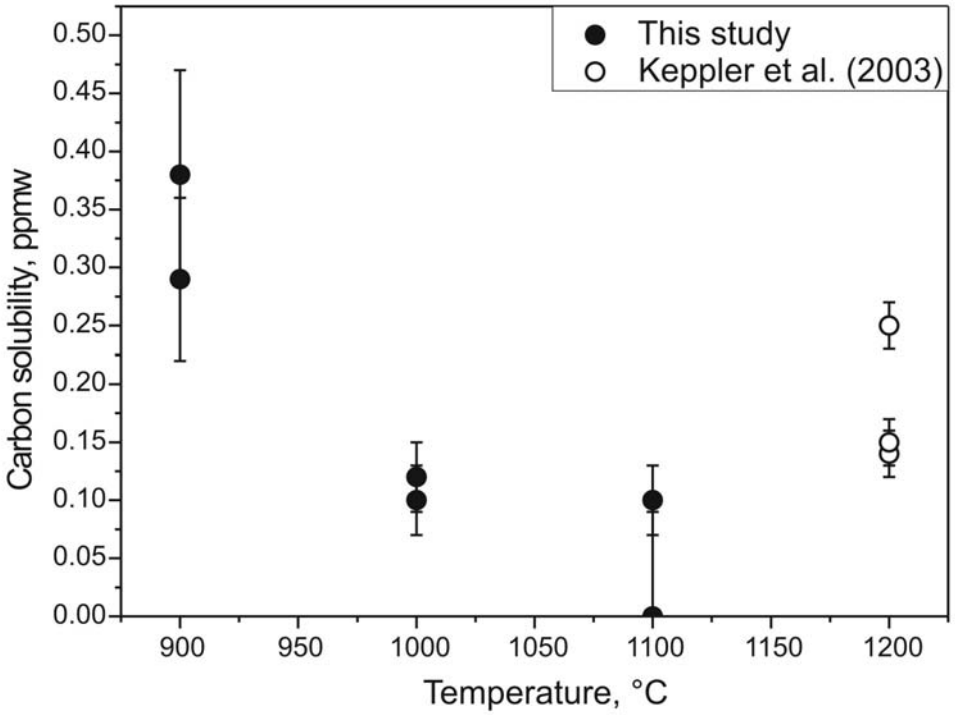

Figure 4.6 Variations of carbon solubility in forsterite with temperature. Data points represent analyses of individual crystals. Error bars correspond to one standard deviation.

previous studies (Catlos et al., 2000; Shimizu et al., 1978 and references therein). Their nature is poorly understood; probably iron reduces the strength of Si bonding in olivine or influences the energy distribution of sputtered silicon ions (the overlap of the Si signal with "exotic" species (e.g. $^{56}Fe_2^{2-}$) is ruled out because the high mass resolution applied (~4300) is sufficient to distinguish the nominal mass difference between them). Thus, the data on Fe-bearing olivine might be underestimated by factor of 1.5-2, because they were all calibrated against pure forsterite.

Table 9 Composition of olivine doped with Fe, Ni and Co

Run	Formula
Ol11N (Ni-capsule)	$Mg_{1.977}Ni_{0.032}Si_{0.995}O_4$
Ol11C (Co-capsule)	$Mg_{1.850}Co_{0.165}Si_{0.993}O_4$
Ol11F1 (Fe-capsule)	$Mg_{1.761}Fe_{0.248}Si_{0.996}O_4$
Ol11F2 (5%Fa in starting mixture)	$Mg_{1.945}Fe_{0.062}Si_{0.997}O_4$
Ol11F3 (10%Fa in starting mixture)	$Mg_{1.887}Fe_{0.122}Si_{0.995}O_4$

Compositions were obtained by electron microprobe

To study the effect of composition on carbon solubility, Fe-bearing crystals were synthesized (runs Ol11F2 and Ol11F3 in Table 8 and 9). They are slightly depleted in fayalite component compared to the average upper mantle olivine (~Fo91, e.g. McDonough and Rudnick, 1998). The experiments show no significant effect of Fe on carbon solubility. Further increasing the fayalite content would result in significant uncertainty due to the effect of iron on silicon ionization mentioned above, which is difficult to quantify. Nevertheless, it is obvious that the Fe/Mg ratio is not a crucial factor controlling carbon solubility in olivine even if the data in Table 8 (runs Ol11F1-Ol11F3) were corrected according to the elevated ion yield of silicon.

4.2.2. Enstatite

Enstatite accounts for ~12 vol.% of uppermost mantle and its modal fraction and structure change with increasing depth. At pressure of 8-9 GPa orthoenstatite transforms to clinoenstatite which in turn reacts with pyrope garnet to form majoritic garnet at pressure of 10-15 GPa (Irifune, 1987). Enstatite was suggested to dissolve more carbon than olivine based on the observed enrichment of mantle enstatite in liquid CO_2 inclusions relatively to olivine (Schwab and Freisleben, 1988).

The dependence of C solubility in enstatite on pressure and temperature was studied in this work (Table 10 and Figure 4.7). In contrast to expectations, the first

precise measurements of carbon-saturated enstatite show that although the pattern of carbon solubility is essentially similar to olivine, enstatite incorporates even less carbon. At lower pressure (1.5 GPa) carbon solubility is in the range of 50-190 parts per billion, which is approximately one order of magnitude lower than recently reported in Keppler et al. (2003) and close to a limit of detection of the technique. Crystals grown at higher pressure are enriched in carbon, but to a lesser degree than olivine. The best fit of the data in Table 10 (except run MA-W-16) to equation 4.1 resulted in A=0.078 ppmw and ΔV=-2.99cm^3/mol.

Table 10 Experimental data on carbon solubility in enstatite

Run	Mineral	*T* (°C)	*P* (GPa)	*t* (h)	C content[a] (wt. p.p.m.)
E9	Enstatite	900	1.5	96	0.07±0.01
					0.14±0.02
					0.15±0.02
E10	Enstatite	1000	1.5	96	0.19±0.04
					0.05±0.01
					0.07±0.01
E11	Enstatite	1100	1.5	168	0.06±0.01
					0.05±0.01
					0.10±0.01
MA-E-6	Enstatite	1100	6	5	0.44±0.03
					0.38±0.03
					0.30±0.02
MA-W-16	Clinoenstatite	1400	16	10	0.69±0.06
					0.65±0.04
					0.80±0.06

Runs with prefix "MA" were carried out in the multi-anvil press, all other experiments were performed in a piston cylinder apparatus. Oxygen fugacity was not buffered but it is probably close to Ni-NiO in piston cylinder runs and between G/DCO and EMOG/D in multianvil runs (see sections 2.1.2.1-2.2.2 for details). Errors are one standard deviation.

[a] If several numbers are given , they represent analysis of different crystals in the charge.

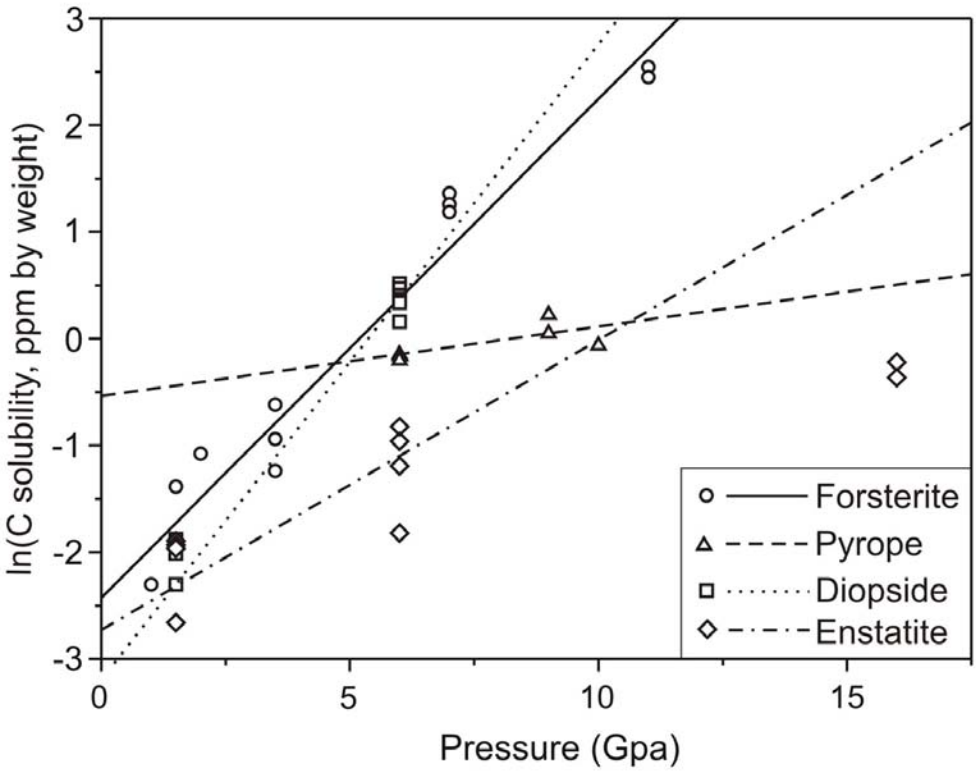

Figure 4.7 Plot of the logarithm of carbon solubility in upper mantle silicates versus pressure for T = 900-1200°C. The slopes of the lines are related to the volume change ΔV of the dissolution reaction. Estimated values of ΔV are -5.47 cm^3/mol for forsterite, - 3.0 cm^3/mol for enstatite, - 6.4 cm^3/mol for diopside and – 0.9 cm^3/mol for pyrope. Except for forsterite, these data are, however, only constrained by few measurement and they may therefore be subject to substantial errors.

Enstatite, coexisting with wadsleyite was recovered from experiment at 16 GPa. High-clinoenstatite rather than orthoenstatite is stable at pressures higher than 8-9 GPa, but it readily transforms to enstatite upon decompression (Angel et al., 1992). Therefore, we attribute the carbon content measured in enstatite from run MA-W-16 to clinoenstatite.

4.2.3. Diopside

Up to 17 vol.% of the pyrolite upper mantle is suggested to be clinopyroxene which undergoes gradual high-pressure transitions as the pyroxenes dissolve into the garnet, with the resulting "garnet–majorite" solid solution ultimately transforming to silicate perovskite. As a major constituent of subducting oceanic crust, clinopyroxene could be considered as potential carrier of carbon to the deep mantle.

Table 11 Experimental data on carbon solubility in diopside

Run	**Mineral**	***T* (°C)**	***P* (GPa)**	***t* (h)**	**C content[a] (wt. p.p.m.)**
D9	Diopside	900	1.5	168	<0.01 [b]
D10	Diopside	1000	1.5	96	0.02±0.01 0.12±0.01 0.10±0.01
D11	Diopside	1100	1.5	96	0.08±0.01 0.16±0.02 0.09±0.01 0.07±0.01
MA-D-6	Diopside	1100	6	8	1.45±0.07 1.60±0.06 1.50±0.07

Runs with prefix "MA" were carried out in the multi-anvil press, all other experiments were performed in a piston cylinder apparatus. Oxygen fugacity was not buffered but it is probably close to Ni-NiO in piston cylinder runs and between G/DCO and EMOG/D in multianvil runs (see sections 2.1.2.1-2.2.2 for details). Errors are one standard deviation.

[a] If several numbers are given , they represent analysis of different crystals in the charge.

[b] Values are below limit of detection.

Experimental results are shown in Table 11. Carbon solubility in diopside at uppermost mantle conditions is the lowest among ordinary silicates and independent on temperature, but increases more sharply with pressure. A fit of experimental data to equation 4.1 yields ΔV=-6.45 cm^3/mol and A=0.051 ppmw. The comparison with low-Ca clinopyroxenes from run MA-W-16 suggests that the presence of Ca probably may favor carbon solubility (see section 5.1 for more details).

4.2.4. Pyrope and $MgAl_2O_4$-spinel

Pyrope makes up about 15 vol.% of upper mantle. Its fraction increases to ~40 vol.% at the top of transition zone due to the formation of a solid solution with pyroxene. Data on carbon solubility in pyrope are presented in Table 12. Carbon solubility in pyrope increases with pressure as for other minerals, but the dependence is not as pronounced as in olivine or pyroxenes. No water was added in experiment MA-Py-9. However, the only difference from water-bearing runs is that crystals grown were smaller in size while the carbon solubility was not affected by the absence of water.

Although spinel $MgAl_2O_4$ is stable only in the Earth's uppermost mantle it was included in this investigation because it is an oxide mineral and the comparison with other mantle minerals could provide some useful insights to probable mechanisms of carbon dissolution (see Section 5.1). We failed to determine any discernible amount of carbon in spinel structure above the limit of detection in 30 ppb by weight (Table 12). Due to the compositional difference between the analyzed and the reference sample (section 2.2) a slight error in the estimated detection limit is possible.

Table 12 Experimental data on carbon solubility in pyrope and spinel

Run	Mineral	*T* (°C)	*P* (GPa)	*t* (h)	C content[a] (wt. p.p.m.)
MA-Py-6	Pyrope	1300	6	10	0.85±0.05
					0.87±0.05
MA-Py-9	Pyrope	1300	9	10	0.83±0.06
					1.27±0.07
					1.07±0.06
MA-Py-10	Pyrope	1300	10	6	0.82±0.04
					0.96±0.05
Sp	Spinel	1100	1.5	168	<0.03 [b]
					<0.02 [b]

Runs with prefix "MA" were carried out in the multi-anvil press, all other experiments were performed in a piston cylinder apparatus. Oxygen fugacity was not buffered but it is probably close to Ni-NiO in piston cylinder runs and between G/DCO and EMOG/D in multianvil runs (see sections 2.1.2.1-2.2.2 for details). Errors are one standard deviation.

[a] If several numbers are given , they represent analysis of different crystals in the charge.

[b] Values are below limit of detection.

4.3 Carbon solubility in minerals of the transition zone and lower mantle

The transition zone begins at a depth of ~410 km, where olivine transforms to wadsleyite, Wadsleyite accounts for ~60 vol.% of the upper part of the transition zone and coexists with ~40 vol.% of majoritic garnet. This assemblage is stable to the depth of ~520 km where the wadsleyite-ringwoodite transformation occurs. At the 670-km discontinuity, ringwoodite decomposes to ferripericlase (Fe,Mg)O and $MgSiO_3$-perovskite. Majorite converts to the perovskite structure, too, thereby making silicate perovskite the most abundant silicate in the Earth.

Table 13 Experimental data on carbon solubility in minerals of the transition zone and lower mantle

Run	Mineral	*T* *(°C)*	*P* *(GPa)*	*t* *(h)*	C content [a] (wt. p.p.m.)
MA-W-16	Wadsleyite	1400	16	10	0.04±0.01
					<0.04 [b]
MA-W-17	Wadsleyite	1400	17	4	<0.07 [b]
					<0.05 [b]
MA-R-21	Ringwoodite	1200	21	10	0.04±0.01
MA-R-23	Ringwoodite	1200	23	4	0.10±0.02
					<0.07 [b]
					<0.08 [b]
MA-I-25	Mg-Ilmenite	1400	25	10	<0.10 [b]
					<0.08 [b]
					<0.11 [b]
MA-Ps-25	Mg-Perovskite	1400	25	10	<0.10 [b]
					<0.07 [b]
					<0.09 [b]
					<0.10 [b]
MA-Ps-26	Mg-Perovskite	1400	26	3	<0.05 [b]
					<0.09 [b]

All experiments were conducted in a multi-anvil press. Oxygen fugacity was not buffered but it is probably between G/DCO and EMOG/D (see section 2.1.2.2 for details).

Errors are one standard deviation.

[a] Each number refers to the analysis of one single crystal in the charge

[b] Values are below limit of detection.

The first experimental results on carbon solubility in minerals of the transition zone and lower mantle are summarized in Table 13. Most of the synthesized crystals show no excess of ^{13}C relatively to the natural ratio $^{13}C/^{12}C$. Therefore, the maximum carbon solubility in wadsleyite, ringwoodite, $MgSiO_3$-ilmenite and $MgSiO_3$-perovskite is estimated to be below the limit of detection of 40-110 ppbw. Since these numbers were obtained using non-matrix matching tholeiite glass standards, systematic errors of a factor of 2-3 is possible. RSFs calculated for crystalline phases in this study are higher than for glass (Table 4). Possibly, the ionization of carbon relative to silicon is higher for a crystalline matrix than for an amorphous matrix. In this case even lower detection limit would result.

5. Discussion and geological implications

5.1 Carbon speciation in silicates

In spite of extensive studies during the past 40 years there is no consensus on the potential mechanism of carbon incorporation in silicates. Neutral carbon has been suggested to dissolve interstitially or in cation vacancies (Freund, 1981). Ernst et al. (1969), Fyfe (1970) and Ernst and Schwab (1972) suggested that carbon may directly substitute for silicon in tetrahedral coordination; they even speculated about a solid solution of "orthocarbonates" with silicates at the conditions of the deep mantle. The exceedingly low carbon solubility in silicates encountered in this study makes direct studies of carbon speciation by spectroscopic methods impossible. However, the analysis of the thermodynamic data provides some insight into speciation. In particular, the observation that carbon solubility in olivine is independent of oxygen fugacity is quite significant.

Carbon in carbonates is in the +4 oxidation state. If it were incorporated in minerals in any other form than C^{4+}, redox exchange reactions would be involved. For example, the reaction

$$C^{4+}_{carbonate} + 2O^{2-}_{mineral} \rightarrow C^{0}_{mineral} + O_2$$

describes the dissolution of carbon in neutral form with the equilibrium constant

$$K = \frac{\left[C^{0}_{mineral}\right] \cdot f_{O_2}}{\left[C^{4+}_{carbonate}\right] \cdot \left[O^{2-}_{mineral}\right]^2} .$$

Consequently, one would expect carbon solubility to decrease with oxygen fugacity according to

$$\left[C^{0}_{mineral}\right] \sim \frac{1}{f_{O_2}} .$$

The expected dependencies of carbon solubility on oxygen fugacity for different substitution mechanisms are plotted in Figure 5.1 together with the experimental data for olivine. Evidently, the experimental data exclude the possibility of a change in oxidation state of carbon during dissolution. Therefore, carbon in olivine is dissolved as C^{4+}. This leaves two possibilities: either, C^{4+} directly

substitutes for Si^{4+}, or C^{4+} may occupy interstitial sites. Considering the small ionic radius of C^{4+} (15 pm, Shannon, 1976) the latter possibility would appear to be quite reasonable. However, the systematic variations in carbon solubility observed for different minerals rather suggest the direct substitution of C^{4+} for Si^{4+}, as the solubility is clearly correlated with the volume of the Si^{4+} site in the respective mineral. While the average length of Si-O bond does not differ much among common upper mantle silicates (Hazen, 1976), the tetrahedral volumes vary more systematically (Table 14). Moreover, polyhedral volumes are more sensitive to compression because of the change in (1) bond angle strain, (2) polyhedral angle variance, and (3) mean polyhedral elongation (Hazen, 1976, Levien et al., 1979). Figure 5.2 gives a plot of carbon solubility versus the volume of the Si tetrahedron in the respective structure ((Smyth and Bish, 1988) and references in Table 14).

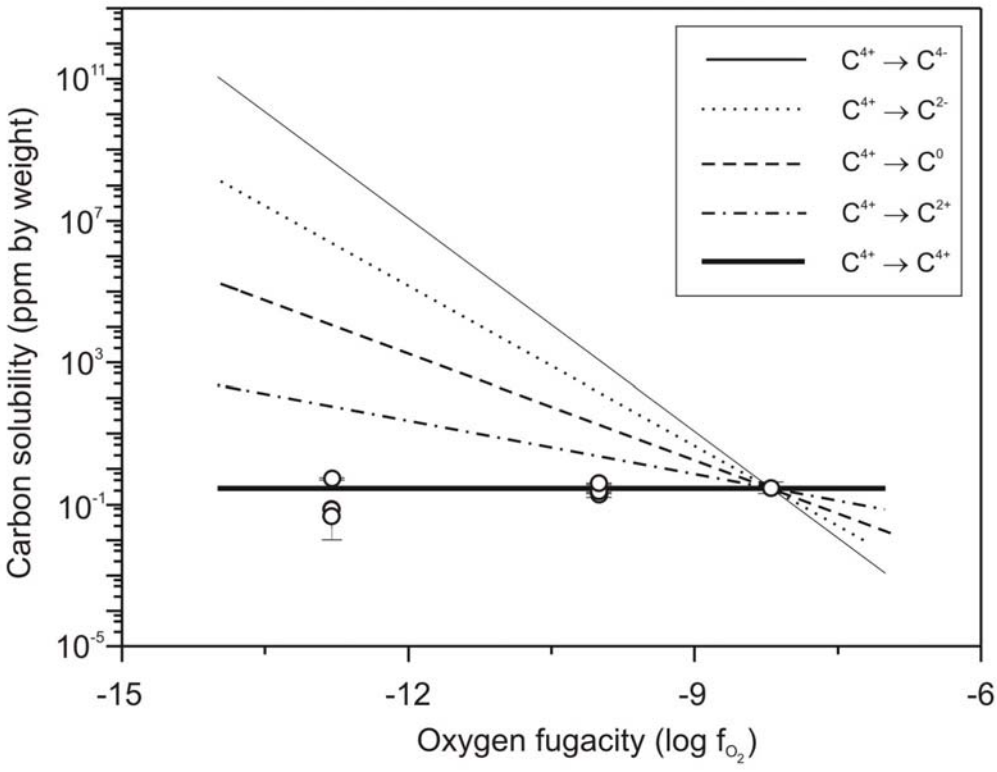

Figure 5.1 Dependence of carbon solubility in olivine on oxygen fugacity at 1.5 GPa and 1100 °C. Theoretical slopes for different solution mechanisms are shown for comparison.

Table 14 Selected structural data for major mantle silicates

Mineral	P, GPa	Si-O bond length, Å	Volume of SiO_4-tetrahedron	Reference
Forsterite	1	1.622-1.650	2.21	Hazen, 1976; Kudoh and Takeuchi, 1985
	1.5	1.611-1.648	2.20	
	2	1.60-1.66	2.19	
	3.5	1.608-1.642	2.165	
	7	1.598-1.614	2.08	
	11	1.57-1.60	2.02	
Enstatite	1.5	1.631-1.646	2.23	Hugh-Jones and Angel, 1994; Hugh-Jones et al., 1997
	6	1.614-1.629	2.16	
High-clinoenstatite	16	1.582-1.676	2.17-2.21	Angel et al., 1992; Wentzcovitch et al., 1995
Diopside	1.5	1.581-1.678	2.16	Levien and Prewitt, 1981
	6	1.587-1.676	2.24	
Pyrope	6	1.619-1.630	2.15	Hazen and Finger, 1978; Levien et al., 1979; Zhang et al., 1998
	10	mean 1.613	2.11	
Wadsleyite	17	1.651	2.30	Horiuchi and Sawamoto, 1981
Ringwoodite	21	1.654	2.32	Sasaki et al., 1982
Ilmenite	24	1.799	7.59[a]	Horiuchi et al., 1982
Perovskite	>25	1.789	7.68[a]	Horiuchi et al., 1987

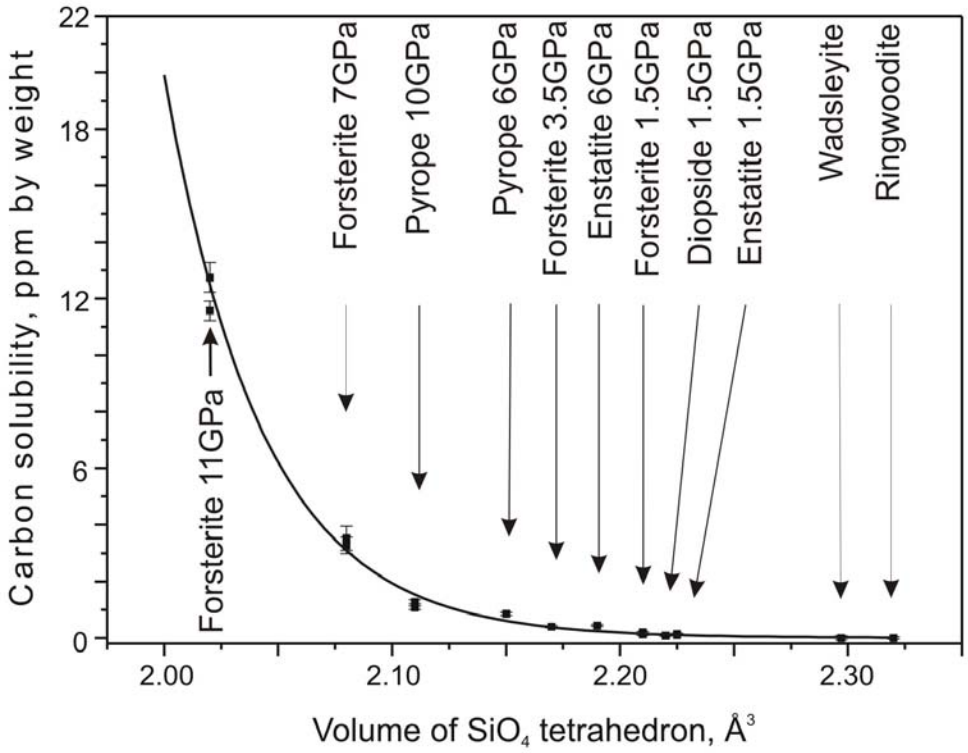

Figure 5.2 Carbon solubility in silicates as a function of the volume of the SiO_4 tetrahedron. Volume data are from Smyth and Bish (1988) and references in Table 14. The curve shown is a guide for the eye only.

This graph explains perfectly the variations of carbon solubility among upper mantle silicates as well as the failure to find any carbon in wadsleyite and ringwoodite. Silicon in $MgSiO_3$-ilmenite and $MgSiO_3$-perovskite is in octahedral coordination. This site, still being the smallest in their structures, has a much longer Si-O bond and larger polyhedral volume (e.g. 7.68 $Å^3$ in perovskite compared to 2.10-2.24 Å in upper mantle minerals), in agreement with the increase of interatomic distances with increasing coordination number (Shannon and Prewitt, 1968). The smallest polyhedra in $MgAl_2O_4$ spinel are MgO_4 tetrahedra with a volume in the range of 3.653-3.827 $Å^3$. It is therefore not surprising, that no carbon was detected in $MgAl_2O_4$ spinel. Figure 5.2 is also in a agreement with our observation that the substitution of Mg by Fe (or Co or Ni) in olivine does not affect carbon solubility, because the volume of the SiO_4 tetrahedron does not vary significantly even among the end-members forsterite, fayalite, liebenbergite and Co-olivine.

The correlation shown in Figure 5.2 can be used to estimate carbon solubility in other silicates. Those with larger polyhedral volume, (e.g. Ca-garnet, 2.255 $Å^3$) would dissolve virtually no carbon, while the smaller volume of the SiO_4 tetrahedron in zircon (2.118 $Å^3$) and plagioclase (2.12-2.15 $Å^3$) should enhance carbon solubility. However, due to their low abundance or limited stability field in the mantle, these minerals are unlikely to be significant reservoirs of carbon.

5.2 Implications for carbon storage in the mantle and global carbon cycle

The geological implications of this study very much depend on the bulk carbon content in the mantle (Section 1.2). Although numerous estimates yield a wide range of carbon abundance in the mantle (Table 1), cosmochemical arguments based on ratios of elements with similar volatility as carbon (for instance, $C/^{36}Ar$, Otting and Zahringer, 1967, or $C/^{3}He$, Marty and Jambon, 1987) in chondrites generally suggest rather high carbon abundances in the bulk earth in the order of 1000 ppm or higher, with most of this carbon probably residing in the mantle.

If the numbers in Table 1 are compared to the carbon solubilities in upper mantle minerals found in this study, it is obvious that throughout almost the entire mantle, most of the carbon must be stored in a separate carbon-rich phase. This could either be a carbonate phase or elemental carbon in the form of graphite or diamond. Considering that estimates of carbon abundance in the upper mantle, although somewhat uncertain, usually range from 100 to more than 1000 ppm, diamond would have to be a common accessory mineral in mantle xenoliths coming from the diamond stability field, if most of the carbon where present as elemental carbon. This does not agree with the observation that diamond is an exceedingly rare mineral, although it could be explained by the rarity of well-preserved samples originating from the diamond stability field or by the prevalence of other forms of elemental carbon (e.g. amorphous films on grain boundaries, Mathez (1987); Mathez et al., 1987, Wilmart et al., 1993) or micro diamonds, which might not be normally recognized. Most likely, however, carbonates, i.e. dolomite or magnesite are the main storage sites of carbon throughout most of the upper mantle (Biellmann et al., 1993; Isshiki et al., 2004; Wang et al., 1996; Wyllie and Huang, 1976). Considering the low melting point of

carbonates (Dalton and Presnall, 1998b) and the low viscosity of carbonatite melts (Dobson et al., 1996) which form close to the solidus of a carbonated mantle, it would be very surprising if carbon were homogeneously distributed in the mantle. Rather, since the mantle geotherm is close to or above the solidus of carbonated peridotite throughout much of the deeper upper mantle, local carbon enrichment due to carbonatite melts will be common. Unfortunately, the density of anhydrous and hydrous carbonatite melts is not known under the relevant conditions of pressure and temperature and therefore it is not possible to predict whether carbonatite melts would tend to rise or to descend in a carbonated mantle. If these melts were less dense than the surrounding peridotite, in agreement with measurements at 1 bar (Dobson et al., 1996), one could imagine a continuous enrichment of the shallow mantle by carbonatite melts generated during mantle convection. These melts would percolate upward through the mantle until they solidify as the mantle geotherm intersects the solidus. In this way, massive carbonate enrichments could be generated, particularly in the shallow mantle below old, cold and stable continental crust. This idea is entirely consistent with the common enrichment of CO_2 in magmas originating in the subcontinental mantle (Wilson, 1989).

If the curve for olivine in Figure 4.5 is extrapolated to the base of the upper mantle at a depth of ~410 km, carbon solubility in olivine reaches 45-50 ppmw. This value is still much smaller than the 1000 ppm often assumed for a fertile mantle peridotite, but it is comparable to some of the lowest values derived for bulk carbon concentration in depleted mantle (Saal et al., 2002; Zhang and Zindler, 1993). Accordingly, for a depleted mantle source composition, there might be a narrow layer just above the transition zone where most of the carbon is stored in olivine (Figure 5.3). Upon subduction or downwelling of such a depleted carbon reservoir, carbonate, probably in the form of a carbonatite melt will exsolve, once the reservoir passes through the olivine to wadsleyite transformation. The geodynamic significance of this effect entirely depends on the density contrast between carbonate melt and surrounding peridotite and permeability of ambient mantle region for these carbonatite melts. If the melt is denser than the peridotite, it will continue to descend into the deeper mantle. However, if the melt were still less dense than the surrounding peridotite and its low viscosity is not affected significantly by pressure increase above 5 GPa (Dobson et al., 1996), it could percolate upward due to low viscosity while the residual peridotite may continue to descend into the lower mantle. In this case, a

situation would arise that in some ways is similar to the water filter model proposed by Bercovici and Karato (2003), but with quite the opposite effect. While the Bercovici and Karato model is a mechanism to retain incompatible elements in the lower mantle, the formation of a carbonatite melt of low density at the 410 km discontinuity could retain CO_2 in the upper mantle and prevent it from being recycled into the lower mantle. However, the geodynamic significance of this effect is questionable, as it would only be relevant for carbon-depleted reservoirs.

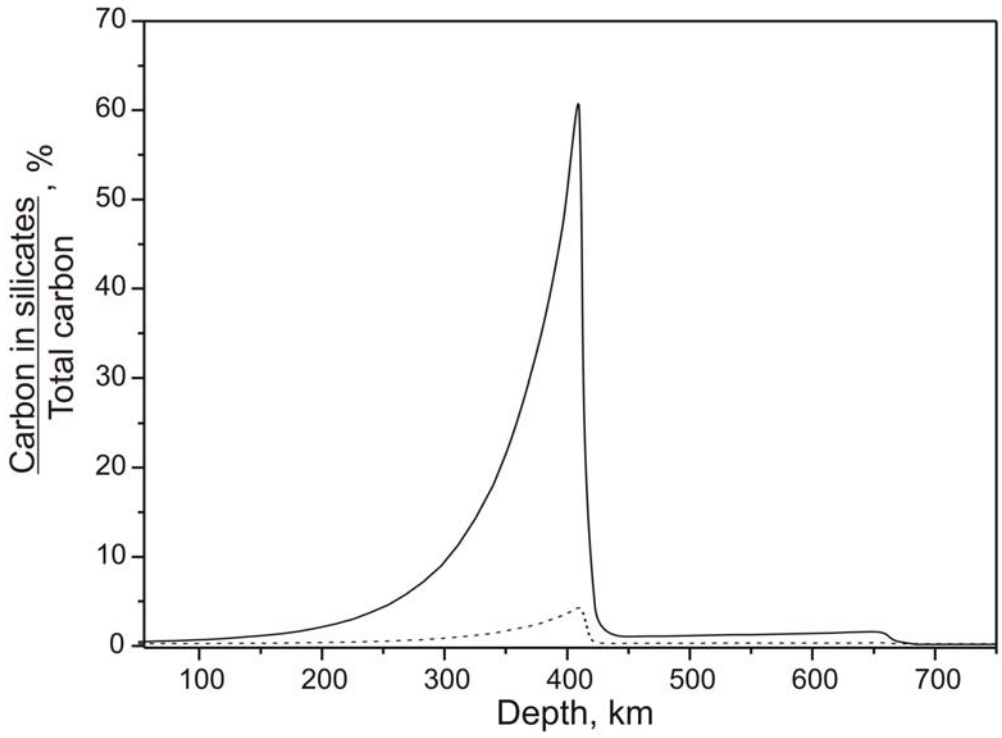

Figure 5.3 Fraction of total mantle carbon, dissolved in silicates as a function of depth for a depleted MORB source (73 ppmw C, Zhang and Zindler, 1993, solid line) and for fertile pyrolitic mantle (1000 ppmw, Jambon, 1994, dotted line). The curves were calculated from the experimental solubility data reported in this study and assuming a pyrolitic mineral assemblage of the mantle.

While carbonate is the most plausible host for carbon in upper mantle(Wang et al., 1996; Dalton and Presnall, 1998a; Dalton and Presnall, 1998b; Dasgupta et al., 2004), changes in ambient oxygen fugacity may stabilize diamond in the transition zone and lower mantle (Bryndzia and Wood, 1990; Canil and O'Neill, 1996; Frost et al., 2004; Luth, 1999; Mathez et al., 1987; O'Neill et al., 1993b). However, the redox equilibria between carbonate and diamond are not well studied under the relevant conditions of pressure and temperature.

5.3 Flood basalt eruptions and mass extinctions

The results of this study suggest that massive carbonate enrichments in the shallow subcontinental mantle are possible. Large shallow carbonate enrichments could be tapped by continental flood basalts with the effect of a sudden injection of large amounts of carbon dioxide into the atmosphere, possibly triggering mass extinctions (Morgan et al., 2004). Although this possibility is strongly supported by the correlation between the ages of large-scale flood basalt events and major life extinctions during the last ~250 my (Figure 5.4, Courtillot, 1999a; Renne et al., 1995) the link between these events remains poorly understood. For instance, Wignall (2001) showed that among the 15 major Phanerozoic extinctions only six coincide with the formation of large igneous provinces (LIPs). However, perturbations in global carbon cycle triggered by volcanism are believed to be the most probable explanation. Even if average volatile-poor basalt magmas are considered (see Table 1), the total amount of carbon dioxide degassed into the atmosphere during relatively short (~1 my) continental flood basalt eruptions (up to $1x10^{19}$ g for Siberian Traps, Grard et al., 2005; McCartney et al., 1990) is comparable to the amount of carbon in all surficial carbon reservoirs ($5x10^{19}$ g, Berner, 1999). However, it was shown on the base of compositional and density data for Columbia River flood basalts (Lange, 2002) that at least some flood basalts have to be exceptionally volatile-rich in order to ascent to the surface. Accordingly, their effect on the surface carbon budget would be the orders of magnitude larger. Morgan et al. (2004) speculated that the eruption of flood basalts was accompanied by a large explosive CO_2 and SO_2 release from the

cratonic lithosphere. Unlike SO_2 and minor volatiles (e.g. Cl, F) which have a short-term (on the order of months and years (Devine et al., 1984; Genin et al., 1995; McCartney et al., 1990; Pinto et al., 1989) influence on climate , injected CO_2 cannot be rapidly removed from the atmosphere and may act as a greenhouse agent for periods of several thousand years. For the Triassic-Jurassic boundary, which coincides with the activity of the Central Atlantic Magmatic Province, stomatal indices in fossil ginkgo leaves suggest a sudden fourfold rise in atmospheric CO_2, corresponding to a "greenhouse warming" of 3-4 °C right at the boundary (Beerling and Woodward, 1995; McElwain et al., 1999). The increase of leaf temperature above a "lethal" limit could contribute to the extinction of terrestrial flora (McElwain et al., 1999). However, the reduction of solar irradiation due to sulfate aerosols and volcanic ash and the enhanced consumption of atmospheric CO_2 by continental weathering of newly formed basalts (Dessert et al., 2003) may compensate for the warming effect, particularly during flood basalt events, which provide a continuous recharging of the atmosphere by repeated eruptions.

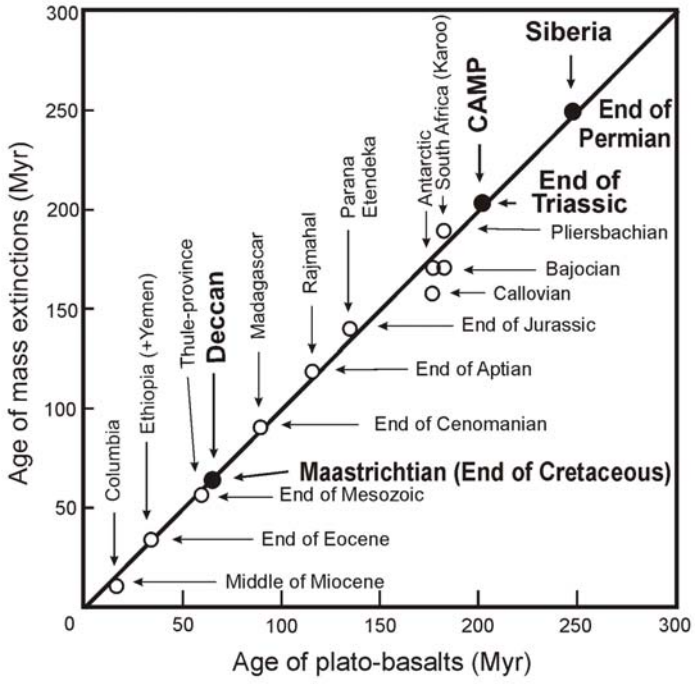

Figure 5.4 Age correlations between large igneous provinces and major extinction events (after Courtillot and Renne, 2003)

Although "greenhouse" warming alone is probably not sufficient to cause extinction, it may stimulate a number of harmful consequences for the biosphere. Warming of oceans leads to lower oxygen solubility in water and lower latitudinal temperature gradient (due to more intensive warming of high-latitude seawater, Grard et al., 2005) which results in less intense convection. Abrupt negative shifts in $\delta^{13}C$ in both organic and inorganic carbon observed, for instance, at Permian-Triassic boundary (e.g. Holser et al., 1989) provide evidence that "greenhouse" warming could be enhanced by dissociation of gas hydrates at the oceanic floor leading to the enrichment of surficial carbon in isotopically light carbon and extreme anoxic and(or) euxinic conditions (Kiehl and Shields, 2005; Knoll et al., 1996). This may provide a major killing mechanism by extensive reduction of sulfur in oxygen-poor seawater and by emission of hydrogen sulfide into the atmosphere (Grice et al., 2005; Wignall and Twitchett, 1996), originally triggered, however, by volcanic activity. Although some of large igneous provinces (LIP's) do not coincide with mass extinction events (Wignall, 2001), all post-Paleozoic global warming/marine anoxia events are well correlated with the intervals of LIP activity (e.g. Kerr, 1998; Sinton and Duncan, 1997).

Another extinction mechanism could be related to the extreme acidification of oceans induced by flood basalt eruptions. Significant fractions of CO_2 and SO_2 released into the atmosphere are adsorbed by seawater (Caldeira and Wickett, 2003; Houghton et al., 1996). Carbon dioxide reacts with water to produce carbonic acid, which dissolves calcium carbonate. Sulfur dioxide reacts with water and oxygen to produce sulfuric acid which enters the ocean through acid rain. While elevated carbon and sulfur fluxes have opposite effect on global temperature, they both increase the acidity of the seawater and make it more difficult for marine organisms to precipitate carbonates for building their shells. This scenario is supported, for example, by the preferred extinction of all marine invertebrates with calcium carbonate exoskeletons at Permian-Triassic boundary (e.g. Liang, 2002) which are most sensitive to the acid-base balance (Knoll, 1996) and by the studies of present-day coral reefs (Kleypas et al., 1999; Orr et al., 2005).

Not all continental flood basalts cause life extinctions. A large number of factors may be responsible for this. In particular, Jourdan et al. (2005) explained the absence of a major mass extinction contemporaneous to the Karoo flood basalt province by the unusually long duration of volcanism (~8 m.y.). Courtillot (1999b)

suggested that the magnitude of biological effects of volcanism depends on the arrangement of continents, sea level and climate at the time of eruptions. Probably most of these factors should be linked to the dynamics of environmental response to the changes caused by flood basalt events (intensity of weathering, rate of the consumption of atmospheric carbon by biosphere etc.). The efficiency of such carbon sinks may control the scale and duration of global warming and accompanied marine anoxia, euxinia or acidification events.

6. References

Andersen, T., O'Reilly, S. Y. and Griffin, W. L. (1984). The trapped fluid phase in upper mantle xenoliths from Victoria, Australia - implications for mantle metasomatism, Contrib. Mineral. Petrol. **88**: 72-85.

Angel, R. J., Chopelas, A. and Ross, N. L. (1992). Stability of high-density clinoenstatite at upper-mantle pressures, Nature **358**: 322-324.

Ballhaus, C. (1993). Redox states of lithospheric and asthenospheric upper-mantle, Contrib. Mineral. Petrol. **114**: 331-348.

Beerling, D. J. and Woodward, F. I. (1995). Stomatal responses of variegated leaves to CO_2 enrichment, Ann. Bot. **75**: 507-511.

Bercovici, D. and Karato, S. (2003). Whole-mantle convection and the transition-zone water filter, Nature **425**: 39-44.

Bergman, S. C. and Dubessy, J. (1984). CO_2-CO fluid inclusions in a composite peridotite xenolith - implications for upper mantle oxygen fugacity, Contrib. Mineral. Petrol. **85**: 1-13.

Berner, R. A., Lasaga, A. C. and Garrels, R. M. (1983). The carbonate-silicate geochemical cycle and its effect on atmospheric carbon dioxide over the past 100 million years, American Journal of Science **283**: 641-683.

Berner, R. A. (1994). 3GeocarbII: A revised model of atmospheric CO_2 over Phanerozoic time, Am. J. Sci. **294**: 56-91.

Berner, R. A. (1999). A new look at the long-term carbon cycle, Geil. Soc. Am. Today **9**: 1-6.

Biellmann, C., Gillet, P., Guyot, F., Peyronneau, J. and Reynard, B. (1993). Experimental evidence for carbonate stability in the Earth's lower mantle, Earth Planet. Sci. Lett. **118**: 31-41.

Bilal, A. and Touret, J. (1977). Fluid inclusions in phenocrysts from basaltic lavas of Puy Beaunit (French Massif Central), Bull. Soc. Fr. Mineral. Cristallogr. **100**: 324-328.

Bina, C. R. (1998). Lower mantle mineralogy and the geophysical perspective, Rev. Mineral. **37**: 205-239.

Bina, C. R. (2003). Seismological constraints upon mantle composition. In: Treatise on Geochemistry, (Ed.) R. W. Carlson, Elsevier, New York, **2**: pp. 39-59.

Blank, J. G. and Brooker, R. A. (1994). Experimental studies of carbon dioxide in silicate melts - solubility, speciation, and stable carbon isotope behavior, Rev. Mineral. **30**: 157-186.

Blundy, J. D., Brodholt, J. P. and Wood, B. J. (1991). Carbon fluid equilibria and the oxidation state of the upper mantle, Nature **349**: 321-324.

Bolfan-Casanova, N. (2000). The distribution of water in the Earth's mantle: an experimental and inrfared study. Ph.D. Thesis, Bayerisches Geoinstitut, Universität Bayreuth: pp 169.

Bottinga, Y. and Javoy, M. (1990). Midocean ridge basalt degassing - bubble nucleation, J. Geophys. Res. **95**: 5125-5131.

Boyd, F. R. and England, J. L. (1960). Apparatus for phase-equilibrium measurements at pressures up to 50 kilobars and temperatures up to 1750 degrees C, J. Geophys. Res. **65**: 741-748.

Boyd, F. R. and England, J. L. (1965). The rhombic enstatite-clinoenstatite inversion, Carnegie Inst. Wash. Year Book **64**: 117-120.

Brewster, D. (1823). On the existence of two new fluids in the cavities of minerals, which are immiscible, and possess remarkable physical properties, Philos. J. **9**: 94-95, 268-270.

Brey, G., Brice, W. R., Ellis, D. J., Green, D. H., Harris, K. L. and Ryabchikov, I. D. (1983). Pyroxene-carbonate reactions in the upper mantle, Earth Planet. Sci. Lett. **62**: 63-74.

Brooker, R., Holloway, J. R. and Hervig, R. (1998). Reduction in piston-cylinder experiments: The detection of carbon infiltration into platinum capsules, Am. Mineral. **83**: 985-994.

Bryndzia, L. T. and Wood, B. J. (1990). Oxygen thermobarometry of abyssal spinel peridotites - the redox state and C-O-H volatile composition of the Earth's sub-oceanic upper mantle, Am. J. Sci. **290**: 1093-1116.

Caldeira, K. and Wickett, M. E. (2003). Anthropogenic carbon and ocean pH, Nature **425**: 365-365.

Canil, D. (1990). Experimental study bearing on the absence of carbonate in mantle-derived xenoliths, Geology **18**: 1011-1013.

Canil, D. (1994). Stability of clinopyroxene at pressure-temperature conditions of the transition region, Phys. Earth Planet. Inter. **86**: 25-34.

Canil, D., O'Neill, H. S. C., Pearson, D. G., Rudnick, R. L., McDonough, W. F. and Carswell, D. A. (1994). Ferric iron in peridotites and mantle oxidation states, Earth Planet. Sci. Lett. **123**: 205-220.

Canil, D. and O'Neill, H. S. C. (1996). Distribution of ferric iron in some upper-mantle assemblages, J. Petrol. **37**: 609-635.

Cartigny, P., Harris, J. W. and Javoy, M. (1998). Eclogitic diamond formation at Jwaneng: No room for a recycled component, Science **280**: 1421-1424.

Catlos, E. J., Sorensen, S. S. and Harrison, T. M. (2000). Th-Pb ion-microprobe dating of allanite, Am. Mineral. **85**: 633-648.

Chapman, D. S. (1986). Thermal gradients in the continental crust. In: The Nature of the Lower Continental Crust, (Ed.) J. B. Dawson, D. A. Carswell, J. Hall and K. H. Wedepohl, Blackwell, London: pp. 63-70.

Christie, D. M., Carmichael, I. S. E. and Langmuir, C. H. (1986). Oxidation states of midocean ridge basalt glasses, Earth Planet. Sci. Lett. **79**: 397-411.

Courtillot, V. (1999a). Das Sterben der Saurier; Erdgeschichtliche Katastrophen. Enke, Stuttgart, pp 150.

Courtillot, V. (1999b). Evolutionary Catastrophes: the Science of Mass Extinctions. Cambridge Univ. Press, Cambridge, pp 237.

Courtillot, V.E. and Renne, P.R., 2003. On the ages of flood basalt events, C. R. Geosci. **335**: 113-140.

Dalton, J. A. and Presnall, D. C. (1998a). The continuum of primary carbonatitic-kimberlitic melt compositions in equilibrium with lherzolite: data from the system CaO-MgO-Al_2O_3-SiO_2-CO_2 at 6 GPa, J. Petrol. **39**: 1953-1964.

Dalton, J. A. and Presnall, D. C. (1998b). Carbonatitic melts along the solidus of model lherzolite in the system CaO-MgO-Al_2O_3-SiO_2-CO_2 from 3 to 7 GPa, Contrib. Mineral. Petrol. **131**: 123-135.

Dasgupta, R., Hirschmann, M. M. and Withers, A. C. (2004). Deep global cycling of carbon constrained by the solidus of anhydrous, carbonated eclogite under upper mantle conditions, Earth Planet. Sci. Lett. **227**: 73-85.

Davies, G. R., Nixon, P. H., Pearson, D. G. and Obata, M. (1993). Tectonic implications of graphitized diamonds from the Ronda peridotite massif, southern Spain, Geology **21**: 471-474.

Deines, P. (2002). The carbon isotope geochemistry of mantle xenoliths, Earth Sci. Rev. **58**: 247-278.

Dessert, C., Dupre, B., Gaillardet, J., Francois, L. M. and Allegre, C. J. (2003). Basalt weathering laws and the impact of basalt weathering on the global carbon cycle, Chem. Geol. **202**: 257-273.

Devine, J. D., Sigurdsson, H., Davis, A. N. and Self, S. (1984). Estimates of sulfur and chlorine yield to the atmosphere from volcanic eruptions and potential climatic effects, J. Geophys. Res. **89**: 6309-6325.

Dobson, D. P., Jones, A. P., Rabe, R., Sekine, T., Kurita, K., Taniguchi, T., Kondo, T., Kato, T., Shimomura, O. and Urakawa, S. (1996). In-situ measurement of viscosity and density of carbonate melts at high pressure, Earth Planet. Sci. Lett. **143**: 207-215.

Duba, A. G. and Shankland, T. J. (1982). Free carbon and electrical conductivity in the Earth's mantle, Geophys. Res. Lett. **9**: 1271-1274.

Eggler, D. H. and Baker, D. R. (1982). Reduced volatiles in the system C-O-H; implications to mantle melting, fluid formation, and diamond genesis. In: High Pressure Research in Geophysics, (Ed.) S. Akimoto and M. H. Manghnani, Center Academic Publisher, Tokyo: pp. 237-250.

Ellis, D. E. and Wyllie, P. J. (1980). Phase relations and their petrological implications in the system MgO-SiO_2-H_2O-CO_2 at pressures up to 100 kbar, Am. Mineral. **65**: 540-556.

Ernst, T., Mages, G. and Schwab, R. G. (1969). Liquid CO_2 in olivine bombs; generated by decomposition of "orthocarbonates"? Fluid Inclusion Res. **69**: 16-17.

Ernst, T. and Schwab, R. G. (1972). A new theory on the formation and ascent of basic magmas with special respect to the undersaturated series, Proc. 24th Int. Geol. Congr., Montreal, **14**: 28-33.

Ernst, T., Schwab, R. G., Scheubel, B. and Brosch, P. (1982). High pressure experiments on the equilibrium olivine-CO_2-enstatite-carbonate in natural system. In: High Pressure in the Geosciences, (Ed.) W. Schreyer.

Falloon, T. J. and Green, D. H. (1989). The solidus of carbonated, fertile peridotite, Earth Planet. Sci. Lett. **94**: 364-370.

Fei, Y. W. and Saxena, S. K. (1990). Internally consistent thermodynamic data and equilibrium phase relations for compounds in the system MgO-SiO_2 at high pressure and high pressure and high temperature, J. Geophys. Res. **95**: 6915-6928.

Fiquet, G., Guyot, F., Kunz, M., Matas, J., Andrault, D. and Hanfland, M. (2002). Structural refinements of magnesite at very high pressure, Am. Mineral. **87**: 1261-1265.

Freund, F., Kathrein, H., Wengeler, H. and Knobel, R. (1980). Carbon in solid-solution in forsterite - a key to the untractable nature of reduced carbon in terrestrial and cosmogenic rocks, Geochim. Cosmochim. Acta **44**: 1319-1333.

Freund, F. (1981). Mechanism of the water and carbon dioxide solubility in oxides and silicates and the role of O^-, Contrib. Mineral. Petrol. **76**: 474-482.

Frost, D. J. and Wood, B. J. (1997). Experimental measurements of the fugacity of CO_2 and graphite/diamond stability from 35 to 77 kbar at 925 to 1650 degrees C, Geochim. Cosmochim. Acta **61**: 1565-1574.

Frost, D. J. and Wood, B. J. (1998). The fugacity of carbon dioxide and the graphite/diamond CO equilibrium between 35 and 77 kbar at 925 to 1650 degrees C, Geochim. Cosmochim. Acta **62**: 725-725.

Frost, D. J., Langenhorst, F. and van Aken, P. A. (2001). Fe-Mg partitioning between ringwoodite and magnesiowustite and the effect of pressure, temperature and oxygen fugacity, Phys. Chem. Miner. **28**: 455-470.

Frost, D. J., Liebske, C., Langenhorst, F., McCammon, C. A., Tronnes, R. G. and Rubie, D. C. (2004). Experimental evidence for the existence of iron-rich metal in the Earth's lower mantle, Nature **428**: 409-412.

Fyfe, W. S. (1970). Lattice energies, phase transformations and volatiles in the mantle, Phys. Earth Planet. Inter. **3**: 196-200.

Gasparik, T. (2003). Phase Diagrams for Geoscientists. An Atlas of the Earth's Interior. Springer-Verlag, Berlin, pp 462.

Genin, A., Lazar, B. and Brenner, S. (1995). Vertical mixing and coral death in the Red Sea following the eruption of Mount Pinatubo, Nature **377**: 507-510.

Gerlach, T. M. and Graeber, E. J. (1985). Volatile budget of Kilauea Volcano, Nature **313**: 273-277.

Gerlach, T. M., McGee, K. A., Elias, T., Sutton, A. J. and Doukas, M. P. (2002). Carbon dioxide emission rate of Kilauea Volcano: Implications for primary magma and the summit reservoir, J. Geophys. Res. **107**: 2189– 2203.

Grandin de L'Eprevier, A. (1972). Synthèse de monocristeaux de forsterite, Mg_2SiO_4 par la méthode des sels fondus. Thèse, La Faculté des Sciences d'Orléans, Orléans.

Grard, A., Francois, L. M., Dessert, C., Dupre, B. and Godderis, Y. (2005). Basaltic volcanism and mass extinction at the Permo-Triassic boundary: Environmental impact and modeling of the global carbon cycle, Earth Planet. Sci. Lett. **234**: 207-221.

Green, H. W. and Radcliffe, S. V. (1975). Fluid precipitates in rocks from Earth's mantle, Geol. Soc.Am. Bull. **86**: 846-852.

Green, H. W. I. (1972). A CO_2 charged asthenosphere, Nature **238**: 2-5.

Green, H. W. I. and Gueguen, Y. (1974). Origin of kimberlite pipes by diapiric upwelling in the upper mantle, Nature **249**: 617-620.

Greenland, L. P., Rose, W. I. and Stokes, J. B. (1985). An estimate of gas emissions and magmatic gas content from Kilauea volcano, Geochim. Cosmochim. Acta **49**: 125-129.

Grice, K., Cao, C. Q., Love, G. D., Bottcher, M. E., Twitchett, R. J., Grosjean, E., Summons, R. E., Turgeon, S. C., Dunning, W. and Jin, Y. G. (2005). Photic zone euxinia during the Permian-Triassic superanoxic event, Science **307**: 706-709.

Gudfinnsson, G. H. and Presnall, D. C. (2005). Continuous gradations among primary carbonatitic, kimberlitic, melilititic, basaltic, picritic, and komatiitic melts in equilibrium with garnet lherzolite at 3-8 GPa, J. Petrol. **46**: 1645-1659.

Gudmundsson, G. and Wood, B. J. (1995). Experimental tests of garnet peridotite oxygen barometry, Contrib. Mineral. Petrol. **119**: 56-67.

Hansen, J. E., Lacis, A., Rind, D. and Russell, G. (1984). Climate Sensitivity to Increasing Greenhouse Gases. In: Greenhouse Effect and Sea Level Rise: A Challenge for This Generation, (Ed.) M. C. Barth and J. G. Titus, Van Nostrand Reinhold Co., New York: pp. 57-77.

Haselton, H. T., Sharp, W. E. and Newton, R. C. (1978). CO_2 fugacity at high temperatures and pressures from experimental decarbonation reactions, Geophys. Res. Lett. **5**: 753-756.

Hazen, R. M. (1976). Effects of temperature and pressure on crystal structure of forsterite, Am. Mineral. **61**: 1280-1293.

Hazen, R. M. and Finger, L. W. (1978). Crystal structures and compressibilities of pyrope and grossular to 60 kbar, Am. Mineral. **63**: 297-303.

Helmstaedt, H. H. (1993). "Primary" diamond deposits - what controls their size, grade, and location? In: Giant Ore Deposits, (Ed.) B. H. Whiting, C. J. Hodgson and R. Mason, Special Publication - Society of Economic Geologists, **2**: pp. 13-80.

Holser, W. T., Schonlaub, H. P., Attrep, M., Boeckelmann, K., Klein, P., Magaritz, M., Orth, C. J., Fenninger, A., Jenny, C., Kralik, M., Mauritsch, H., Pak, E., Schramm, J. M., Stattegger, K. and Schmoller, R. (1989). A unique geochemical record at the Permian-Triassic boundary, Nature **337**: 39-44.

Horiuchi, H. and Sawamoto, H. (1981). Beta-Mg_2SiO_4: single crystal X-ray diffraction study, Am. Mineral. **66**: 568-575.

Horiuchi, H., Hirano, M., Ito, E. and Matsui, Y. (1982). $MgSiO_3$ (ilmenite-type): single crystal X-ray diffraction study, Am. Mineral. **67**: 788-793.

Horiuchi, H., Ito, E. and Weidner, D. J. (1987). Perovskite-type $MgSiO_3$: single crystal X-ray diffraction study, Am. Mineral. **72**: 357-360.

Hugh-Jones, D. A. and Angel, R. J. (1994). A compressional study of $MgSiO_3$ orthoenstatite up to 8.5 GPa, Am. Mineral. **79**: 405-410.

Hugh-Jones, D. A., Chopelas, A. and Augel, R. (1997). Tetrahedral compression in $(Mg,Fe)SiO_3$ orthopyroxenes, Phys. Chem. Miner. **24**: 301-310.

Ingrin, J. and Skogby, H. (2000). Hydrogen in nominally anhydrous upper-mantle minerals: concentration levels and implications, Eur. J. Mineral. **12**: 543-570.

Ionov, D. and Harmer, R. E. (2002). Trace element distribution in calcite-dolomite carbonatites from Spitskop: inferences for differentiation of carbonatite magmas and the origin of carbonates in mantle xenoliths, Earth Planet. Sci. Lett. **198**: 495-510.

Ionov, D. A., Dupuy, C., O'Reilly, S. Y., Kopylova, M. G. and Genshaft, Y. S. (1993). Carbonated peridotite xenoliths from Spitsbergen - Implications for trace element signature of mantle carbonate metasomatism, Earth Planet. Sci. Lett. **119**: 283-297.

Irifune, T. (1987). An experimental investigation of the pyroxene garnet transformation in a pyrolite composition and its bearing on the constitution of the mantle, Phys. Earth Planet. Inter. **45**: 324-336.

Isshiki, M., Irifune, T., Hirose, K., Ono, S., Ohishi, Y., Watanuki, T., Nishibori, E., Takata, M. and Sakata, M. (2004). Stability of magnesite and its high-pressure form in the lowermost mantle, Nature **427**: 60-63.

Ita, J. and Stixrude, L. (1992). Petrology, elasticity, and composition of the mantle transition zone, J. Geophys. Res. **97**: 6849-6866.

Ito, J. (1975). High temperature solvent growth of orthoenstatite, $MgSiO_3$ in air, Geophys. Res. Lett. **2**: 533-536.

Jambon, A. (1994). Earth degassing and large-scale geochemical cycling of volatile elements, Rev. Mineral. **30**: 479-517.

Javoy, M., Pineau, F. and Allegre, C. J. (1982). Carbon geodynamic cycle, Nature **300**: 171-173.

Javoy, M., Pineau, F. and Delorme, H. (1986). Carbon and nitrogen isotopes in the mantle, Chem. Geol. **57**: 41-62.

Javoy, M. (1997). The major volatile elements of the Earth: Their origin, behavior, and fate, Geophys. Res. Lett. **24**: 177-180.

Johannes, W. (1973). Eine vereinfachte Piston-Zylinder Apparatur hoher Genauigkeit, N. Jb. Mineral. **1973**: 337–351.

Jourdan, F., Feraud, G., Bertrand, H., Kampunzu, A. B., Tshoso, G., Watkeys, M. K. and Le Gall, B. (2005). Karoo large igneous province: Brevity, origin, and relation to mass extinction questioned by new Ar-40/Ar-39 age data, Geology **33**: 745-748.

Kadik, A., Pineau, F., Litvin, Y., Jendrzejewski, N., Martinez, I. and Javoy, M. (2004). Formation of carbon and hydrogen species in magmas at low oxygen fugacity, J. Petrol. **45**: 1297-1310.

Kadik, A. A., Shilobreeva, S. N., Minaev, V. M. and Kovalenko, V. I. (1996). The carbon measurements in the upper mantle minerals by the $^{12}C_{(d,n)}{}^{13}N$ nuclear reaction, Lunar Planet. Sci. **27**: 631-632.

Kamenetsky, M. B., Sobolev, A. V., Kamenetsky, V. S., Maas, R., Danyushevsky, L. V., Thomas, R., Pokhilenko, N. P. and Sobolev, N. V. (2004). Kimberlite melts rich in alkali chlorides and carbonates: A potent metasomatic agent in the mantle, Geology **32**: 845-848.

Karato, S. (2004). The role of volatiles on the physical properties of mantle minerals, Geochim. Cosmochim. Acta **68**: A273 (abstract).

Kathrein, H., Gonska, H. and Freund, F. (1983). Subsurface segregation and diffusion of carbon in magnesium oxide, Appl. Phys. **30**: 33-41.

Katsura, T. and Ito, E. (1990). Melting and subsolidus phase-relations in the $MgSiO_3$-$MgCO_3$ system at high pressures: Implications to evolution of the Earth's atmosphere, Earth Planet. Sci. Lett. **99**: 110-117.

Keppler, H., Wiedenbeck, M. and Shcheka, S. S. (2003). Carbon solubility in olivine and the mode of carbon storage in the Earth's mantle, Nature **424**: 414-416.

Kerr, A. C. (1998). Oceanic plateau formation: a cause of mass extinction and black shale deposition around the Cenomanian-Turonian boundary? J. Geol. Soc. **155**: 619-626.

Kerrick, D. M. (2001). Present and past nonanthropogenic CO_2 degassing from the solid Earth, Rev. Geophys. **39**: 565-585.

Kerrick, D. M. and Connolly, J. A. D. (2001). Metamorphic devolatilization of subducted marine sediments and the transport of volatiles into the Earth's mantle, Nature **411**: 293-296.

Kiehl, J. T. and Shields, C. A. (2005). Climate simulation of the latest Permian: Implications for mass extinction, Geology **33**: 757-760.

Kleypas, J. A., Buddemeier, R. W., Archer, D., Gattuso, J. P., Langdon, C. and Opdyke, B. N. (1999). Geochemical consequences of increased atmospheric carbon dioxide on coral reefs, Science **284**: 118-120.

Knoche, R., Sweeney, R. J. and Luth, R. W. (1999). Carbonation and decarbonation of eclogites: the role of garnet, Contrib. Mineral. Petrol. **135**: 332-339.

Knoll, A. H., Bambach, R. K., Canfield, D. E. and Grotzinger, J. P. (1996). Comparative Earth history and Late Permian mass extinction, Science **273**: 452-457.

Kohlstedt, D. L., Keppler, H. and Rubie, D. C. (1996). Solubility of water in the alpha, beta and gamma phases of $(Mg,Fe)_2SiO_4$, Contrib. Mineral. Petrol. **123**: 345-357.

Kudoh, Y. and Takeuchi, Y. (1985). The crystal structure of forsterite Mg_2SiO_4 under high pressure up to 149 kb, Z. Kristallogr. **171**: 291-302.

Lange, R. A. (2002). Constraints on the preeruptive volatile concentrations in the Columbia River flood basalts, Geology **30**: 179-182.

Lasaga, A. C., Berner, R. A. and Garrels, R. M. (1985). An improved geochemical model of atmospheric CO_2 fluctuations over the past 100 million years. In: The Carbon Cycle and Atmospheric CO_2: Natural Variations Archean to Present, Geophysical Monograph, (Ed.) E. T. Sundquist and W. S. Broecker, American Geophysical Union, Washington, D.C., **32**: pp. 397-411.

Laurora, A., Mazzucchelli, M., Rivalenti, G., Vannucci, R., Zanetti, A., Barbieri, M. A. and Cingolani, C. A. (2001). Metasomatism and melting in carbonated peridotite xenoliths from the mantle wedge: The Gobernador Gregores case (Southern Patagonia), J. Petrol. **42**: 69-87.

Lecuyer, C., Simon, L. and Guyot, F. (2000). Comparison of carbon, nitrogen and water budgets on Venus and the Earth, Earth Planet. Sci. Lett. **181**: 33-40.

Lee, C. T., Rudnick, R. L., McDonough, W. F. and Horn, I. (2000). Petrologic and geochemical investigation of carbonates in peridotite xenoliths from northeastern Tanzania, Contrib. Mineral. Petrol. **139**: 470-484.

Levien, L., Prewitt, C. T. and Weidner, D. J. (1979). Compression of pyrope, Am. Mineral. **64**: 805-808.

Levien, L. and Prewitt, C. T. (1981). High-pressure structural study of diopside, Am. Mineral. **66**: 315-323.

Liang, H. D. (2002). End-Permian catastrophic event of marine acidification by hydrated sulfuric acid: Mineralogical evidence from Meishan Section of South China, Chin. Sci. Bull. **47**: 1393-1397.

Luth, R. (1999). Carbon and carbonates in the mantle. In: Mantle Petrology: Field Observations and High Pressure Experimentation: A Tribute to Francis R. (Joe) Boyd., (Ed.) Y. Fei, C. M. Bertka and B. O. Mysen, Geochemical Society, Houston: pp. 297-316.

Luth, R. W., Virgo, D., Boyd, F. R. and Wood, B. J. (1990). Ferric iron in mantle-derived garnets - implications for thermobarometry and for the oxidation state of the mantle, Contrib. Mineral. Petrol. **104**: 56-72.

Luth, R. W. (1993). Diamonds, eclogites, and the oxidation state of the Earth's mantle, Science **261**: 66-68.

Luth, R. W. (1995). Experimental determination of the reaction dolomite + 2 coesite = diopside + 2 CO_2 to 6 GPa, Contrib. Mineral. Petrol. **122**: 152-158.

Luth, R. W. (2003). Mantle volatiles - distribution and consequences. In: Treatise on Geochemistry, (Ed.) W. Carlson, Elsevier, New York, **2**: pp. 319-361.

Marty, B. and Jambon, A. (1987). C/He^3 in volatile fluxes from the solid Earth. Implications for carbon geodynamics, Earth Planet. Sci. Lett. **83**: 16-26.

Mathez, E. A., Blacic, J. D., Beery, J., Maggiore, C. and Hollander, M. (1984). Carbon abundances in mantle minerals determined by nuclear-reaction analysis, Geophys. Res. Lett. **11**: 947-950.

Mathez, E. A. (1987). Carbonaceous matter in mantle xenoliths - composition and relevance to the isotopes, Geochim. Cosmochim. Acta **51**: 2339-2347.

Mathez, E. A., Blacic, J. D., Beery, J., Hollander, M. and Maggiore, C. (1987). Carbon in olivine - results from nuclear-reaction analysis, J. Geophys. Res. **92**: 3500-3506.

Mathez, E. A., Fogel, R. A., Hutcheon, I. D. and Marshintsev, V. K. (1995). Carbon isotopic composition and origin of SiC from kimberlites of Yakutia, Russia, Geochim. Cosmochim. Acta **59**: 781-791.

McCammon, C. (1997). Perovskite as a possible sink for ferric iron in the lower mantle, Nature **387**: 694-696.

McCammon, C. (2001). Deep diamond mysteries, Science **293**: 813-814.

McCammon, C. and Kopylova, M. G. (2004). A redox profile of the Slave mantle and oxygen fugacity control in the cratonic mantle, Contrib. Mineral. Petrol. **148**: 55-68.

McCammon, C. (2005a). The paradox of mantle redox, Science **308**: 807-808.

McCammon, C. (2005b). Mantle oxidation state and oxygen fugacity: constraints on mantle chemistry, structure and dynamics. In: Structure, Composition, and Evolution of Earth's Mantle, (Ed.) R. D. van der Hilst, J. Bass, J. Matas and J. Trampert, American Geophysical Union, Washington, D.C.

McCartney, K., Huffman, A. R. and Tredoux, M. (1990). A paradigm for endogenous causation of mass extinctions. In: Global catastrophes in Earth History, (Ed.)

V. L. Sharpton and P. D. Ward, Geological Society of America, Boulder, Colorado, **247**: pp. 125-138.

McDonough, W. F. and Rudnick, R. L. (1998). Mineralogy and composition of the upper mantle, Rev. Mineral. **37**: 139-164.

McElwain, J. C., Beerling, D. J. and Woodward, F. I. (1999). Fossil plants and global warming at the Triassic-Jurassic boundary, Science **285**: 1386-1390.

Melton, C. E., Giardini, A. A. and Salotti, C. A. (1972). Observation of nitrogen, water, carbon dioxide, methane and argon as impurities in natural diamonds, Am. Mineral. **57**: 1518-1523.

Mierdel, K. and Keppler, H. (2004). The temperature dependence of water solubility in enstatite, Contrib. Mineral. Petrol. **148**: 305-311.

Moine, B. N., Gregoire, M., O'Reilly, S. Y., Delpech, G., Sheppard, S. M. F., Lorand, J. P., Renac, C., Giret, A. and Cottin, J. Y. (2004). Carbonatite melt in oceanic upper mantle beneath the Kerguelen Archipelago, Lithos **75**: 239-252.

Molina, J. F. and Poli, S. (2000). Carbonate stability and fluid composition in subducted oceanic crust: an experimental study on H_2O-CO_2-bearing basalts, Earth Planet. Sci. Lett. **176**: 295-310.

Morgan, J. P., Reston, T. J. and Ranero, C. R. (2004). Contemporaneous mass extinctions, continental flood basalts, and 'impact signals': are mantle plume-induced lithospheric gas explosions the causal link? Earth Planet. Sci. Lett. **217**: 263-284.

Nakamura, A. and Schmalzried, H. (1983). On the nonstoichiometry and point defects of olivine, Phys. Chem. Miner. **10**: 27-37.

Newton, R. C. and Sharp, W. E. (1975). Stability of forsterite + CO_2 and its bearing on role of CO_2 in mantle, Earth Planet. Sci. Lett. **26**: 239-244.

O'Neill, H. S., Rubie, D. C., Canil, D., Geiger, C. A., Ross, C. R., Seifert, F. and Woodland, A. B. (1993a). Ferric iron in the upper mantle and in transition zone assemblages: Implication for relative oxygen fugacities in the mantle. In: Evolution of the Earth and Planets. Geophysical monograph, (Ed.) E. Takahashi, R. Jeanloz and D. C. Rubie, American Geophysical Union, Washington, D.C., **14**: pp. 73-88.

O'Neill, H. S. C., McCammon, C. A., Canil, D., Rubie, D. C., Ross, C. R. and Seifert, F. (1993b). Mossbauer spectroscopy of mantle transition zone phases and determination of minimum Fe^{3+} content, Am. Mineral. **78**: 456-460.

O'Nions, R. K. and Oxburgh, E. R. (1988). Helium, volatile fluxes and the development of continental crust, Earth Planet. Sci. Lett. **90**: 331-347.

Oberheuser, G., Kathrein, H., Demortier, G., Gonska, H. and Freund, F. (1983). Carbon in olivine single crystals analyzed by the $^{12}C_{(d,p)}{}^{13}C$ method and by photoelectron spectroscopy, Geochim. Cosmochim. Acta **47**: 1117-1129.

Orr, J. C., Fabry, V. J., Aumont, O., Bopp, L., Doney, S. C., Feely, R. A., Gnanadesikan, A., Gruber, N., Ishida, A., Joos, F., Key, R. M., Lindsay, K., Maier-Reimer, E., Matear, R., Monfray, P., Mouchet, A., Najjar, R. G., Plattner, G. K., Rodgers, K. B., Sabine, C. L., Sarmiento, J. L., Schlitzer, R., Slater, R. D., Totterdell, I. J., Weirig, M. F., Yamanaka, Y. and Yool, A. (2005). Anthropogenic ocean acidification over the twenty-first century and its impact on calcifying organisms, Nature **437**: 681-686.

Otting, W. and Zahringer, J. (1967). Total carbon content and primordial rare gases in chondrites, Geochim. Cosmochim. Acta **31**: 1949-1960.

Parkinson, I. J. and Arculus, R. J. (1999). The redox state of subduction zones: insights from arc-peridotites, Chem. Geol. **160**: 409-423.

Parkinson, I. J., Arculus, R. J. and Eggins, S. M. (2003). Peridotite xenoliths from Grenada, Lesser Antilles Island Arc, Contrib. Mineral. Petrol. **146**: 241-262.

Pasteris, J. D. (1988). Secondary graphitization in mantle-derived rocks, Geology **16**: 804-807.

Pineau, F. and Javoy, M. (1975). O^{18}/O^{16} and $^{13}C/^{12}C$ ratios in trace carbonates associated to high-temperature peridotites, C. R. Hebdomadair. Seances l'Academie Sci. Ser.D **280**: 809-812.

Pineau, F. and Mathez, E. A. (1990). Carbon isotopes in xenoliths from the Hualalai volcano, Hawaii, and the generation of isotopic variability, Geochim. Cosmochim. Acta **54**: 217-227.

Pinto, J. P., Turco, R. P. and Toon, O. B. (1989). Self-limiting physical and chemical effects in volcanic-eruption clouds, J. Geophys. Res. **94**: 11165-11174.

Rasool, S. I. and Debergh, C. (1970). Runaway greenhouse and accumulation of CO_2 in Venus atmosphere, Nature **226**: 1037-1045.

Renne, P. R., Zhang, Z. C., Richards, M. A., Black, M. T. and Basu, A. R. (1995). Synchrony and causal relations between Permian-Triassic boundary crises and Siberian flood volcanism, Science **269**: 1413-1416.

Rimini, E. (1995). Ion Implantation: Basics to Device Fabrication. Kluwer Academic Publishers, Boston, pp 393.

Ringwood, A. E. (1962). Model for the upper mantle, J. Geophys. Res. **67**: 857-867.

Ringwood, A. E. (1989). Constitution and evolution of the mantle. In: Kimberlites and Related Rocks: Vol. 1 - their composition, occurrence, origin and emplacement, (Ed.), Blackwell, Melbourn: pp. 457-485.

Roberts, J. J., Duba, A. G., Mathez, E. A., Shankland, T. J. and Kinzler, R. (1999). Carbon-enhanced electrical conductivity during fracture of rocks, J. Geophys. Res. **104**: 737-747.

Roedder, E. (1965). Liquid CO_2 inclusions in olivine-bearing nodules and phenocrysts from basalts, Am. Mineral. **50**: 1746-1782.

Roedder, E. (1984). Fluid inclusions. Min. Soc. of America, pp 644.

Rubie, D. C., Karato, S., Yan, H. and Oneill, H. S. C. (1993). Low differential stress and controlled chemical environment in multianvil high-pressure experiments, Phys. Chem. Miner. **20**: 315-322.

Rubie, D. C. (1999). Characterising the sample environment in multianvil high-pressure experiments, Phase Transit. **68**: 431-451.

Saal, A. E., Hauri, E. H., Langmuir, C. H. and Perfit, M. R. (2002). Vapour undersaturation in primitive mid-ocean-ridge basalt and the volatile content of Earth's upper mantle, Nature **419**: 451-455.

Santillan, J., Williams, Q. and Knittle, E. (2003). Dolomite-II: A high-pressure polymorph of $CaMg(CO3)_2$, Geophys. Res. Lett. **30**: 1054 doi:10.1029/2002GL016018.

Santos, F. A. M., Mateus, A., Almeida, E. P., Pous, J. and Mendes-Victor, L. A. (2002). Are some of the deep crustal conductive features found in SW Iberia caused by graphite? Earth Planet. Sci. Lett. **201**: 353-367.

Sasaki, S., Prewitt, C. T., Sato, Y. and Ito, E. (1982). Single crystal X-ray study of gamma-Mg_2SiO_4, J. Geophys. Res. **87**: 7829-7832.

Schilling, F. and Wunder, B. (2004). Temperature distribution in piston-cylinder assemblies: Numerical simulations and laboratory experiments, Eur. J. Mineral. **16**: 7-14.

Schrauder, M. and Navon, O. (1993). Solid carbon dioxide in a natural diamond, Nature **365**: 42-44.

Schwab, R. G. and Freisleben, B. (1988). Fluid CO_2 inclusions in olivine and pyroxene and their behavior under high-pressure and temperature conditions, Bull. Mineral. **111**: 297-306.

Scott, H. P., Williams, Q. and Knittle, E. (2001). Stability and equation of state of Fe_3C to 73 GPa: Implications for carbon in the Earth's core, Geophys. Res. Lett. **28**: 1875-1878.

Scott, H. P., Hemley, R. J., Mao, H. K., Herschbach, D. R., Fried, L. E., Howard, W. M. and Bastea, S. (2004). Generation of methane in the Earth's mantle: In situ

high pressure-temperature measurements of carbonate reduction, Proc. Natl. Acad. Sci. U. S. A. **101**: 14023-14026.

Shannon, R. (1976). Revised effective ionic radii and systematic studies of interatomic distances in halides and chalcogenides, Acta Crystallogr. **32**: 751-767.

Shannon, R. D. and Prewitt, C. T. (1968). Effective ionic radii in oxides and fluorides, Acta Crystallogr. **B25**: 925-945.

Shimizu, N., Semet, M. P. and Allegre, C. J. (1978). Geochemical applications of quantitative ion-microprobe analysis, Geochim. Cosmochim. Acta **42**: 1321-1334.

Sinton, C. W. and Duncan, R. A. (1997). Potential links between ocean plateau volcanism and global ocean anoxia at the Cenomanian-Turonian boundary, Econ. Geol. **92**: 836-842.

Skorodumova, N. V., Belonoshko, A. B., Huang, L., Ahuja, R. and Johansson, B. (2005). Stability of the $MgCO_3$ structures under lower mantle conditions, Am. Mineral. **90**: 1008-1011.

Smyth, J. R. and Bish, D. L. (1988). Crystal structures and cation sites of the rock-forming minerals. Allen and Unwin, Boston, pp 332.

Stachel, T., Brey, G. P. and W., H. J. (2005). Inclusions in sublithospheric diamonds: glimpses of deep Earth, Elements **1**: 73-78.

Sutton, S. R., Karner, J., Papike, J., Delaney, J. S., Shearer, C., Newville, M., Eng, P., Rivers, M. and Dyar, M. D. (2005). Vanadium K-edge XANES of synthetic and natural basaltic glasses and application to microscale oxygen barometry, Geochim. Cosmochim. Acta **69**: 2333-2348.

Taylor, W. R. and Green, D. H. (1988). Measurement of reduced peridotite-C-O-H solidus and implications for redox melting of the mantle, Nature **332**: 349-352.

Tingle, T. N., Green, H. W. and Finnerty, A. A. (1988). Experiments and observations bearing on the solubility and diffusivity of carbon in olivine, J. Geophys. Res. **93**: 15289-15304.

Trull, T., Nadeau, S., Pineau, F., Polve, M. and Javoy, M. (1993). C-He systematics in hotspot xenoliths - Implications for mantle carbon contents and carbon recycling, Earth Planet. Sci. Lett. **118**: 43-64.

Tsirelson, V. G., Belokoneva, E. L., Nozik, Y. Z. and Urusov, V. S. (1986). $MgAl_2O_4$ spinel - peculiarities of its atomic and electronic structure deduced from precision x-ray diffraction data, Geokhimiya: 1035-1042.

Tsong, I. S. T., Knipping, U., Loxton, C. M., Magee, C. W. and Arnold, G. W. (1985). Carbon on surfaces of magnesium oxide and olivine single crystals - diffusion from the bulk or surface contamination, Phys. Chem. Miner. **12**: 261-270.

Tsong, I. S. T. and Knipping, U. (1986). Solute carbon and carbon segregation in magnesiumoxide single crystals - a secondary ion mass spectrometry study - comment, Phys. Chem. Miner. **13**: 277-279.

Ueltzen, M. (1993). The Verneuil Flame Fusion Process - Substances, J. Cryst. Growth **132**: 315-328.

van Achterbergh, E., Griffin, W. L., Ryan, C. G., O'Reilly, S. Y., Pearson, N. J., Kivi, K. and Doyle, B. J. (2004). Melt inclusions from the deep Slave lithosphere: implications for the origin and evolution of mantle-derived carbonatite and kimberlite, Lithos **76**: 461-474.

van Keken, P. E., Kiefer, B. and Peacock, S. M. (2002). High-resolution models of subduction zones: implications for mineral dehydration reactions and the transport of water into the deep mantle, Geochem. Geophys. Geosyst. **3**: 1056 doi:10.1029/2001GC000256.

Verneuil, A. (1902). The artificial production of the ruby by fusion, C. R. Hebdomadair. Seances l'Academie Sci. Ser.D **135**: 791.

Viljoen, K. S. (1995). Graphite-bearing and diamond-bearing eclogite xenoliths from the Bellsbank kimberlites, Northern Cape, South-Africa, Contrib. Mineral. Petrol. **121**: 414-423.

Vogelsang, H. (1869). Nachtrag zu der Abhandlung "Über Flüssigskeiteinschlüsse in Gesteinen", Ann. Phys. Chem. **137**: 257-271.

Vogelsang, H. and Geissler, H. (1869). Über die Natur der Flüssigkeitseinschlüsse in gewissen Mineralien, Ann. Phys. Chem. **137**: 56-74.

Walker, D., Carpenter, M. A. and Hitch, C. M. (1990). Some simplifications to multianvil devices for high pressure experiments, Am. Mineral. **75**: 1020-1028.

Wang, A., Pasteris, J. D., Meyer, H. O. A. and Dele-Duboi, M. L. (1996). Magnesite-bearing inclusion assemblage in natural diamond., Earth Planet. Sci. Lett. **141**: 293-306.

Wentzcovitch, R. M., Hughjones, D. A., Angel, R. J. and Price, G. D. (1995). Ab initio study of $MgSiO_3$ C2/e enstatite, Phys. Chem. Miner. **22**: 453-460.

Wiedenbeck, M., Rhede, D., Lieckefett, R. and Witzki, H. (2004). Cryogenic SIMS and its applications in the earth sciences, Appl. Surf. Sci. **231-2**: 888-892.

Wignall, P. B. and Twitchett, R. J. (1996). Oceanic anoxia and the end Permian mass extinction, Science **272**: 1155-1158.

Wignall, P. B. (2001). Large igneous provinces and mass extinctions, Earth-Sci. Rev. **53**: 1-33.

Wilmart, E., Mosbah, M. and Pineau, F. (1993). Carbon in igneous minerals of granulites from Rogaland (Norway) - nuclear microanalysis and isotope geochemistry, Eur. J. Mineral. **5**: 269-280.

Wilson, M. (1989). Igneous petrogenesis. Unwin Hyman, London, pp 466.

Wood, B. J. and Virgo, D. (1989). Upper mantle oxidation state - ferric iron contents of lherzolite spinels by Fe^{57} Mossbauer spectroscopy and resultant oxygen fugacities, Geochim. Cosmochim. Acta **53**: 1277-1291.

Wood, B. J., Bryndzia, L. T. and Johnson, K. E. (1990). Mantle oxidation state and its relationship to tectonic environment and fluid speciation, Science **248**: 337-345.

Wood, B. J. (1991). Oxygen barometry of spinel peridotites, Rev. Mineral. **25**: 417-431.

Wood, B. J. (1993). Carbon in the core, Earth Planet. Sci. Lett. **117**: 593-607.

Wood, B. J., Pawley, A. and Frost, D. R. (1996). Water and carbon in the Earth's mantle, Philosophical Transactions of the Royal Society of London **354**: 1495-1511.

Woodland, A. B., Kornprobst, J. and Wood, B. J. (1992). Oxygen thermobarometry of orogenic lherzolite massifs, J. Petrol. **33**: 203-230.

Woodland, A. B. and Koch, M. (2003). Variation in oxygen fugacity with depth in the upper mantle beneath the Kaapvaal craton, Southern Africa, Earth Planet. Sci. Lett. **214**: 295-310.

Wyllie, P. J. and Huang, W. L. (1976). Carbonation and melting reactions in system CaO-MgO-SiO_2-CO_2 at mantle pressures with geophysical and petrological applications, Contrib. Mineral. Petrol. **54**: 79-107.

Wyllie, P. J., Huang, W. L., Otto, J. and Byrnes, A. P. (1983). Carbonation of peridotites and decarbonation of siliceous dolomites represented in the system CaO-MgO-SiO_2-CO_2 to 30 kbar, Tectonophysics **100**: 359-388.

Yaxley, G. M. and Green, D. H. (1994). Experimental demonstration of refractory carbonate-bearing eclogite and siliceous melt in the subduction regime, Earth Planet. Sci. Lett. **128**: 313-325.

Zhang, J., Martinez, I., Guyot, F., Gillet, P. and Saxena, S. K. (1997). X-ray diffraction study of magnesite at high pressure and high temperature, Phys. Chem. Miner. **24**: 122-130.

Zhang, L., Ahsbahs, H. and Kutoglu, A. (1998). Hydrostatic compression and crystal structure of pyrope to 33 GPa, Phys. Chem. Miner. **25**: 301-307.

Zhang, Y. and Zindler, A. (1993). Distribution and evolution of carbon and nitrogen in Earth, Earth Planet. Sci. Lett. **117**: 331-345.

Zheng, Y. F., Gong, B., Li, Y. L., Wang, Z. R. and Fu, B. (2000). Carbon concentrations and isotopic ratios of eclogites from the Dabie and Sulu terranes in China, Chem. Geol. **168**: 291-305.

Zhu, Y. F. and Ogasawara, Y. (2002). Carbon recycled into deep Earth: Evidence from dolomite dissociation in subduction-zone rocks, Geology **30**: 947-950.

Erklärung

Name: Shcheka
Vorname: Svyatoslav
Straße: Rückertweg 21
PLZ Ort: 95447 Bayreuth

Ich erkläre hiermit, dass

- ich die Dissertation ohne andere als die in ihr erwähnte Hilfe verfasst habe,
- ich keine früheren Promotionen oder Promotionsversuche unternommen habe.

Bayreuth, den 22.11.2005

Svyatoslav Shcheka